

FORCED PERIODIC OSCILLATIONS IN CHEMICAL REACTORS:
VAPOR-PHASE CONSECUTIVE-COMPETITIVE HYDROGENATION
ON SUPPORTED METAL CATALYSTS

A Dissertation
Presented to
the Faculty of the Department of Chemical Engineering
University of Houston
Houston, Texas

In Partial Fulfillment
of the Requirements for the Degree
Doctor of Philosophy in Chemical Engineering

by

MAHEYAR RUSTOM BILIMORIA

December, 1978

*To my parents and the
memory of my sister*

ACKNOWLEDGEMENTS

I am extremely grateful to my advisor, Professor James E. Bailey, for his guidance, encouragement and understanding throughout the duration of this work. I sincerely appreciate his comments and constructive criticism of the preliminary draft of this dissertation. I feel especially fortunate in having had such an exceptional, friendly and amiable boss to work for.

Grateful acknowledgements are extended to:

Professor James T. Richardson for valuable suggestions and discussions during the work and for serving on the thesis committee.

Professor Dan Luss for his expressed interest during the study and for serving on the thesis committee.

Professors John F. Andrews and John W. Rabalais for serving on the thesis committee.

Ms. Margaret Sanchez, Mrs. Joanne Davidson and Ms. Paula Papandreou for typing the manuscript.

Ms. Janice Chelton, Mrs. Debbie Schrekenghost, Mr. Joe Chetta, Mr. Gary Willison, Mr. Stanley and Mr. Srinivas Bette for their assistance in preparing the figures.

The Engineering Systems Simulation Laboratory for the use of computing facilities.

The following organizations are acknowledged for their generous financial support:

The Chemical Engineering Department of the University of Houston.

The National Science Foundation.

The Camille and Henry Dreyfus Foundation.

The J. N. Tata Endowment for the Higher Education of Indians.

I am especially grateful to Dr. Duane D. Bruns and to Mr. Roy Priest for their help in the design and fabrication of the reactor and to Mr. James Payne for his help with all the electronic equipment.

Finally, but most importantly I am deeply indebted to my parents and my family, my host parents David and Addell Delony and my close friends for continuous encouragement throughout this study. For their cheerful forbearance and unflinching support I will always be grateful.

TABLE OF CONTENTS

CHAPTER		PAGE
1.	INTRODUCTION	1
1.1	Introduction to Periodic Processes and Literature Review	1
1.2	Chemistry, Thermodynamics and Kinetics of the Chosen Reaction System	7
2.	FACTORS LEADING TO THE SELECTION AND DESIGN OF THE REACTOR	21
2.1	Objectives of the Study	21
2.2	Characteristics of the Reaction and Catalyst	22
2.3	Physical Effects	24
2.4	Catalyst Deactivation	26
2.5	Available Reactors and Their Characteristics	27
2.5.1	Integral Packed Bed Reactors	27
2.5.2	Differential Packed Bed Reactors	29
2.5.3	Recycle Reactors	30
2.5.4	Microcatalytic Reactors	31
2.5.5	Continuous Stirred Gas-Solid Reactors	32
3.	THE EXPERIMENTAL SYSTEM	36
3.1	Overall System	36
3.2	Reactants and Inert Gas Feed System	42
3.3	The Reactor	43

CHAPTER	PAGE
3.	
3.4	The Heating and Temperature Control System 52
3.5	The Multichannel Timer 58
3.6	Product Gas Sampling and Analysis 62
4.	EXPERIMENTAL PROCEDURES AND LIMITATIONS 67
4.1	System Leak Test 67
4.2	Catalyst Pretreatment 68
4.3	System Start-up and Shut-down 69
4.4	Run Procedures 71
a.	Steady State 71
b.	Periodic 72
c.	Step Response 74
4.5	Limitations on the Operating Conditions and Equipment 74
5.	PRESENTATION OF RESULTS AND DISCUSSION 81
5.1	Introduction 81
5.2.1	Catalyst I - Experiments 82
5.2.2	Catalyst I - Steady State Modeling 90
5.2.3	Catalyst I - Unsteady State Modeling 97
5.2.4	Catalyst I - Plug Flow Simulations 112
5.3	Catalyst II 115
5.4	Catalyst III 116
5.5	Catalyst IV 129
5.6	Catalyst V 136

CHAPTER	PAGE
6. CONCLUSIONS AND RECOMMENDATIONS	147
6.1 Conclusions	147
6.2 Recommendations for Future Work	149
REFERENCES	152
APPENDIX 1 Flowmeter Calibrations	160
APPENDIX 2 Multichannel Timer Settings	164
APPENDIX 3 Estimation of Parameters	165
APPENDIX 4 Catalyst Properties	168

LIST OF TABLES

TABLE	PAGE
1.1 A Sampling of Simulation Findings on Alteration of Time-Averaged Reactor Performance by Forced Cycling Operation	8
1.2 A Summary of Experimental Research on Forced Cyclic Catalytic Reactions	10
1.3 Heats of Reaction and Equilibrium Constants for Hydrogenation of Acetylene to Ethylene and Ethane	14
4.1 Values of Parameters and Operating Conditions Used in the Experiments	76
5.1 Steady State Data Fit for Catalyst I	94
5.2 Steady State Data Fit for Catalyst II	118
5.3 Comparison between the Two Reactors	144
5.4 Comparison between Catalyst I and Catalyst V	145

LIST OF FIGURES

FIGURE	PAGE
3.1 Experimental reaction system highlighting cyclic feed makeup apparatus and effluent analysis equipment	37
3.2 Overall view of the experimental system	38
3.3 Detailed schematic diagram of the feed gas supply and metering system	44
3.4 Top seal plate for reactor-cum-jacket showing radial positions of the thermocouples	45
3.5 Top view of reactor showing baffles and feed gas inlet	47
3.6 Elevation section of the reaction chamber and jacket assembly	48
3.7 View of the bearing housing and drive shaft showing rotary seal unit	49
3.8a View of the seal housing flush gland	50
3.8b Elevation section showing seal housing, bearing housing and internals	51
3.9 Schematic diagram of seal housing showing its function	53
3.10 Dismantled view of one of the spinning baskets showing the wire mesh screens and support panels	54
3.11 Views of the stationary basket and the agitator assembly	55
3.12 Another view of the reactor-cum-jacket assembly showing heater coils wrapped around the reaction chamber	57
3.13 Schematic wiring diagram of the temperature controlling and recording system	59

FIGURE	PAGE
3.14 View of the assembly of switches, motors and relays constituting the multichannel timer	60
3.15 Schematic Wiring Diagram of the Timing Device	61
3.16 Infra-Red Spectrogram for acetylene	63
3.17 Infra-Red Spectrogram for ethylene	64
3.18 Infra-Red Spectrogram for ethane	65
5.1 Steady-state and periodic effluent hydrocarbon distributions for various time-average hydrogen/acetylene feed ratios for Catalyst I	83
5.2 Instantaneous effluent compositions for cycling with Catalyst I and a period of 300 s	85
5.3 The results of a step-up in feed hydrogen mole fractions (A) show overshoots and much longer transients than the reverse step-down experiment (B) for Catalyst I	87
5.4 SEM photograph of Catalyst I - (fresh sample)	88
5.5 SEM photograph of Catalyst I - (prepoisoned sample)	88
5.6 SEM photograph of Catalyst I - (after-reaction sample)	89
5.7 Comparison of the spinning basket and stationary basket mixing characteristics to an ideal CSTR	91
5.8 Experimental traces of temperature-time profiles for the spinning basket reactor	98
5.9 Comparisons between experimentally measured effluent compositions and compositions calculated from Equation 5.11 (Steady-state Catalyst I)	102
5.10 Comparisons between experimentally measured effluent compositions and compositions calculated from Equation 5.11 for a step increase in feed hydrogen (Catalyst I)	103

FIGURE

PAGE

- 5.11 Comparisons between experimentally measured effluent compositions and compositions calculated from Equation 5.11 for a step decrease in feed hydrogen (Catalyst I) 105
- 5.12 Comparison of the instantaneous concentration trajectories for (A) Simulations with the dynamic model and (B) Experiments (Catalyst I) 107
- 5.13 Comparison of the instantaneous concentration trajectories for (A) Simulations with the dynamic model and (B) Experiments (Catalyst I) 108
- 5.14 Comparison of the instantaneous concentration trajectories for (A) Simulations with the dynamic model and (B) Experiments (Catalyst I) 109
- 5.15 Comparison of periodic time-average and steady-state effluent compositions obtained by simulation with the dynamic model to the corresponding compositions measured experimentally (Catalyst I) 110
- 5.16 "Attainable Sets" of effluent compositions obtained by simulations of a plug-flow reactor and from cyclic experiments with the spinning basket reactor (Catalyst I) 114
- 5.17 Steady-state effluent compositions obtained by experiments with Catalyst II 117
- 5.18 The shaded region shows the domain of ethane yields obtained in several different steady-state experiments at different stages of deactivation of Catalyst III. The curves show ethane yields obtained by cycling feed hydrogen concentration with different periods. 121
- 5.19 Effect of fouling on steady-state effluent compositions for Catalyst III 122
- 5.20 Feed hydrogen step-up (A) for Catalyst III produces a damped oscillation in effluent ethylene in contrast to a step-down in feed hydrogen (B) 123

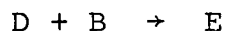
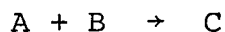
FIGURE	PAGE
5.21 Instantaneous effluent compositions for feed hydrogen cycling with Catalyst III for nine sets of periods (τ) and mean hydrogen feed rates (directly related to γ)	124
5.22 Periodic effluent concentrations for three different switching fractions as measured continuously using the ir analyzer (≈ 180 s, Catalyst III)	126
5.23 SEM photograph of Catalyst III - (fresh sample)	127
5.24 SEM photograph of Catalyst III - (fouled sample)	127
5.25 SEM photograph of Catalyst III - (pre-poisoned sample)	128
5.26 SEM photograph of Catalyst III - (magnified view of a small region of Figure 5.25)	128
5.27 Experimental step-response data for Catalyst IV	130
5.28 Experimental step-response data for Catalyst IV	131
5.29 Experimental step-response data for Catalyst IV	133
5.30 Experimental step-response data for Catalyst IV	134
5.31 Steady-state (solid line) and periodic (broken lines-see legend) effluent hydrocarbon distributions for various time-average hydrogen/acetylene ratios for Catalyst IV	135
5.32 SEM photograph of Catalyst IV - (fresh sample)	137
5.33 SEM photograph of Catalyst IV - (pre-poisoned sample)	137
5.34 SEM photograph of Catalyst IV - (fouled sample)	138
5.35 SEM photograph of Catalyst IV - (enlarged view of a portion of Figure 5.34)	138
5.36 Steady-state (solid line) and periodic (broken lines-see legend) effluent hydrocarbon distributions for various time-average hydrogen/acetylene ratios for Catalyst V (stationary basket)	140

FIGURE	PAGE
5.37 Steady-state (solid line) and periodic (broken lines-see legend) effluent hydrocarbon distributions for various time-average hydrogen/acetylene ratios for Catalyst V (spinning basket)	141
5.38 Experimental Infra-Red records of response to step feed tracer	143
A1.1 Nitrogen Flowmeter Calibration	161
A1.2 Acetylene Flowmeter Calibration	162
A1.3 Hydrogen Flowmeter Calibration	163

CHAPTER 1
INTRODUCTION

1.1 Introduction to Periodic Processes and Literature Review

In the last decade, the demand and the available supply of energy and other resources have begun to converge. Unsteady-state operation is significant and viable among current alternatives for improving process capacity and efficiency. Especially interesting in the contexts of both unsteady-state operation and importance to chemical reaction engineering are consecutive-competitive reactions, whose general stoichiometry is given by:



The kinetics of such reaction systems are often complex, very nonlinear and highly coupled - all attributes which are indicative of potential sensitivity to, and which may be favorably exploited by, intentional unsteady operation. An interesting kind of unsteady-state operation is the cyclic or periodic process where the inputs and the process variables are periodic functions of time.

Most chemical processes, even to this day, continue to be conventionally operated in a steady-state or batch mode. Periodic processing emerged as yet another mode of operation in 1935 when

Van Dijck patented the design of a pulsed extractor column. However, it was only in the early fifties that this concept was introduced to the chemical and petroleum engineering literature by Cannon and coworkers whose experiments showed that the efficiency and the capacity of a distillation column could be improved by controlled cycling of the vapor flow-rate (1952, 1956, 1961a, 1961b, 1961c).

These findings led Schrodt and his colleagues (1965, 1966a, 1966b, 1967a, 1967b) to examine the conditions under which periodic operation of a distillation column was superior to conventional methods. Horn (1964, 1967) was the first to extend the concept of controlled cycling to multistage counter-current separation processes. At this point it will suffice to say that research and development interest in unsteady-state separation processes continues to remain at a high level (Wankat, 1974; Duffy et al., 1978). Having undertaken this brief historical excursion to put certain events in their proper chronological order, all further discussion will be restricted to chemical reaction engineering.

The periodic operation of chemical reactors and the associated optimization theory has been summarized in extensive reviews by Bailey (1973, 1977), and in a student thesis (Fjeld, 1971). Hence, no attempt will be made here to conduct an exhaustive literature survey. A few of the basic concepts and certain important applications of the theory of periodic processes will be introduced and other pertinent topics will be discussed in the context of this particular research.

Periodic conditions within a chemical reactor may emerge spontaneously or they may be forced upon it. The classic studies of Aris and Amundson (1958) on CSTR dynamics are perhaps the earliest and best known illustrations of free oscillations. They demonstrated that nonlinearity and coupling within the system can lead to spontaneous concentration and temperature cycling. Such autonomous or free oscillations have been discussed in detail by Douglas and his students (Douglas and Rippin, 1966; Douglas and Gaitonde, 1967, Dorawala and Douglas, 1971; Douglas, 1972) among many others and will not be dealt with in this study.

Forced cycling is promoted by fluctuations or oscillations in the immediate vicinity of a chemical reactor. These forced fluctuations may be further classified into two groups depending on whether the periodic input is accidental or deliberate. The phenomenon of "flickering," a systematic pulsation in the temperature of catalytic gauze convertors (Edwards et al., 1974) is a very good example of unintentional forced oscillations. However, according to Bailey (1977), "Intentionally forced oscillations offer promise of a new generation of reaction engineering methodology." Such forced periodic phenomena are characterized by regular oscillations in the process variables, which in turn are driven by systematic cyclic changes in at least one of the system inputs.

In some of the first papers on the intentional unsteady-state operation of chemical reactors for performance improvement, Douglas and Rippin (1966) examined the effect of sinusoidal variations in

feed concentration on the time-average conversion for a second order reaction taking place in a continuous stirred tank reactor (CSTR). Since then, a whole spate of theoretical studies have shown that several benefits including improved selectivity, increased conversion and reduced sensitivity may in some cases be realized by periodic operation. The most important among these is perhaps the contribution of Horn and Lin (1967) in which they laid the foundations of the theory of optimum periodic processing. Other notable and significant contributions to periodic reactor theory are cited below.

In any periodic process we are confronted with two very important system parameters: τ , the period or cycle time, and τ_c , the characteristic response time of the system. Bailey, in his first review on the subject, used the relative magnitudes of these two time constants to define the different regimes of periodic operation: Process Life Cycles and Quasi-Steady Periodic Operation are characterized by $\tau \gg \tau_c$ whereas on the opposite end of the scale, Relaxed Steady State Operation is defined by $\tau \ll \tau_c$. The remaining class in which both τ and τ_c are comparable is called Intermediate Periodic Operation. The major distinction between the first two classes is that a Quasi-Steady Periodic Operation is made so by choice, whereas a Process Life Cycle is intrinsically periodic. This scheme of classification is unique in that it can be universally applied to all kinds of periodic phenomena and helps put the various branches of the mathematical theory in their proper perspective.

Bailey and Horn (1968, 1969, 1970a, 1970b, 1971a, 1971b, 1972), and Bailey (1968, 1972a, 1972b, 1972c, 1972d, 1974) further developed the theory of periodic processes, emphasizing selectivity improvement. Motivated by the possible complexity of the objective function for the selectivity in the case of complex reactions, Horn and Bailey appealed to the concept of the attainable set (which was first introduced by Horn) to calculate reactor performance.

Bittanti et al. (1973) developed a criterion for testing whether an optimal steady-state process can be improved by cyclic operation and recently, Guardabassi (1975) further extended its applicability.

Renken (1972) was the first to theoretically study the intentional periodic operation of a CSTR in which a homogeneous, irreversible consecutive-competitive reaction took place. Here again, selectivity improvements were reported. The difference between Lin's work (1967) and this one by Renken is that the latter assumed a control policy whereas the former computed an optimal policy. Farhadpour et al. (1975a, 1975b) complemented Renken's work and argued that the control policy used by Renken was indeed the optimum. They also showed that by relaxing the symmetry condition for the input cycle used by Renken, further improvements were possible.

It is also relevant to mention the experimental work of Renken and Wandrey (1973, 1974, 1976) who demonstrated various advantages of periodic operation, and that of Al-Taie (1977) who investigated the hydrogenation of butadiene over a commercial

nickel oxide catalyst in a periodic fixed bed reactor.

In his most recent review, Bailey (1977) has identified three important classes of forced oscillation applications:

- a) Determination of chemical kinetics and mechanism: When investigating various possible reaction paths, several postulated mechanistic models may predict almost identical steady-states and yet produce markedly distinct time-averaged responses when forced periodically. Thus, besides revealing new operational policies for chemical reactors, unsteady state reaction studies may serve as a valuable tool for model discrimination. (Horn and Bailey, 1969, 1970a).
- b) Improvement of dynamic characteristics: In his work on stability and control of periodic processes, Fjeld (1972, 1974) showed how a small amplitude forced cycle could help stabilize an otherwise unstable chemical reactor which exhibited a large amplitude autonomous limit cycle. In addition to proving the existence of multiple stable forced periodic states and demonstrating other pathological dynamic behavior, Sincić (1974) pointed out with the aid of several practical examples that widespread use of Fjeld's "Asynchronous quenching concept" is not likely. Bruns and Bailey (1977) demonstrated that autonomous oscillations generated by a nonlinear feedback control element can be successfully used to control unstable chemical reaction processes.
- c) Alteration of time average performance: This is perhaps the original and largest single application of all periodic processes. Bailey has given a whole list of examples of this application in his writings and the highlights of a few typical theoretical and

experimental studies are presented in Tables 1.1 and 1.2 respectively. These alterations in reactor performances arise because, in dynamic operation, the governing rate processes may assume different relationships than those that occur in the more constrained steady state case.

1.2 Chemistry, Thermodynamics and Kinetics of the Chosen Reaction System

The reaction chosen for experimental study is the catalytic hydrogenation of acetylene which is a very good example of consecutive-competitive stoichiometry. In industry gas phase hydrogenation is not used for preparative purposes; rather it finds an extensive application in purification of olefin feedstocks. Ethylene used for the manufacture of polyethylene must be freed of acetylenic impurities before it is processed further.

The stoichiometry of the reaction can be represented by the following equations:



An undesirable subsidiary manifestation (given by equation (1.3)) is the tendency of the acetylene to hydrogenative polymerization, which can shorten the lifetime of the catalyst.



Although it is very difficult to quantify the extent of the last reaction, Mars and Gorgels (1964) have reported that the

Table 1.1 A SAMPLING OF SIMULATION FINDINGS ON ALTERATION OF TIME-AVERAGED REACTOR PERFORMANCE BY FORCED CYCLING OPERATION

REACTION	REACTOR TYPE	OSCILLATED INPUT	RESULT	REFERENCES
single irreversible, exothermic reaction	packed bed with catalyst decay	reactant feed, bed regeneration	optimal policies for operation and regeneration of the fixed bed were constructed	Ogunye and Ray (1971)
consecutive	CSTR	reactor temperature	under some conditions cycling gives more of the intermediate product than does the optimal steady state process	Dorawala (1969)
heterogeneously catalyzed parallel reactions	packed bed	feed reactant concentration	for certain reaction mechanisms which include surface species dynamics, large alterations in selectivity result from cycling	Bailey and Horn (1971)

Table 1.1 cont.

REACTION	REACTOR TYPE	OSCILLATED INPUT	RESULT	REFERENCES
single reversible exothermic reaction	stirred tank	inlet, exit flow rates, reactor temperature	obtain yield improvement relative to steady state	Codell and Engel (1971)
living end polycondensation polymerization	CSTR	feed monomer	cycling can produce either broadening or narrowing of the molecular weight distribution depending on the frequency of the periodic process	Ray (1968)
irreversible consecutive competitive	CSTR (isothermal)	feed concentration	improvement in selectivity for the intermediate over optimum steady-state	Renken (1972)

TABLE 1.2 A SUMMARY OF EXPERIMENTAL RESEARCH ON FORCED CYCLIC CATALYTIC REACTIONS

REACTION	REACTOR TYPE	OSCILLATED INPUT	RESULT	REFERENCES
ammonia synthesis	fixed bed	feed composition	conversions greater than steady state equilibrium	Unger and Rinker (1976)
ethanol dehydration	fixed bed	flow rate or reactor temperature	conversion is decreased by flow oscillation, increased by temperature oscillation	Denis and Kabel (1970, a & b)
olefin (co) polymerization	CSTR	feed hydrogen pressure	broadened molecular weight distribution	Claybaugh <u>et al.</u> (1969)
hydrogen or ammonia oxidation	catalytic wire	gas composition	irregular temperature fluctuations (flickering)	Edwards <u>et al.</u> (1974)
ethylene oxidation	fixed bed	feed composition	improved selectivity for ethylene oxide	Renken <u>et al.</u> (1976)

Table 1.2 cont.

REACTION	REACTOR TYPE	OSCILLATED INPUT	RESULT	REFERENCES
hydrocarbon oxidation	catalytic wire	feed composition	improved selectivity, regular rather than chaotic catalyst temperature fluctuations	Wandrey and Renken (1973)
SO ₂ oxidation	packed bed	feed composition	enhanced SO ₂ conversion	Unni <u>et al.</u> (1973)
ethanol dehydration	catalytic CSTR	reactor temperature	modified selectivity	Tellis and Hulburt (1975)
ethylene hydrogenation ethanol dehydration	fixed bed	feed composition	improved time average conversion and yield	Renken <u>et al.</u> (1974)
propylene oxidation	catalytic wire	feed composition	enhanced yield of desired product	Wandrey and Renken (1974)
SO ₂ oxidation	fixed bed	feed composition	enhanced rate of SO ₂ oxidation	Briggs <u>et al.</u> (1977)

Table 1.2 cont.

REACTION	REACTOR TYPE	OSCILLATED INPUT	RESULT	REFERENCES
propylene oxidation	catalytic gauze	feed composition	stable forced cyclic operation was obtained at temperatures corresponding to unstable steady states	Wandrey and Renken (1977)
butadiene hydrogenation	packed bed	feed composition	improved selectivity and yield	Al-Taie and Kershenbaum (1978)
acetylene hydrogenation	catalytic CSTR	feed composition	increased conversion and modified selectivity	Bilimoria and Bailey (1978)

"green oil" (as these polymers are often called) formed over a palladium-on-alumina catalyst is roughly equivalent to 5% of the acetylene supplied at ~ 25 atm and 200°C .

The thermodynamics of the reaction has been extensively studied by several investigators (Wagman et al., 1945; Prosen et al., 1945; Kilpatrick et al., 1946). The most important factors with respect to process design and catalyst life and activity are the heats of reaction and the equilibrium constants for reactions (1.1) and (1.1)+(1.2), and these are summarized in Table 1.3 within the range of 300° to 1000°K . The equilibrium constants are strong functions of temperature whereas the heats of reaction seem to be relatively constant. The hydrogenation of hydrocarbons containing a triple bond takes place in two consecutive steps. First, the alkyne is hydrogenated to form an alkene or olefin. This alkene, also being unsaturated can add a pair of hydrogen atoms to form an alkane. Since the hydrogen for both reactions comes from the same source, the alkene and its precursor both compete for the available hydrogen. Hence a selectivity is imposed upon these competing reactions and this selectivity is determined by the relative strengths of the interactions between the reactants, the adsorbed species and the active surface of the catalyst.

Selectivity can also be affected by several other factors, such as intraparticle diffusion, geometry and chemical nature of the catalyst and temperature.

Of the various group VIII metals (of the periodic table) used as hydrogenation catalysts, the most frequently used is palladium,

TABLE 1.3 HEATS OF REACTION & EQUILIBRIUM CONSTANTS FOR
HYDROGENATION OF ACETYLENE TO ETHYLENE AND ETHANE

TEMPERATURE		HEAT OF REACTION ΔH , Cal/g mole		$K = \frac{(C_2H_4)}{(C_2H_2)(H_2)}$	$K = \frac{(C_2H_6)}{(C_2H_2)(H_2)^2}$
$^{\circ}K$	$^{\circ}C$	EQ. (1.1)	EQ. (1.1+1.2)		
300	27	-41.711	-74.451	3.37×10^{24}	1.19×10^{42}
400	127	-42.368	-75.553	7.63×10^{16}	2.65×10^{28}
500	227	-42.911	-76.485	1.65×10^{12}	1.31×10^{20}
600	327	-43.311	-77.211	1.19×10^9	3.31×10^{14}
700	427	-43.645	-77.767	6.50×10^6	3.10×10^{10}
800	527	-43.676	-78.157	1.28×10^5	2.82×10^7
900	627	-44.014	-78.432	5.88×10^3	1.17×10^5
1000	727	-44.099	-78.584	2.23×10^2	1.46×10^3

usually on suitable carriers, and then nickel. These catalysts are often modified with salts of heavy metals such as lead, zinc and copper and/or are poisoned by the addition of organic bases or sulfides (Anderson, 1975).

To achieve high selectivity for the intermediate, the catalyst must fulfill the condition that the partially hydrogenated product (i.e. ethylene) which is formed on the surface is not altered any further. Gutmann and Lindlar (1969) say that the above condition can be fulfilled in two ways:

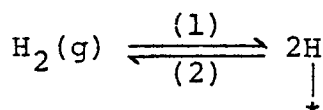
- a) When the subsequent reaction proceeds at a much slower rate than the partial hydrogenation, the selectivity is based on a mechanistic or kinetic factor.
- b) If that is not the case, the partially hydrogenated product can also be protected from subsequent reactions by being rapidly desorbed from the catalyst surface and then not being re-adsorbed again. This thermodynamically dependent selectivity is based on the triple bond being more strongly adsorbed than the corresponding double bond, because of its more electrophilic character. Even relatively small differences in the adsorption energy are sufficient for the acetylene to immediately displace the primarily resulting hydrogenation product from the catalyst surface and accordingly act as a "poison" for the subsequent reaction. This poisoning action is naturally only effective as long as the triple bonded compound is still present.

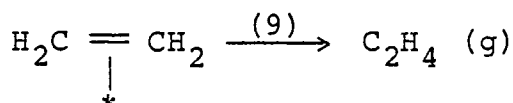
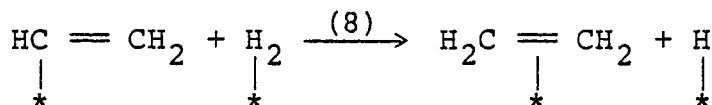
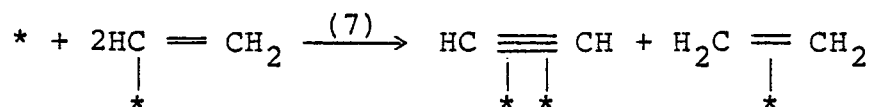
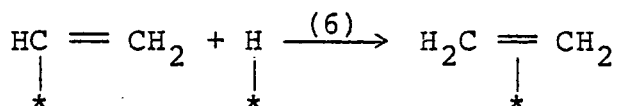
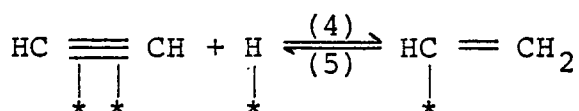
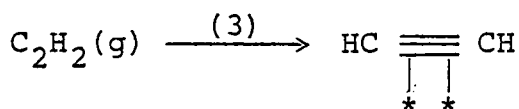
As noted by Gutmann and Lindlar, kinetic and thermodynamic effects are frequently combined and they cannot always be readily distinguished. However, the findings of Bond and Wells (1964) lead one to conclude that acetylene hydrogenation over

palladium catalysts is a good example of thermodynamically controlled selectivity. They observed that although palladium catalysts have 10 to 100 times greater activity for the hydrogenation of ethylene than for the hydrogenation of acetylene, the primarily resulting ethylene contains only 1-5% ethane. From the experiments of Bond et al. (1964) and their own work, Mars and Gorgels concluded that even traces of acetylene suffice to stop ethylene hydrogenation completely and also that the direct formation of ethane from acetylene can be neglected.

These reactions have been the subject of extensive studies by Bond (1962, 1964) and Sheridan (1944, 1945). Bond and co-workers conducted several types of experiments on various metals including acetylene deuteration because they felt that these would reveal information, which in turn would influence interpretation of the kinetics and elucidation of the reaction mechanisms. While all the details are not very clear the orders of acetylene hydrogenation, as determined from initial rates, appear to be in the range of 1.0 - 1.5 for hydrogen and zero or negative with respect to acetylene. Complex hydrogen orders have also been reported for some nickel catalysts. When deuterium was used, all possible isotopic isomers of ethylene were always observed.

Based on the above-mentioned experiments, Bond and Wells (1964) deduced three mechanisms. The sequence of steps involved is shown below:





Mechanism I: This includes steps (1) through (6) and (9) and was designed to explain an order of unity in hydrogen and a zero or negative order in acetylene. After going through a series of arguments, Bond and Wells showed that in this case, the ratio of ethylene formation was given by

$$r = \frac{k_4 k_6}{k_5} \theta_{\text{C}_2\text{H}_2} \theta_{\text{H}}^2$$

where k's are rate constants and θ 's represent surface coverages.

Mechanism II: This mechanism like the one above was also meant to explain the very same dependencies on hydrogen and acetylene. However, the major differences were that hydrogen adsorption was

assumed to be irreversible so that steps (1), (3) through (7), and (9) were included and the ethylene formation rate was given by

$$r = k_7 \theta_{C_2H_3}^2$$

Mechanism III: Here as in mechanism II, hydrogen adsorption was assumed to be irreversible and so step (2) was absent. In this mechanism, which was proposed in order to account for a 1.5 order in hydrogen, step (8) was assumed to be rate-determining. The ethylene formation rate was given by

$$r = k_8 P_{H_2}^{1.5}$$

where P denotes partial pressure. Bond and Wells say that mechanism I applies to ruthenium, osmium and iridium, mechanism II to nickel and palladium and the last one to platinum.

Ethylene hydrogenation is perhaps one of the most widely studied reactions in heterogeneous catalysis. Bond (1964) stated that while the general picture of the hydrogenation of ethylene over Group VIII metals was fairly clear, the least satisfactory aspect was the paucity of precise mechanistic information. He cited the large number of contributing elementary steps and the lack of extensive and accurate kinetics of the various possible exchange processes, as reasons for his conclusion. Recently, Bianchi, et al. (1975) and Richardson and Friedrich (1975) have reviewed the subject and postulated reaction sequences.

It should be noted that the relative rates of olefin desorption and hydrogenation in the presence and in the absence of acetylene may be significantly different in view of the earlier discussion on selectivity. Hence, due care must be exercised in using rate expressions for reaction (1.2), which have been derived under conditions when acetylene is not present.

Komiyama and Inoue (1968) studied the consecutive hydrogenation of acetylene over a nickel-on-keisulguhr catalyst with different particle diameters. Their results showed a similar trend as predicted by Wheeler (1956) viz. selectivity increased with diminishing particle size. They observed, however, that a considerable discrepancy existed between their experiments and the theoretical values obtained with simple first order kinetics and the uniform pore model used by Wheeler. This led them to invoke Langmuir-Hinshelwood kinetics and a micro-macro pore model which seemed to resolve the above discrepancy. Later Komiyama and Inoue (1970) extended their work to include several Langmuir-Hinshelwood type mechanisms. The rates of reaction postulated by them for reactions (1.1) and (1.2) are given by:

$$r_1 = \frac{k_1 P_{H_2} P_A}{1 + K_A P_A}$$

$$r_2 = \frac{k_2 P_{H_2}^{1/2} P_E}{1 + K_A P_A}$$

where k_1 and k_2 are rate constants, K_A is the equilibrium constant of adsorption and P_{H_2} , P_A and P_E are partial pressures of hydrogen,

acetylene and ethylene, respectively.

Toei et al. (1974) investigated the consecutive hydrogenation of acetylene with a nickel-on-keiselguhr catalyst whose micropores were obliterated by annealing in order to eliminate the effect of micropore diffusion resistance. They observed that the numerical value of the selectivity for ethylene formation increased by diminishing the pellet size, but it never approached unity in the limit of zero conversion. They tried to explain such an observation by speculating that certain steps were controlling the reaction, e.g. (i) combined surface reaction and adsorption of acetylene and (ii) combined surface reaction and desorption of ethylene were separately considered as limiting steps. They noted that the surface reaction cannot be omitted from the rate limiting steps because the reaction under consideration is irreversible. Their experimental results seemed to be in fairly good agreement with the surface reaction and desorption limiting mechanism with Langmuir-Hinshelwood rate forms. Using their model they deduced the following relation:

$$\left(\frac{1}{S_0} - 1\right) = \alpha \left(\frac{P_H}{P_A}\right) + \beta$$

which appears to agree with the work of Bond (1961) and Sheridan (1945). Here S_0 is the intrinsic selectivity, α and β are constants and P's are partial pressures. Both of the Japanese studies mentioned above modeled the system as consecutive reactions, neglecting the competitive aspect.

CHAPTER 2

FACTORS LEADING TO THE SELECTION AND DESIGN OF THE REACTOR

2.1 Objectives of the Study

The most important criterion to be considered in designing laboratory reactors is the purpose for studying the reaction. Chemical reactions are studied for a wide variety of reasons (e.g. reaction kinetics, catalyst testing and evaluation, process optimization, stability studies, etc.) and the objectives of the study dictate certain aspects of laboratory reactor design. In any case, several questions have to be answered before making a suitable choice.

Past studies, (Bailey, 1973; Douglas, 1972) almost entirely theoretical, have suggested that significant improvements in selectivity and yield can be realised by intentional dynamic operation of chemical reactors. The principal objective of this study is to demonstrate experimentally this phenomenon and thereby lend credence to earlier modelling studies, illustrate successful utilization of the available theory, and to spur development of other applications. In addition to verification of the results predicted by Lee's (1972) simulations, the objectives for designing the reactor include capability to measure repetitive instantaneous concentration profiles and to study the dynamics of acetylene hydrogenation on supported nickel catalysts.

Owing to the difficulty of obtaining the Japanese catalysts for which the kinetics have been published (Komiyama and Inoue, 1968) and used in Lee's study, an additional objective of this work was to investigate the kinetics of the reaction on the catalysts employed in this work.

A basic requirement in the analysis of catalytic reactors is a rate expression for the specific reaction. The equations used to represent the rate contain certain basic physical-chemical coefficients whose values must be known. There is no method available by which the kinetic rate parameters of a chemical reaction can be predicted and hence experimental determination of these parameters is unavoidable. So, fundamental to the other goals mentioned above, the design of the reactor must be made to allow measurements which are useful in evaluating kinetic parameters.

2.2 Characteristics of the Reaction and Catalyst

1. The acetylene hydrogenation reaction takes place in two steps, both of which are highly exothermic (the heats of hydrogenation being 42.3 kcal/mole and 32.6 kcal/mole respectively (Bond, 1962)). Adequate means of removing this heat must be provided unless differential conversions are involved. Alternately, an inert gas must be used to moderate the reaction by decreasing the partial pressure of the reactants (Komiyama and Inoue, 1968).

2. Metals which themselves catalyze this reaction (Ni, Pd, Pt, etc.) must not be used in any part of the reaction apparatus unless absolutely necessary. In the event their use is unavoidable, the amount of reaction occurring due to these should be determined in advance and be taken into consideration in the subsequent analysis.

3. Materials like copper and silver should be avoided because of safety considerations. (The compounds formed by acetylene with these metals, viz. copper acetylide and silver acetylide, are explosive.)

4. The temperature in the reactor should not exceed 400°C because, at higher temperatures, the aggregates of nickel crystals on the catalyst tend to sinter (Toei et al., 1974). Further, at higher temperatures the reaction rates drop considerably (see Table 1.3).

5. Acetylene tends to be strongly adsorbed on the catalyst and this can lead to deactivation (Komiyama and Inoue, 1970). During the reaction there is some "polymer" formed (Thomas, 1970) on the catalyst which reduces its effectiveness. This sticky mess, commonly referred to as "green oil", tends to coat the catalyst and the reaction apparatus. As a result the catalyst must regularly be regenerated or replaced. One way to minimize this effect is to maintain an excess of hydrogen in the reactor (Toei et al., 1974).

2.3 Physical Effects

The phenomena which occur during a heterogeneously catalysed reaction can be classified into physical and chemical steps (Young and Hougen, 1950). The physical steps occurring are the transfer of the reactant gases to the catalyst surface, diffusion of reactants into the catalyst particle, diffusion of products back to the exterior surface of the particle and transfer of products from the surface to the bulk gas. These physical steps are usually present, and, to simplify the interpretation of experimental data, it is both necessary and desirable to minimize the resistances offered by each. The chemical steps involve activated adsorption of reactants with or without dissociation, surface reactions on active sites, and activated desorption of products. Further the uncatalyzed reaction also takes place in the bulk gas stream simultaneously with the surface reaction. In addition to the above possibilities, fouling and changes in catalyst activity can further complicate matters.

Whether laboratory studies of heterogeneous catalysis are devoted to securing kinetic models or to evaluating catalysts, it is imperative that the information derived accurately reflects only chemical events. The effects of interphase and intraparticle heat and mass transport and spatial nonuniformities in the temperature profiles of the gas and catalyst phases tend to distort the data and make subsequent analyses difficult.

Reaction rate data obtained without evaluation of diffusional effects can yield rate expressions of very restricted applicability.

Since physical and chemical events are coupled together and occur simultaneously, the investigation of gas-solid catalytic reactions is no mean task. Depending on the reaction conditions, the geometry of the reactor and the characteristics of the reaction, physical or chemical events may dominate.

Physical events which tend to falsify kinetic data primarily depend upon the physical and transport properties of the reaction mixture, the gas velocity past the catalyst pellets, and the catalyst pellet size and internal pore structure. These variables in turn affect the rates of external mass transfer and intrapellet diffusion, both of which should be significantly more rapid than the reaction rate if diffusional disguises are to be minimized. Doraiswamy and Rajadhyaksha (1976), Carberry (1964), Bennett and co-workers (1972), Mears (1971) and Weisz and Prater (1954) have explained the role of these factors and have shown how they can be manipulated for proper reactor design. They have also presented a summary of the various transport effects that must be accounted for and the criteria used to determine when they can be neglected. Also, a set of diagnostic tests have been described and some warnings are given to pitfalls among them.

2.4 Catalyst Deactivation

In general, the activity of a catalyst decreases with the passage of time. This may cause changes in selectivity patterns and hinder the analysis of kinetic data. Loss in catalytic activity may be brought about by poisoning, fouling and aging.

Poisoning is caused by impurities in the feed gas streams, especially compounds of sulfur, arsenic, antimony and lead. These compounds or "poisons" react with the active sites and change their chemical composition. If oxygen is present in the feed as an impurity and the temperature is sufficiently high, portions of the nickel catalyst can be oxidised to NiO. Since nickel and nickel oxide show different catalytic activity, such alterations in catalyst composition only serve to falsify kinetic behaviour (Pareja et al., 1975).

Fouling is caused by carbonaceous deposits on the surface of the catalyst. Under certain conditions hydrocarbons decompose or react to produce elemental carbon (Bernardo and Lobo, 1975). Also, during the hydrogenation of acetylene some "polymer" is almost always formed (Thomas, 1970). These carbonaceous deposits and the polymer plug the pores of the catalyst with the result that only a fraction of the total active sites are available for the reaction.

Aging is primarily caused by a thermal process called sintering. Luss (1970) has shown by order of magnitude

calculations, that temperature differences between metal crystallites and the support surface for typical exothermic conditions and particle dimensions can reach hundreds of degrees ($^{\circ}\text{C}$) for extremely short periods of time. It may be for this reason that some degree of crystallite growth is almost invariably noted in supported nickel catalysts which have been used for any length of time in exothermic processes.

2.5 Available Reactors and Their Characteristics:

This section is not intended to be an exhaustive description of the different types of catalytic reactors. Excellent reviews have been written by Carberry (1964), Weekman (1973), Doraiswamy and Tajbl (1974) and Bennett et al. (1972). However, the salient features of the major types of laboratory reactors will be reviewed so that the reasoning behind the final choice of reactor for this study can be fully appreciated. Although it is possible to obtain rate data from nonisothermal reactors, due to the availability of isothermal reactors which yield precise kinetic information, only the latter will be considered.

2.5.1. Integral Packed Bed Reactors:

As the name suggests, this reactor consists of a tube packed with catalyst pellets. It is perhaps the most widely used device because it is inexpensive and is easy to operate. Also, in many instances involving elevated temperatures and pressures, it is the only alternative. Hence, it can be useful for modeling industrial reactors and testing the performance of

catalysts under industrial conditions. Integral reactor data are intrinsically more accurate than differential reactor data because of the high conversions involved so that routine analytical methods are adequate.

By its very nature, the integral reactor produces rates integrated over a concentration range; point rates must be obtained by the process of differentiation. For integral reactors, the rate of a complex reaction is obtained from the relation

$$\frac{dF_i}{dV_R} = \sum_{j=1}^n a_{ij} r_j$$

where F_i is the molar flow rate of species i , V_R is the volume of the reactor, a_{ij} are the stoichiometric coefficients and r_j is the reaction rate for the j^{th} independent reaction. Hence, the data must be differentiated and compared with proposed rate expressions or the rate equations integrated and compared with the data. The former method is inherently inaccurate, so the only other alternative is simultaneous integration and parameter fitting. Rates are often deduced from these data on the assumption of plug flow behaviour, an assumption which is quite often invalidated by the existence of radial and axial dispersion, and possible channeling or incomplete contacting.

The main reason for errors in integral data is the lack of isothermicity, which is particularly serious in highly

exothermic or endothermic reactions. This main disadvantage of this type of reactor may be overwhelming, because the effect of temperature on the rate of a chemical reaction is frequently exponential as described by the Arrhenius law. In light of this discussion and the arguments stated in the previous section on physical effects it is not difficult to see why the integral packed bed reactor is ill-suited for the procurement of accurate kinetic data.

2.5.2. Differential Packed Bed Reactors:

If a differential quantity of catalyst is used, it is readily seen that the conversion obtained would be so small that the compositions of the inlet and outlet streams would be almost identical. Under these conditions, the experimentally measured conversion gives the rate directly. In principle, this is the ideal situation for kinetic measurements. The differential reactor is clearly superior to the integral reactor for kinetic studies in that the various gradients involved are minimized.

In practice, however, differential reactors closely approximating their definition are difficult to operate. This is so in view of the small differences between the composition of the inlet and outlet streams which call for a high degree of analytical precision. Further, it is necessary to prepare synthetic feeds conforming to various compositions to facilitate the measurement of the reaction rate as a function of composition. While this is possible in simple reactions with well known

reaction paths, in complex reactions, certain compounds may be formed which may be difficult to introduce in the feed or whose presence may not be known a priori.

2.5.3. Recycle Reactors:

When a differential reactor is operated such that most of the effluent stream is recycled, a small amount of feed is continuously added and a small product stream continuously removed, a reactor system is obtained which has several advantages over the type of reactor described in the previous section. This reactor may be regarded as a 'pseudo-differential' reactor in that it gives a direct measurement of the reaction rate, but at integral conversion levels.

Since recirculation rates fifteen to twenty times the feed rate are usually employed, the system tends to be more or less isothermal. Further, the resultant high velocities past the catalyst pellets tend to eliminate almost any external transport influence. By varying the recirculation rate and catalyst pellet size, conditions under which the reaction rate limitation by mass transfer is negligible can be established. All measurements of the observed rate of reaction are then made under these conditions.

In the recycle reactor another advantage of operation at high rates of recirculation is that the measured reaction rate corresponds to the exit conditions. This use of exit conditions

obviates the need for employing several synthetic feeds of different compositions. Also, the degree of mixing can be varied by changing the recycle rate, and, depending on its value, this reactor can be operated in the extremes of zero to complete backmixing.

A critical hardware problem associated with reactors of this class is the recirculation pump itself. The primary requirement for this device is that it should be non-catalytic and non-contaminating, and, further, it should have a low hold-up so that steady state is reached rapidly.

One major disadvantage of this reactor is that the recycle gas often has to be heated or cooled to protect the pump and the flow-rate measuring device.

2.5.4. Microcatalytic Reactors

Advances in analysis have made micro reactors a practical proposition in recent years. As the name implies, this reactor is characterized by the use of a very small quantity of catalyst with correspondingly small quantities of reactants. Essentially the method of operation consists in injecting a pulse of reactant into an inert stream passing over a fixed bed of catalyst. The effluent is directed into a chromatographic column for separation and identification of the reaction products.

The very small sample size limits the heat generation, even when the conversion is as high as 100%, thus assuring virtually isothermal operation. Since a carrier gas has to be used in

relatively larger quantities very high space velocities can be used to eliminate external mass transfer resistances.

It should be noted however that kinetic data from micro-catalytic reactors are often considered suspect. This is so because catalyst activity is time dependent and the unsteady-state nature of the reactant pulse exposure to a catalyst can at best describe the initial transient response of the catalyst surface. Another disadvantage of this reactor is that the residence time of the reacting species may not all be the same because of adsorption-desorption differences and resultant chromatographic separations.

2.5.5. Continuous Stirred Gas-Solid Reactors:

From the remarks in the preceding sections, it can be inferred that the ideal catalytic reactor is one which operates isothermally over a wide range of conversions in a steady state with respect to the catalyst and reactants, under clearly defined residence time conditions while facilitating direct rate law determinations. The continuous stirred gas-solid reactor, in principle, possesses these ideal characteristics.

The stirred gas-solid reactor is fundamentally similar to the recycle reactor described earlier in that both give a direct measure of the rate at exit conditions which are identical to the conditions prevailing inside the reactor. Due to the principle feature that gas-solid mass transfer resistance is essentially eliminated and excellent mixing can be achieved, this reactor is often referred to as a gradientless reactor.

This type of reactor was first developed by Carberry and coworkers (Simons et al., 1966) and since then because of its obvious benefits has been used by many others with several modifications in the design. (Tajbl et al., 1967; Brisk et al., 1968; Tajbl, 1969a and 1969b; Smith, 1970; Choudhary and Doraiswamy, 1972; Halladay and Mrazek, 1973; Trifiro et al., 1973.)

The Continuous Stirred Gas-Solid reactor is superior to the recycle reactor in that very high speeds of rotation (e.g. 5000 rpm) can be employed to ensure the absence of any mass transfer effect. Although it is very difficult to estimate the gas velocity past the catalyst particles, order of magnitude calculations using the mass transfer correlation for packed beds (Bird et al., 1960)

$$j_D = \frac{k_g}{u} (Sc)^{2/3} = 0.91 (Re)^{-0.51} \psi \quad (Re < 50)$$

indicate that for first-order kinetics, even with relative velocities as low as 0.5 cm/s, the Biot number (Bi_m) $\gg \phi \tanh(\phi)$ where ϕ is the Thiele modulus. In the above equation k_g is the mass transfer coefficient, u is the velocity, Sc is the Schmidt number, Re is the Reynolds number and ψ is a shape factor. In most of these reactors, typical velocities are much greater than 10 cm/s.

Though the basic principles and general features of all stirred reactors are the same, they can be further classified

depending on whether the catalyst is rotating or stationary and according to the arrangement of the catalyst and the stirring assembly. The spinning basket reactor, the reactor with catalyst impregnated on the walls, the reactor with the catalyst placed in an annular basket and the internal recirculation reactor have specific advantages and disadvantages relative to each other. The spinning-basket reactor described in the next chapter was chosen for this study.

CHAPTER 3

THE EXPERIMENTAL SYSTEM

The spinning-basket reactor and the auxiliary equipment used to investigate the dynamics of acetylene hydrogenation on supported nickel catalysts are described in this chapter. The system was so designed that it permitted the investigation of the chemical reaction behaviour as a function of flow rate, gas composition and temperature under "perfectly mixed" conditions. Further, it enabled instantaneous product gas analysis measurements to be made during periodic and transient response operation with negligible error due to hydraulic and mixing lags.

3.1 Overall System

The apparatus used in this study consisted of five major sections: the feed gas supply and measurement section, the reactor, the heating and temperature control system, the multichannel timer and the product gas sampling and analysis equipment. Figure 3.1 is a schematic diagram of the overall system, highlighting the cyclic feed makeup apparatus and the effluent analysis equipment. A colour picture consisting of most of the apparatus is shown next in Figure 3.2.

In these experiments, acetylene and hydrogen were the reactants, and, as stated in Section 2.2, nitrogen was used as an inert to modify the heat liberated during the reaction and thus make it easier to maintain isothermal conditions.

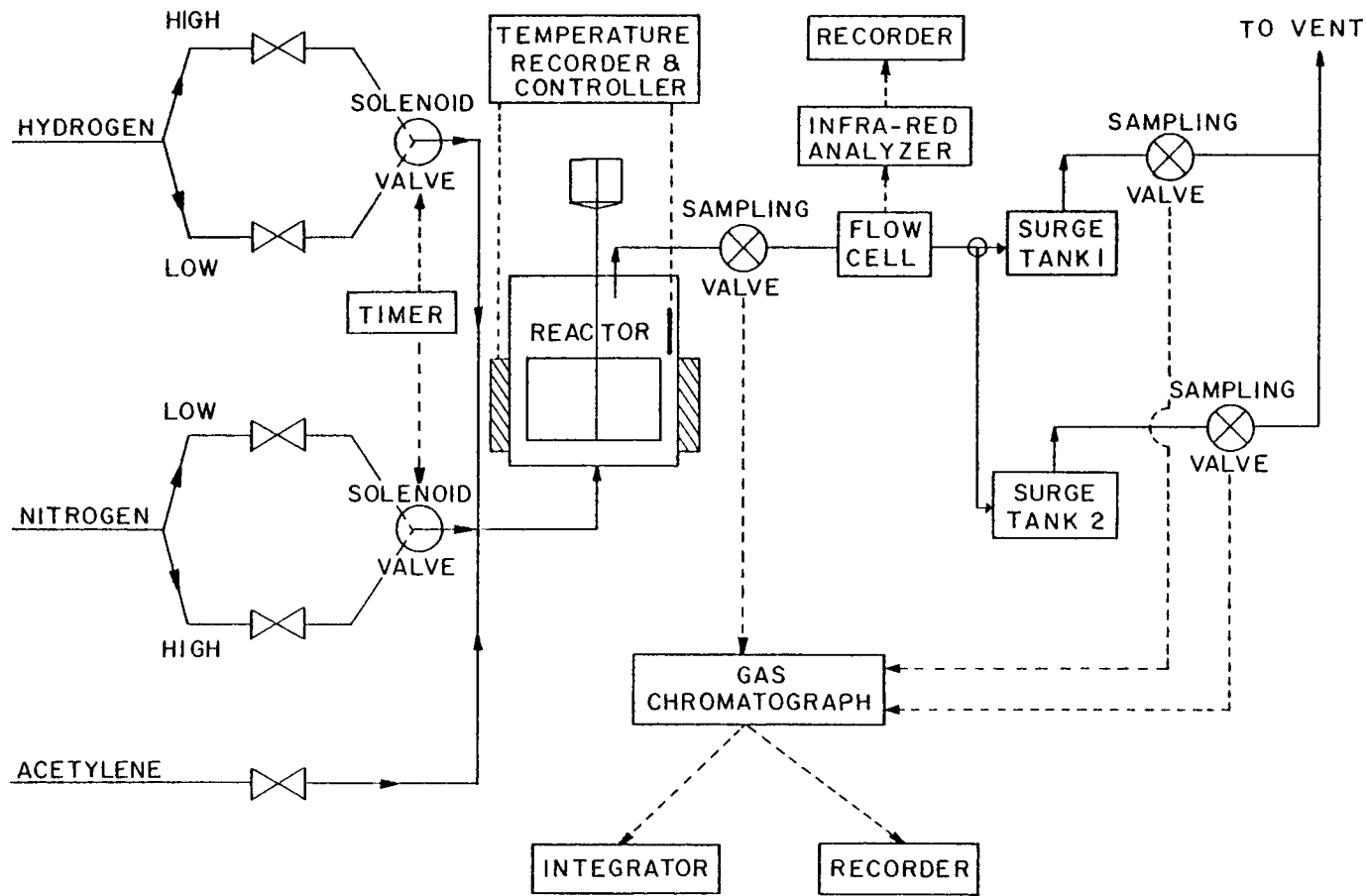


Figure 3.1 Experimental reaction system highlighting cyclic feed makeup apparatus and effluent analysis equipment.

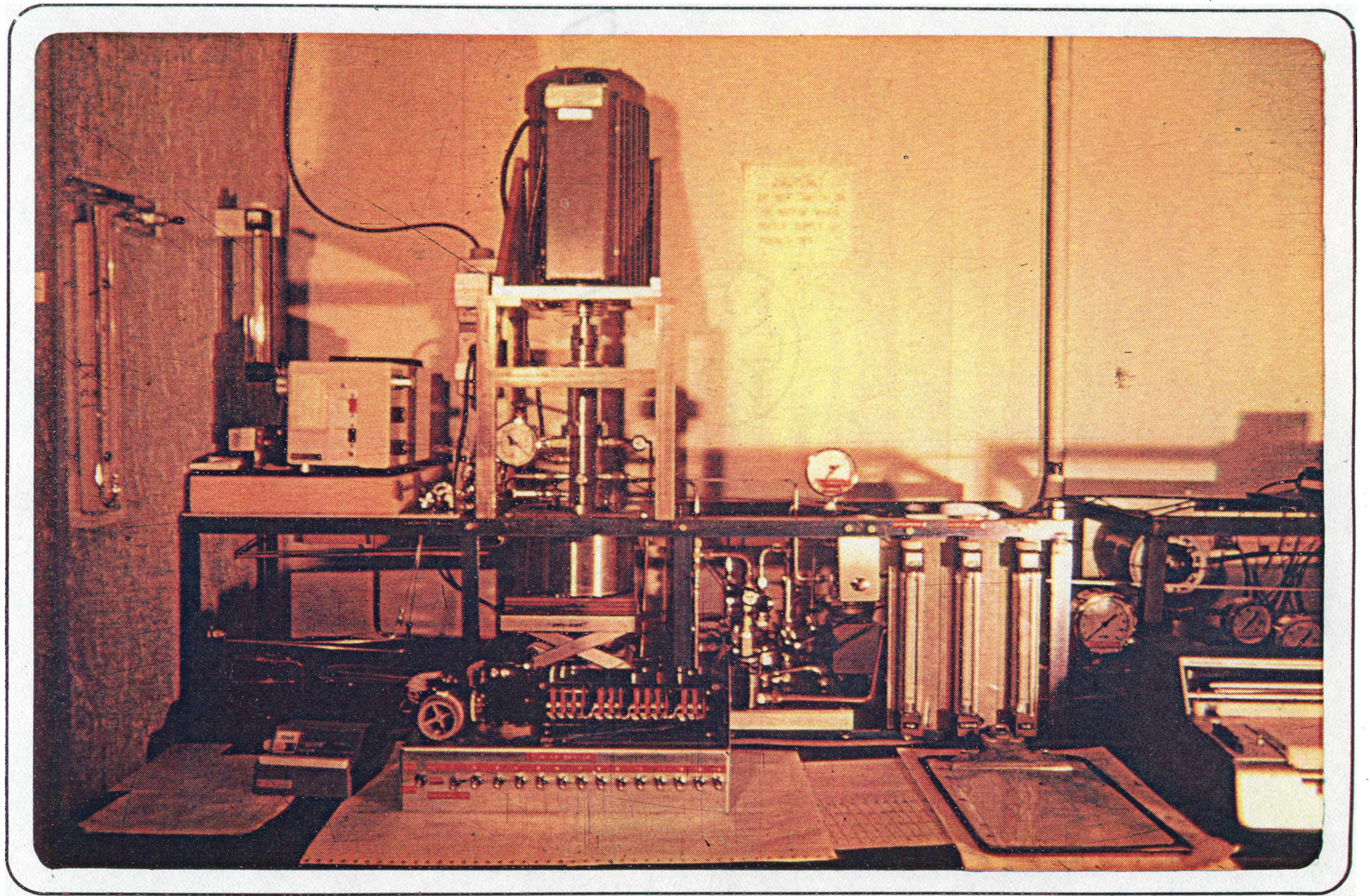


Figure 3.2 Overall view of the experimental system

This also served to keep the acetylene partial pressure well below the explosive limit which is 15 psig (outside the cylinder). Acetylene gas was made to pass through a bed of activated charcoal to remove the solvent phase (Linde, 1975). This was found necessary (as revealed by preliminary experiments) to avoid the occurrence of side-reactions, catalyst poisoning and interference with product analysis.

The pressure in each line was verified using a low range standard gauge and the nitrogen stream was further regulated with an in-line regulator.

Three rotameters were used to measure and monitor the gas flow rates. Before the actual operation, each rotameter was calibrated for the entire range of flow rates used in this study using the method described in Appendix 1. The calibration curves for each gas along with the corresponding float and tube combination are also presented in Appendix 1.

The flow-rates of the feed gases were set using Whitey metering valves located downstream of the rotameters. The acetylene feed to the reactor was kept constant, whereas the flow-rates of hydrogen and nitrogen were adjusted in a complementary manner so as to maintain a constant total gas feed rate. Therefore, the mean residence time in the reactor was identical for both steady and unsteady reactor operation, thus insuring that any observed influences of unsteady operation were due to feed composition changes only. The details showing how this was accomplished, using a dosing system composed

of a multichannel timer, metering valves and solenoid valves, can be found elsewhere in this chapter.

The metered reactants and diluent were combined in a mixing cross located at the exit of the solenoid valves and fed to the bottom of the reactor. This feed line to the reactor was provided with a three-way ball valve just upstream of the mixing cross and a septum arrangement. The ball valve was installed to permit the feed gases to by-pass the reactor and be vented in case of an emergency, whereas the septum allowed gas samples to be drawn out with a hypodermic syringe for purposes of analysis.

The reaction was conducted at a pressure slightly above atmospheric (~ 1 psig) in a stainless steel spinning basket reactor. Nearly isothermal operation at 439° K was maintained by automatic on-off control of a 1000 watt heater in an air-cooled jacket surrounding the reactor.

At the exit of the reactor which is co-axial with the agitator shaft, the product gases were directed into a special mechanical filter containing a sintered stainless steel cartridge. This filter served to trap any catalyst fines which may be created by attrition and swept up into the gas stream. This practice protects the delicate and sensitive sampling and analysis equipment located further downstream. The filtered gas was then cooled by forcing it through a single-pass shell-and-tube heat exchanger using tap water as the cooling medium.

A metering valve placed at the exit of the heat-exchanger helped maintain the desired pressure in the reactor. At this

point a six-port sampling valve permitted injection of a fixed volume (0.25 cm^3) of product gas into the gas chromatograph for analysis. The effluent gas composition was also monitored continuously by a variable filter infra-red analyzer with a flow-through cell and acetylene, ethylene and ethane were detected at 3.05, 5.25, and 6.55 (all μm), respectively.

From the flow-through cell the product gas passed through another Lab Crest rotameter into a three way ball-valve which directed the flow into either one of two surge tanks. These surge tanks were used to damp oscillating effluent concentrations during periodic operation to obtain a time-invariant process effluent which was subsequently injected into the gas chromatograph.

The entire apparatus was put together with the help of stainless steel 6.35 mm outside diameter tubing. The only exceptions to this practice were the use of brass Swagelok fittings and 6.35 mm outside diameter, refrigeration type copper tubing for the cooling water and the compressed air streams. Further, a small portion of the tubing leading to the flow-through cell of the infra-red analyzer was replaced by 6.35 mm outside diameter transparent Tygon tubing. This change was dictated by experience from earlier experiments which revealed that the appearance of a yellowish-brown liquid in this line was a sure indication of extensive fouling in the reactor.

Additional details on each major subsystem are provided in the following sections.

3.2 Reactants and Inert Gas Feed System

The gases used in the experiments were Linde Lab 145 Atomic absorption grade acetylene (>99.6%), Prepurified grade hydrogen (>99.99%) and Prepurified grade nitrogen (>99.997%). The gases were fed from high pressure cylinders, each fitted with two-stage pressure regulators (Linde Model TS-A-200 for H_2 and N_2 and Linde Model SG-9048 for C_2H_2) to provide a constant output with a minimum of pressure fluctuation. A septum arrangement was provided on each line to permit samples to be taken with a hypodermic syringe for gas analysis.

For reasons stated above, the acetylene stream was passed through a Linde model MS-1920 inline gas purifier column filled with Fisher #5-685A adsorbing activated charcoal. From the outlet of the two-stage regulator a portion of the nitrogen was sent to a Moore Nullmatic Model 41N15 inline pressure regulator and then to nitrogen purge section in the seal housing of the reactor. The line carrying the purge stream was standard 3.175 mm outside diameter stainless steel tubing. The main nitrogen feed stream was further regulated with a Linde Model SS-C5 Low pressure line regulator. The gas flow rates for the three feed streams were monitored by Lab Crest Low Flow rotameters (Fischer and Porter #10A1460) with interchangeable tubes and floats.

In order to generate the square-wave type oscillations in the manipulated input variable $u(t)$ (explained in Chapter 4) the hydrogen and nitrogen streams were split into two parts.

Figure 3.3 explains the detailed configuration of the five Whitey #SS-21RS4 metering valves in relation to the two three-way Skinner #V54DB2 solenoid valves used to generate the periodic oscillations. Just downstream of the metering and solenoid valves, a Whitey #SS-42XS4 three-way ball valve was installed in each feed stream before the gases were mixed. A similar ball valve was used after the mixing cross at the reactor feed/by-pass junction.

3.3 The Reactor

Most of the experiments in this study were done in a spinning basket reactor. The reactor was built entirely of type 303 and type 316 stainless steel and consists of four main parts: the reaction chamber and jacket, the bearing housing, the seal housing and the drive shaft and catalyst baskets. Each of these will be discussed below in considerable detail and wherever possible illustrated with the help of diagrams.

The reaction chamber and jacket were machined from type 316 stainless steel and consist of two coaxial cylinders. The reaction chamber was mounted on a cylindrical support which in turn rested on the bottom plate of the jacket. A single highly-machined flat plate (figure 3.4) served as the top seal for both the reactor and jacket and was fixed to the frame support. This meant that for catalyst loading and reactor cleaning operations, the reactor-cum-jacket had to be raised and lowered using a jack-type apparatus positioner. In order to promote good mixing of the gases, four vertical baffles were provided

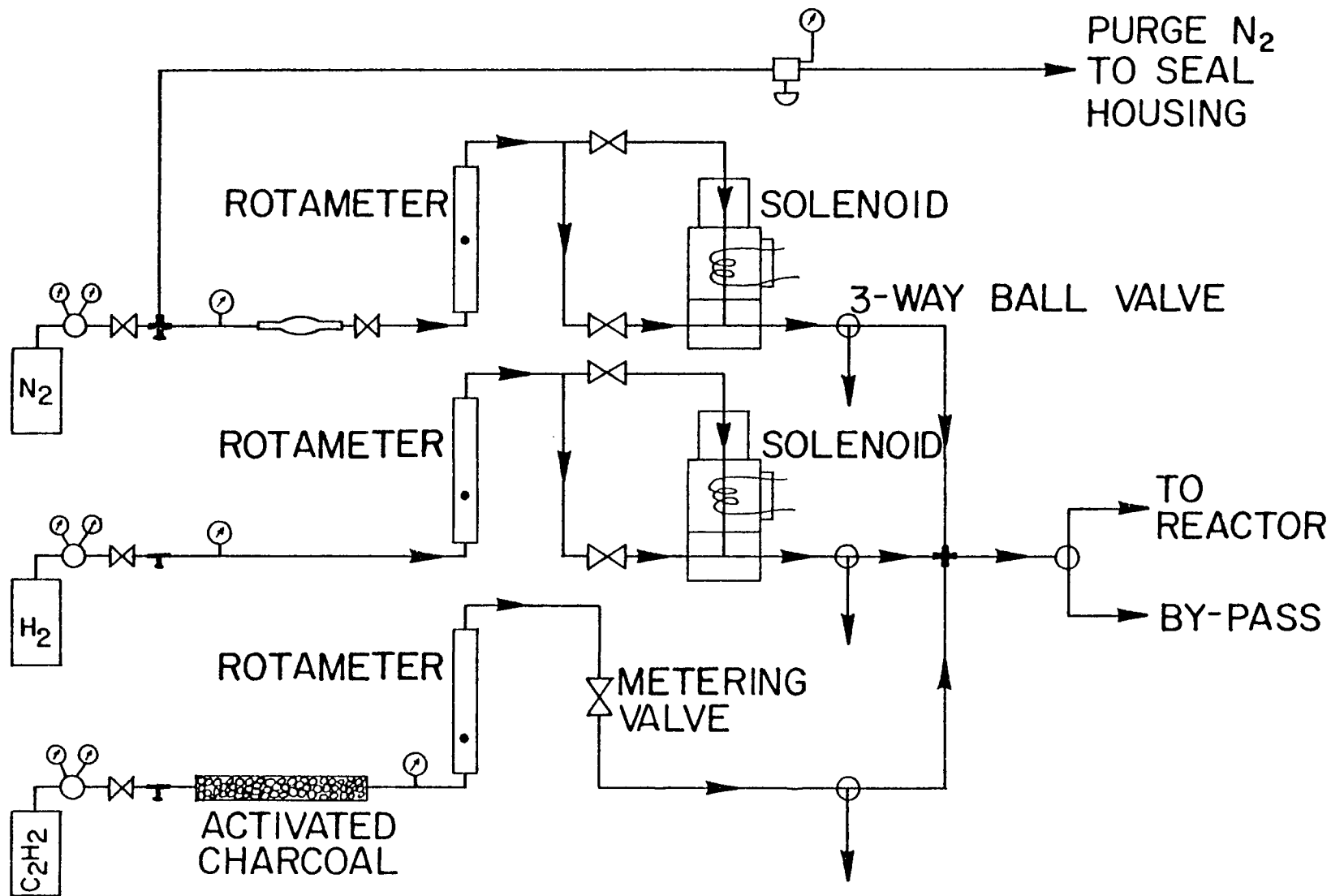


Figure 3.3 Detailed schematic diagram of the feed gas supply and metering system

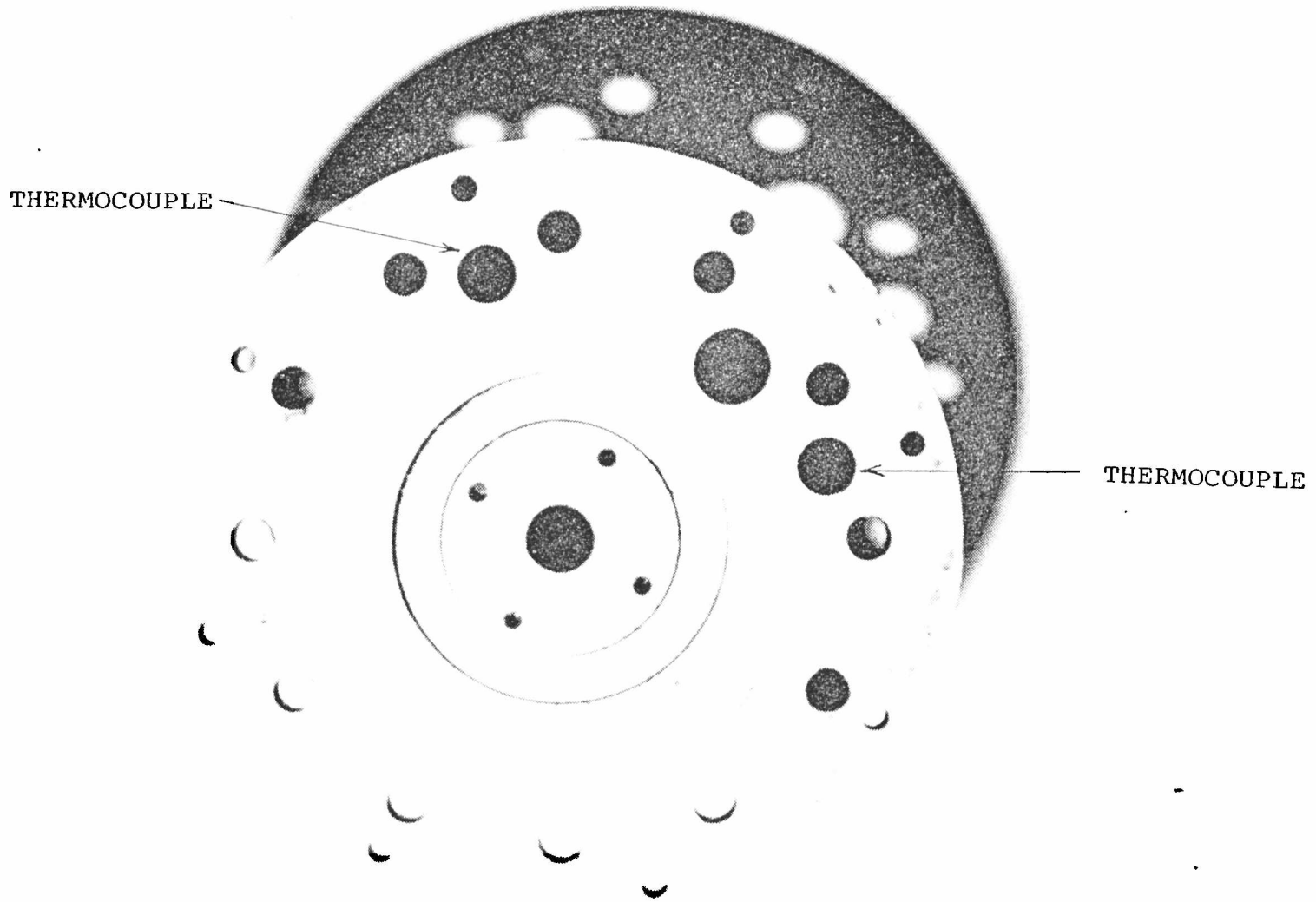


Figure 3.4 Top seal plate for reactor-cum-jacket showing radial positions of the thermocouples

in the reaction chamber, and the feed gases were introduced from the bottom, along the axis. These are shown in figure 3.5. The relative dimensions and positions of the different parts are shown in figure 3.6.

The bearing housing, as the name suggests, contains the ball bearings and their packing seats. Figure 3.7 is a view of the bearing housing and the drive shaft. This unit was built with type 303 stainless steel and its main function is to support the drive shaft and hold it in place. The entire bearing housing rests on top of the seal housing, as shown in figure 3.8. It is very critical that the packing seats for the bearings be positioned just right without excessive tightening of the screws that bind the seats to the housing. Owing to the fact that clearances between the catalyst baskets and the baffles are small and that the drive shaft is long and turns at the rate of 104.7 radians per second, the above warning cannot be over-emphasized.

The seal housing and its major components are shown in figure 3.8. It consists of the seal housing flush gland, the stationary unit, the rotary unit and the sleeve bearing. The sleeve bearing was made out of graphite whereas the flush gland and stationary unit were machined from type 303 stainless steel. The rotary unit (Crane Mechanical Type 79) was mounted at a predetermined position on the shaft and its mating surface on the stationary seat was plated with silicon carbide. This rotary unit is shown mounted on the drive shaft in figure 3.7.

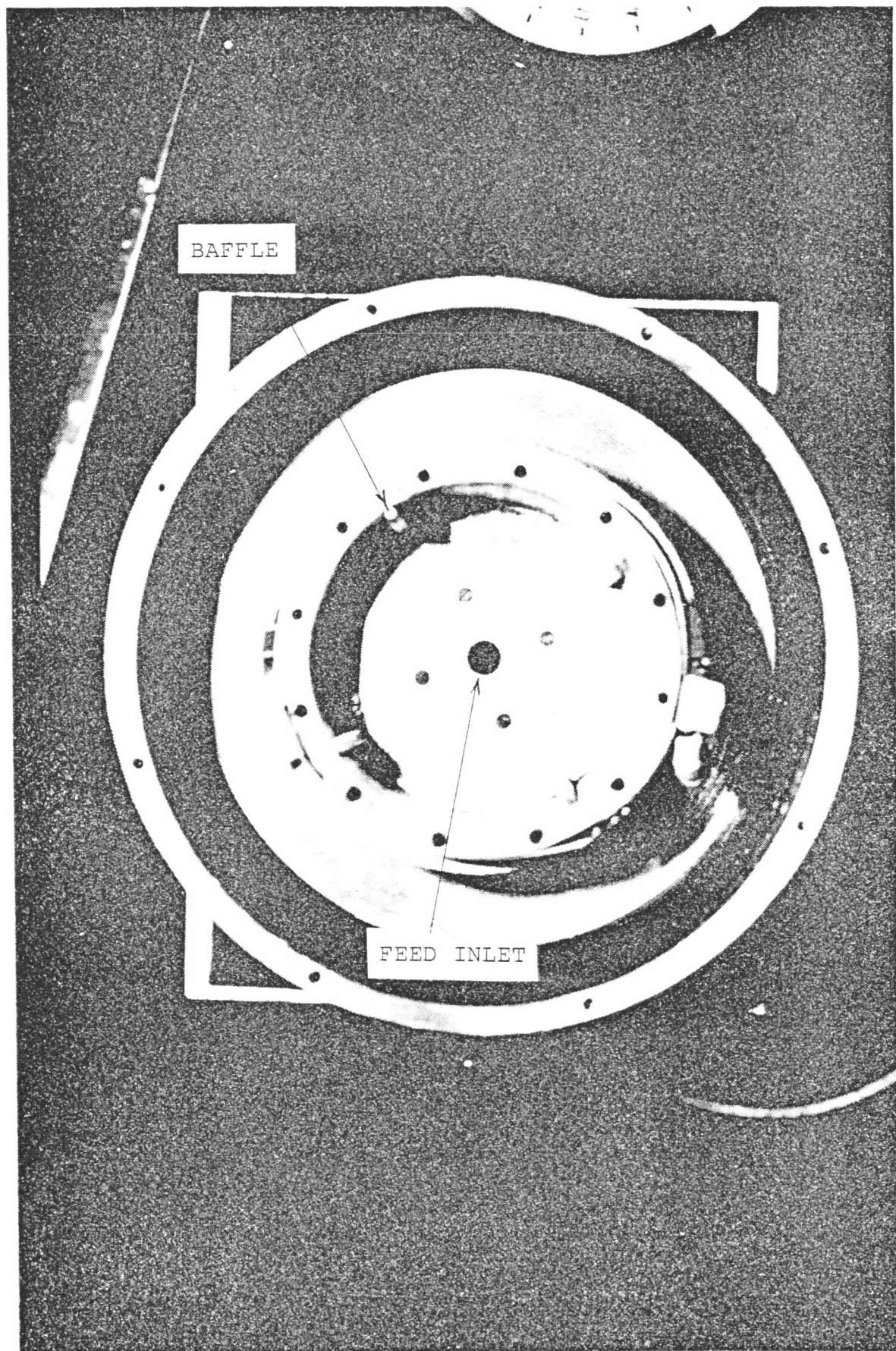


Figure 3.5 Top view of reactor showing baffles and feed gas inlet.

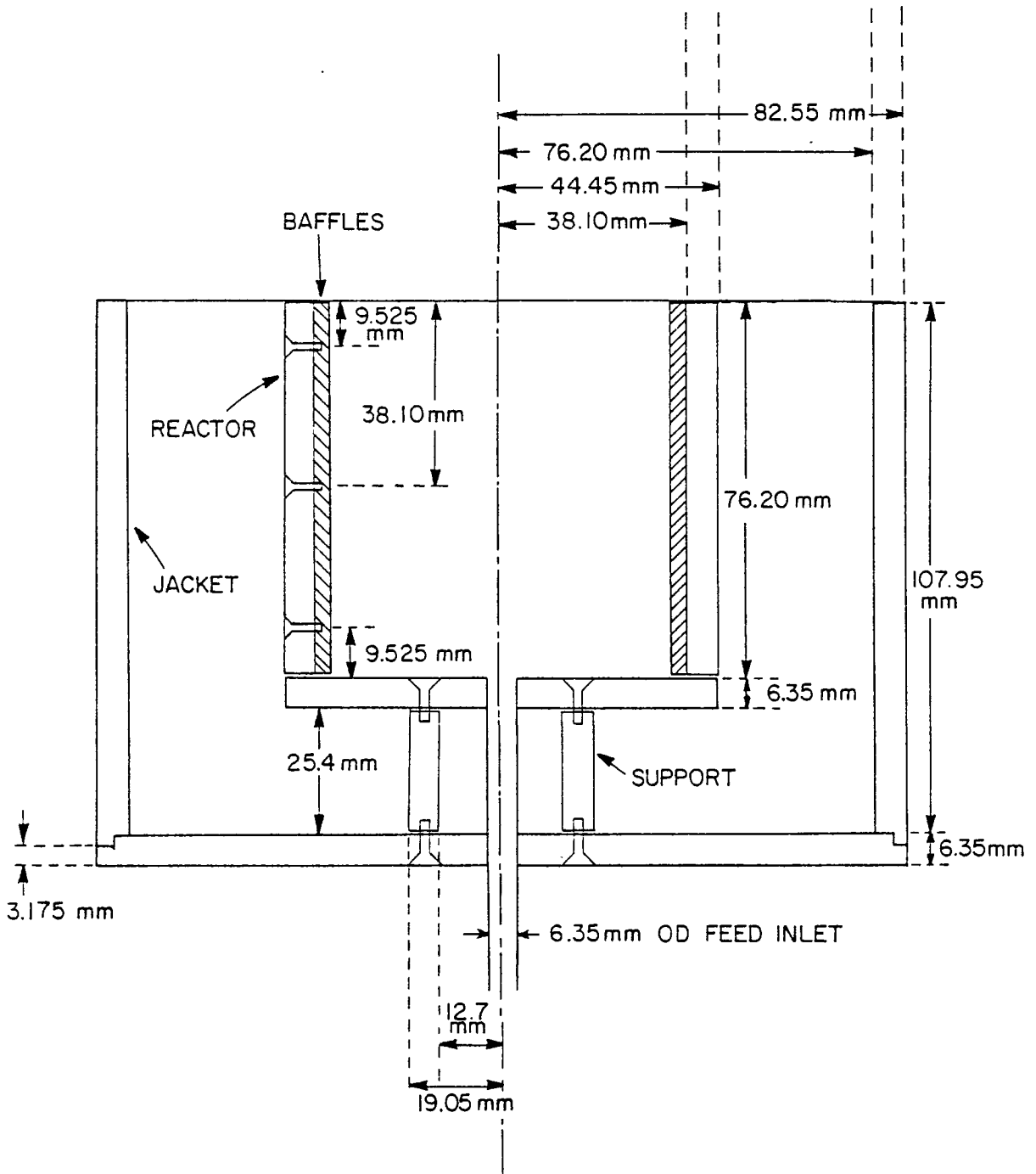


Figure 3.6 Elevation section of the reaction chamber and jacket assembly

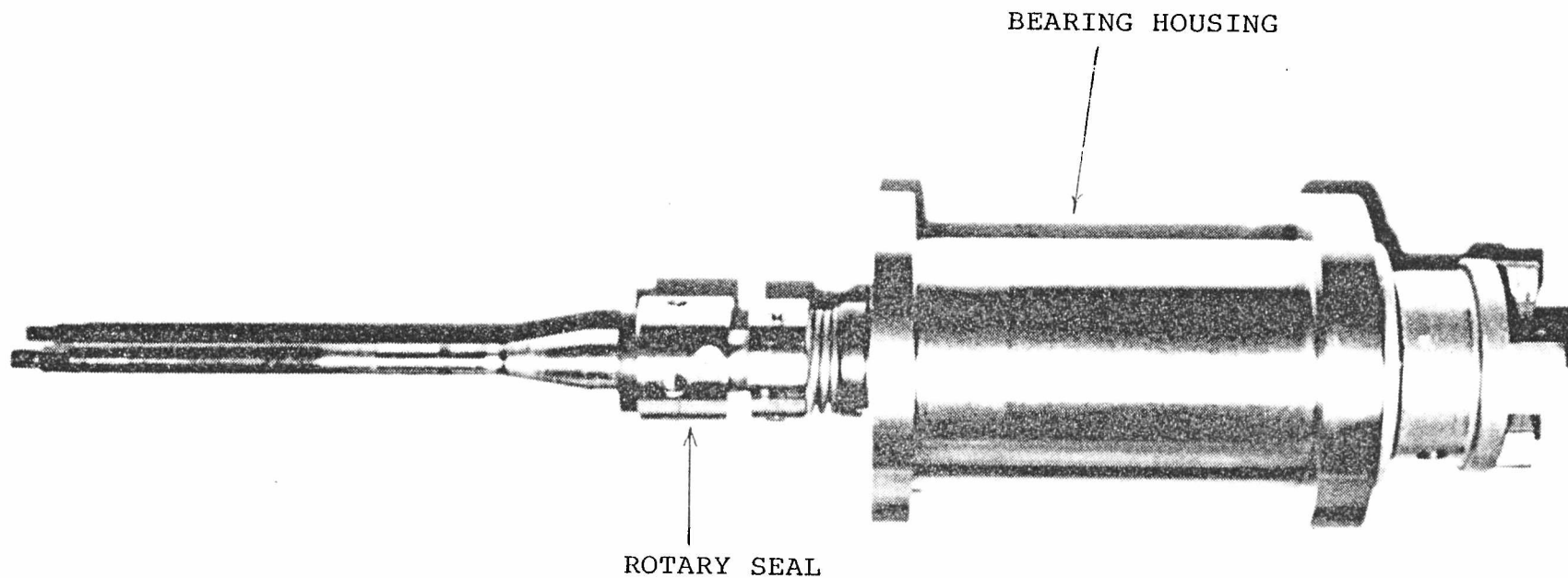


Figure 3.7 View of the bearing housing and drive shaft showing rotary seal unit

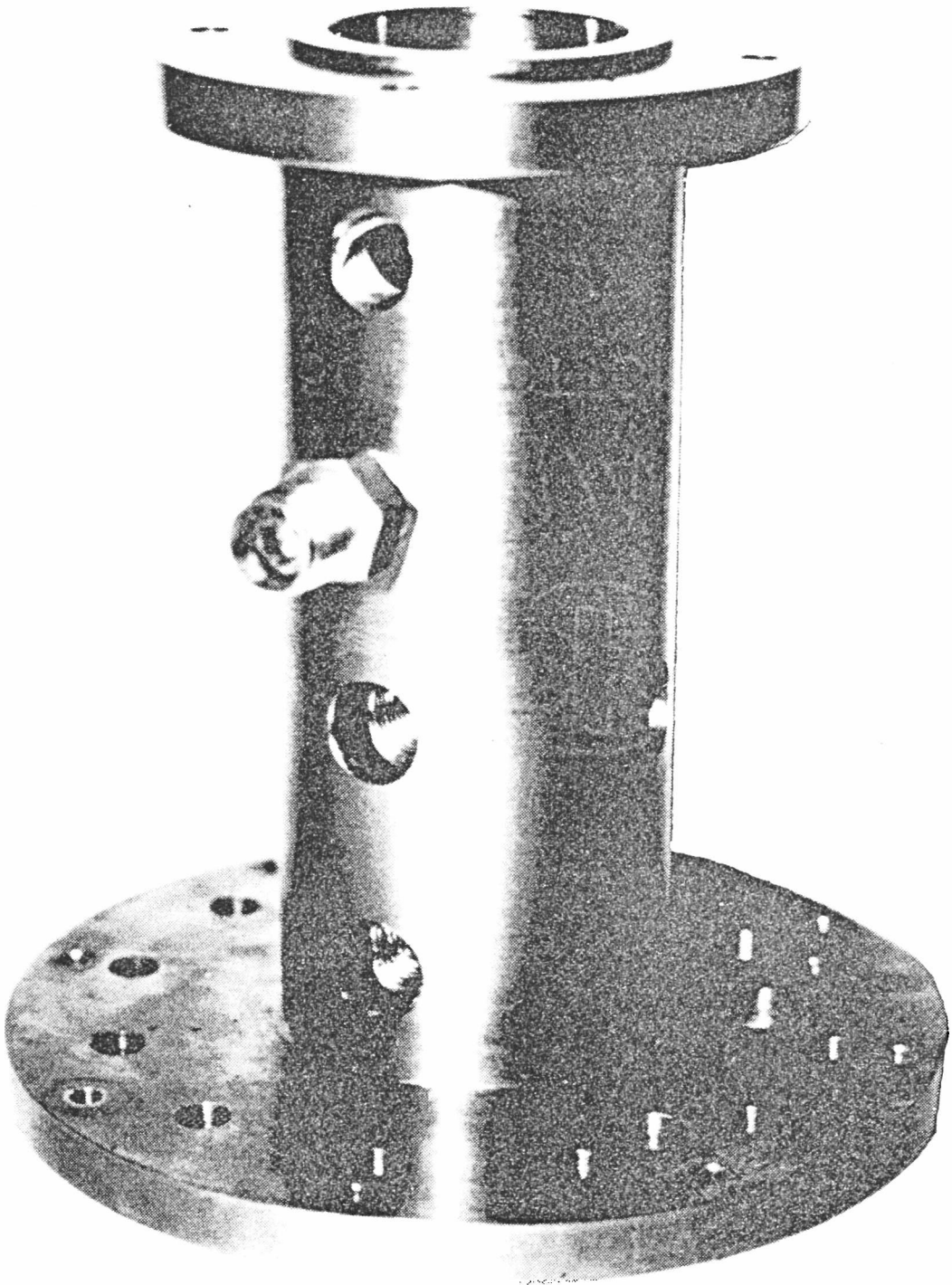


Figure 3.8a View of the seal housing flush gland

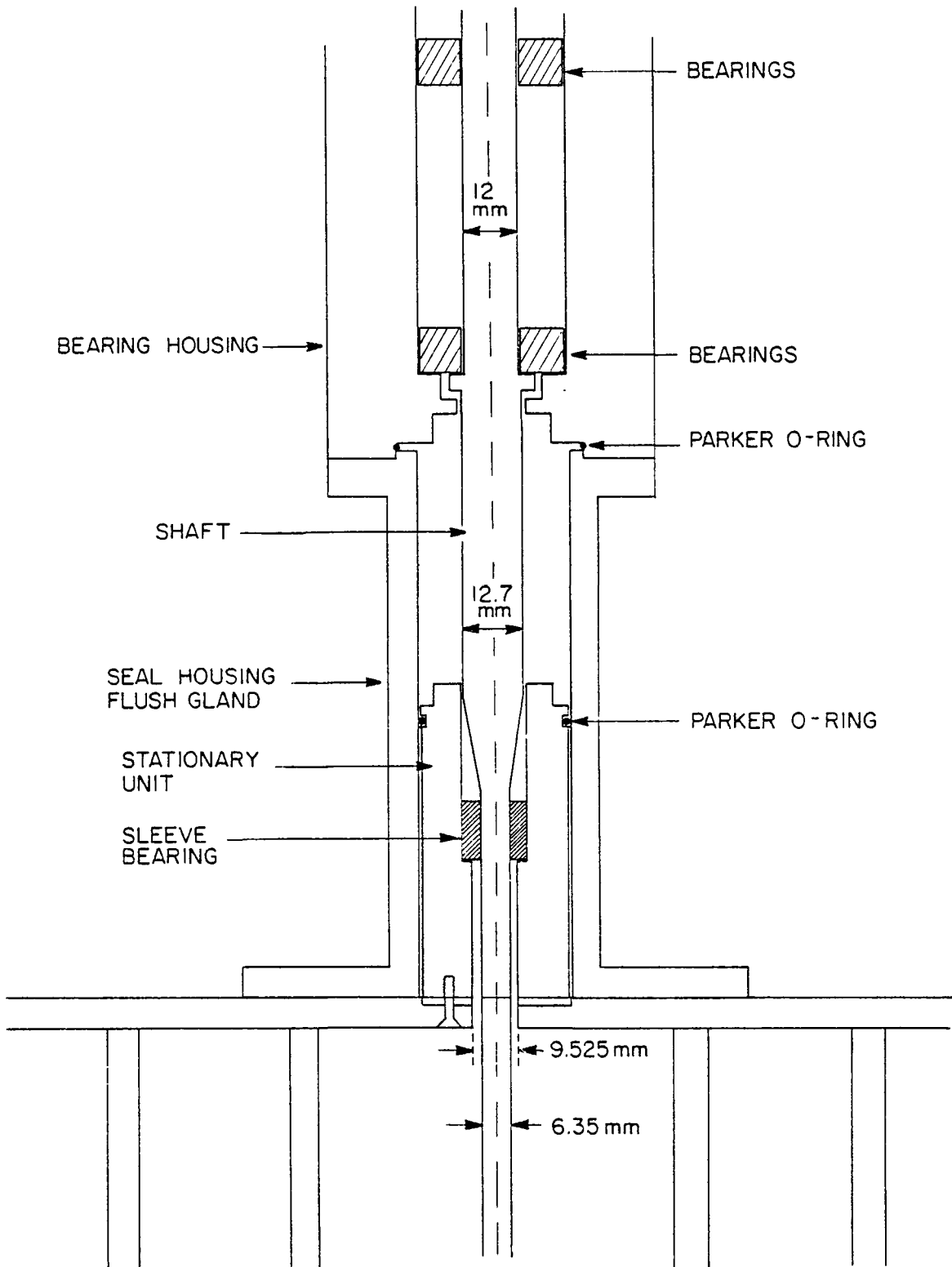


Figure 3.8b Elevation section showing seal housing, bearing housing and internals.

Figure 3.9 is a self-explanatory schematic diagram which illustrates the function of this assembly.

The above parts were common to both the spinning basket and stationary basket operations. The entire drive shaft was made of type 316 stainless steel and coated with a 0.1016mm thick chrome plating. The bottom portion of the shaft had a square section and a threaded portion. The support bracket for the catalyst baskets was mounted on the square section and secured with the help of a hexagonal nut. Figure 3.10 is a view of one of the dismantled spinning baskets showing the metal screens and panel frames. Four such catalyst baskets were mounted at right-angles to each other on the support bracket.

One set of experiments was done, in which the reaction chamber internals were modified to accommodate a stationary basket so that a thermocouple could be inserted into the catalyst bed.

The stationary basket was annular in shape like an automobile air filter. Four stainless steel panels were attached to the support bracket and these served as agitator blades. These are shown in figure 3.11. It should be noted that the stationary basket design was a later modification and was built constrained by the structure of the existing reactor assembly.

3.4 The Heating and Temperature Control System

The spinning basket reactor was operated at 439°K under nearly isothermal conditions. The temperature in this reactor

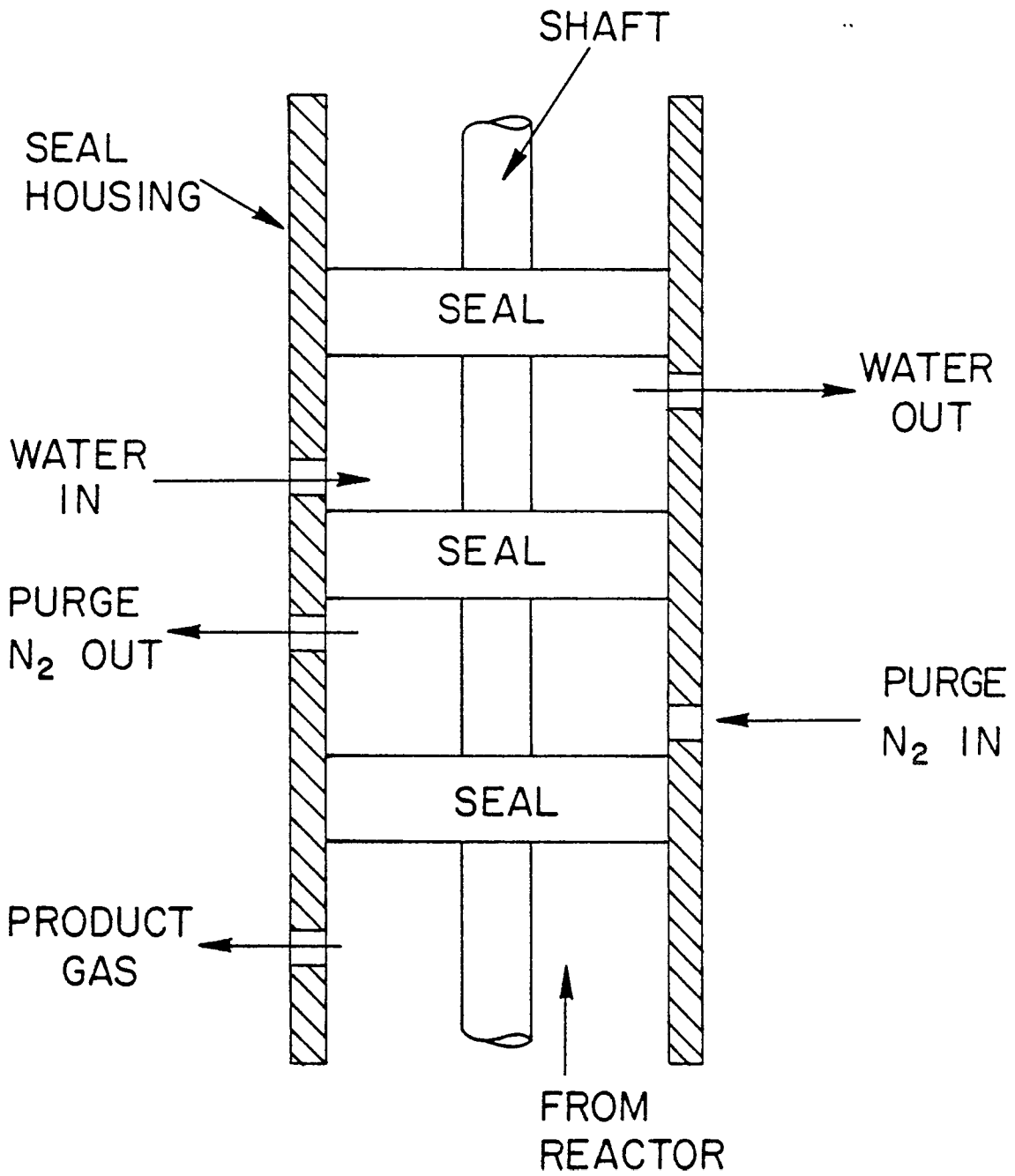


Figure 3.9 Schematic diagram of seal housing showing its function

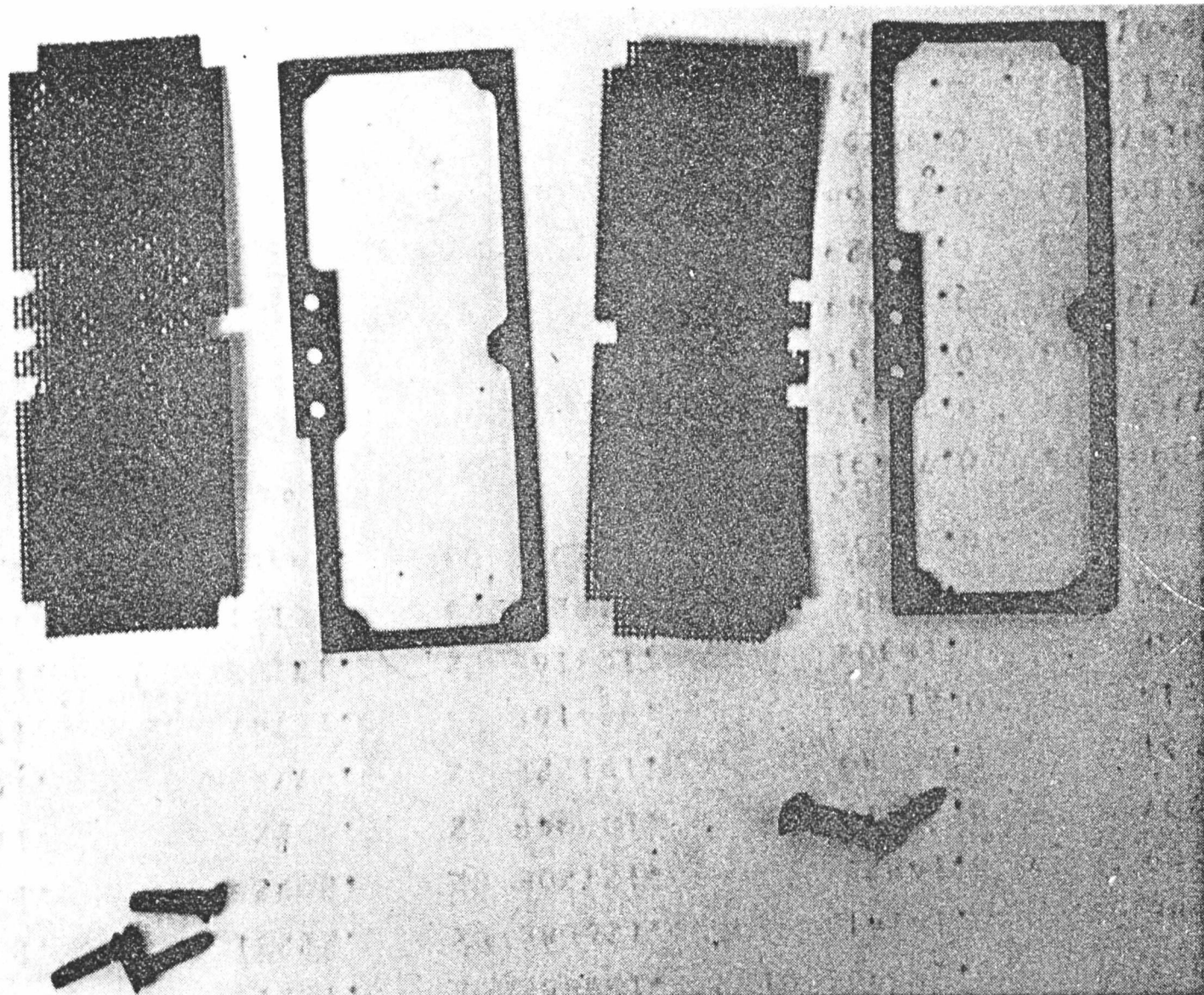
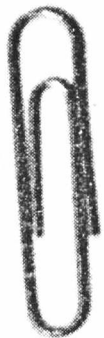
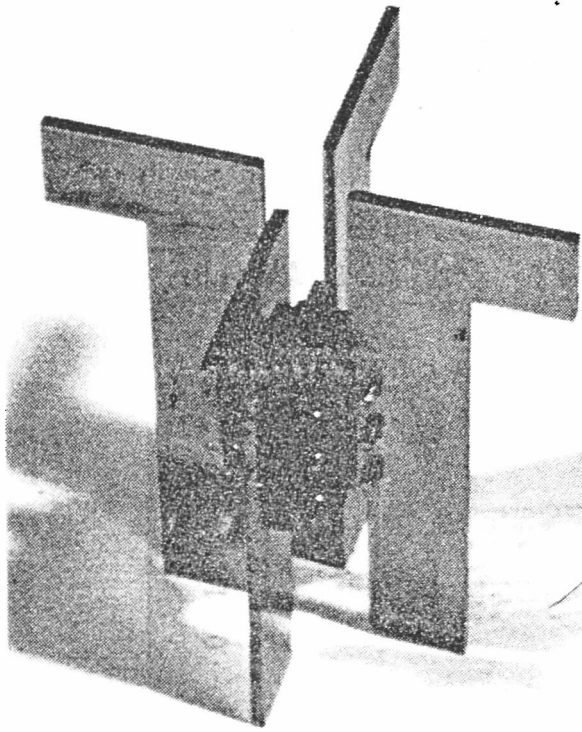
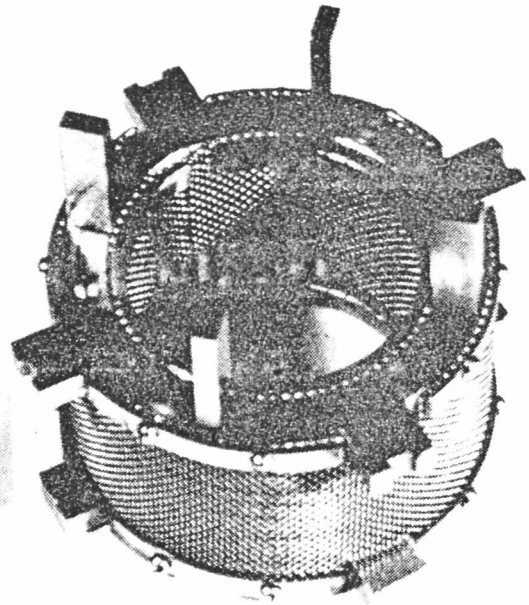


Figure 3.10 Dismantled view of one of the spinning baskets showing the wire mesh screens and support panels



AGITATOR ASSEMBLY



OVERTURNED BASKET

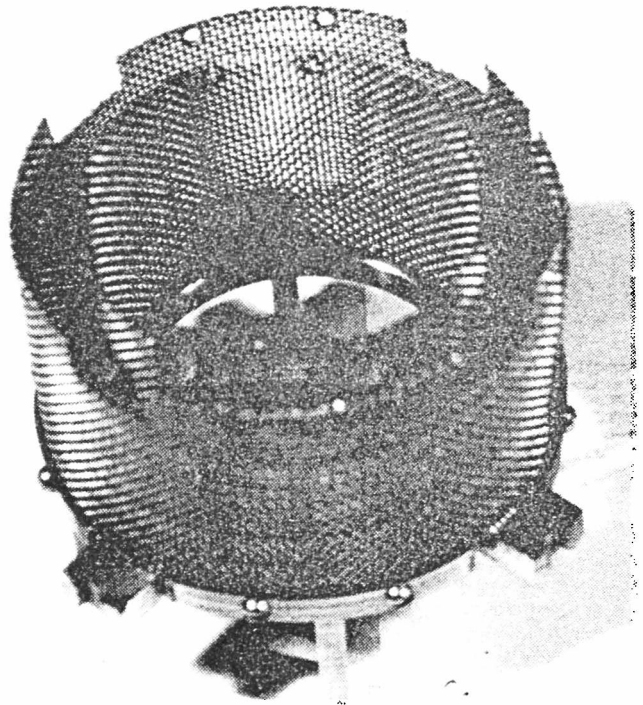


Figure 3.11 Views of the stationary basket and the agitator assembly

was measured by two exposed junction Type J (iron-constantan) thermocouples (Instrumatics #11C1J) protected by a stainless-steel sheath. The radial positions of these thermocouples in the spinning basket reactor are shown in figure 3.4. One of the thermocouples was hooked up to the temperature controller whereas the other was connected to the digital temperature indicator (Omega Model 175 JC1-05). Although the exposed junctions of these thermocouples were located at different depths, owing to the excellent mixing in the reactor, either of them could have been used as the sensor element for the controller with no noticeable difference in the isothermality of the operation. In the stationary basket reactor, however, a grounded junction Type J thermocouple was installed through the bottom of the reactor into the catalyst basket to measure the catalyst temperature, and this thermocouple was connected to the digital temperature indicator. Thus, in both reactors the well-mixed-gas-phase temperature was the controlled variable.

The heater was made up of a 1000 watt nichrome heating coil enclosed in ceramic beads and wrapped around the reactor as shown in figure 3.12. The temperature controller (Love Controls Model 49) maintained the gas phase temperature at the desired level to within $\pm 0.5^{\circ}\text{C}$ during steady-state operations and to within $\pm 1.5^{\circ}\text{C}$ during rapid cyclic operations ($\tau=30$ seconds). This controller has an automatic rate action which varies the proportioning cycle time in accordance with the demands of the process.

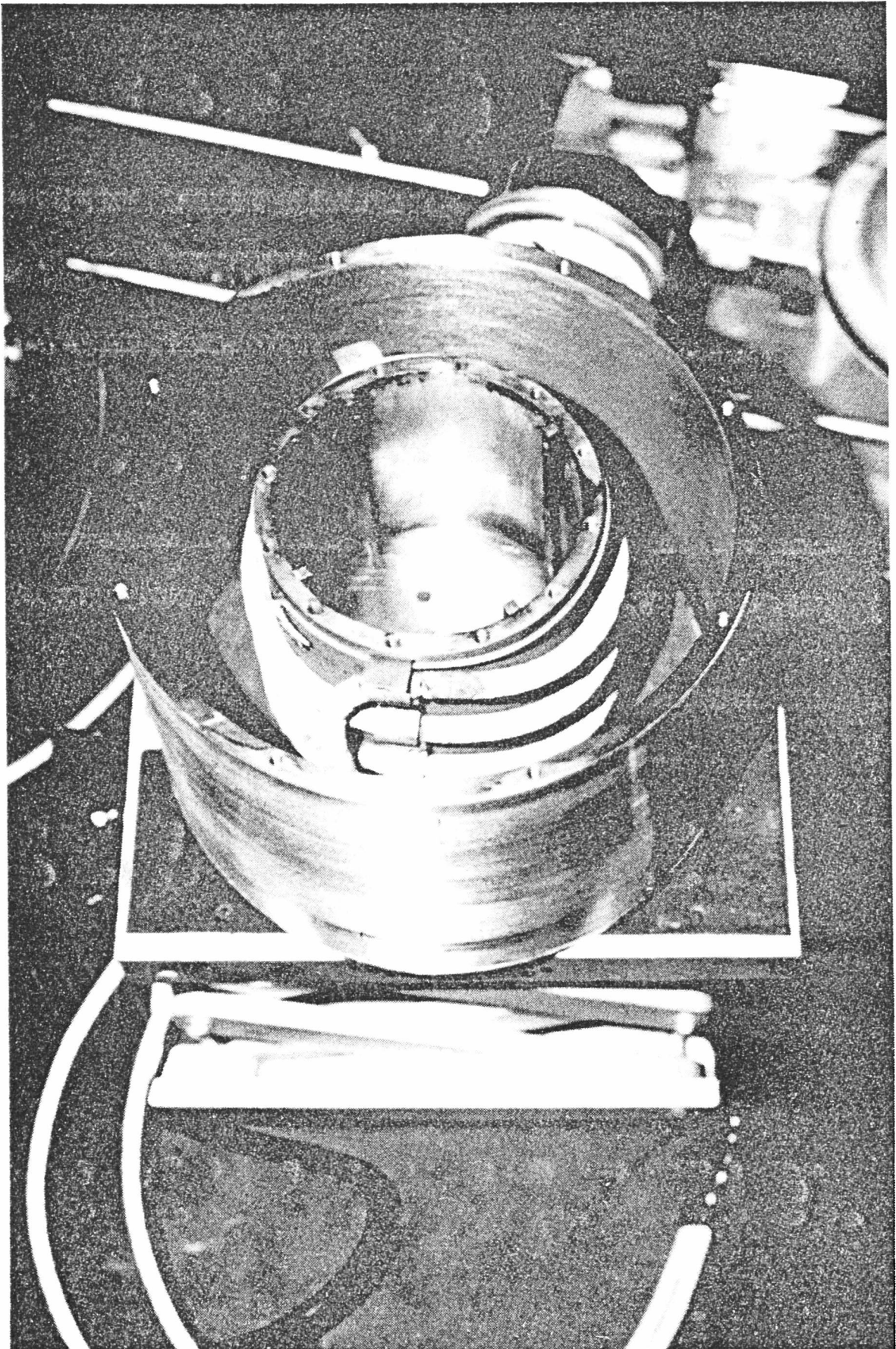


Figure 3.12 Another view of the reactor-cum-jacket assembly showing heater coils wrapped around the reaction chamber

In order to obtain a permanent record the output of both thermocouples was noted on a strip chart recorder (Houston Instrument Omniscribe Model A5113-5). The accuracy and sensitivity of this record was further enhanced by using a suppression network so that one division on the chart paper corresponded to 1°C. A schematic wiring diagram of the entire temperature controlling and recording system is shown in figure 3.13.

3.5 The Multichannel Timer

A picture of the assembly of switches, motors and relays which comprise the multichannel timer is shown in figure 3.14 whereas a schematic wiring diagram of the same is presented in figure 3.15.

Switch S1 turns on the power to the entire unit and drives the synchronous type stepping motor M2 which controls the step initiate switch S3. K1, K1A and K1B are continuous duty relays. M1 is another stepping drive motor which receives power through S3 and K1A or through the snap action step index switch S2.

The sequence of operations that take place during a single step is described below. When the power is turned on via switch S1 the relay K1 is pulled in. When switch S3 is actuated by the motor M2, motor M1 receives power through S3 and K1A and starts to drive. Switch S2 transfers and relay K1 drops out. This assures a single step regardless of how long S3 is actuated beyond a minimum of 150 milliseconds. Motor M1 now receives power through switch S2 and returns S2 to the rest position. Thus, motor M1 stops and the step is complete.

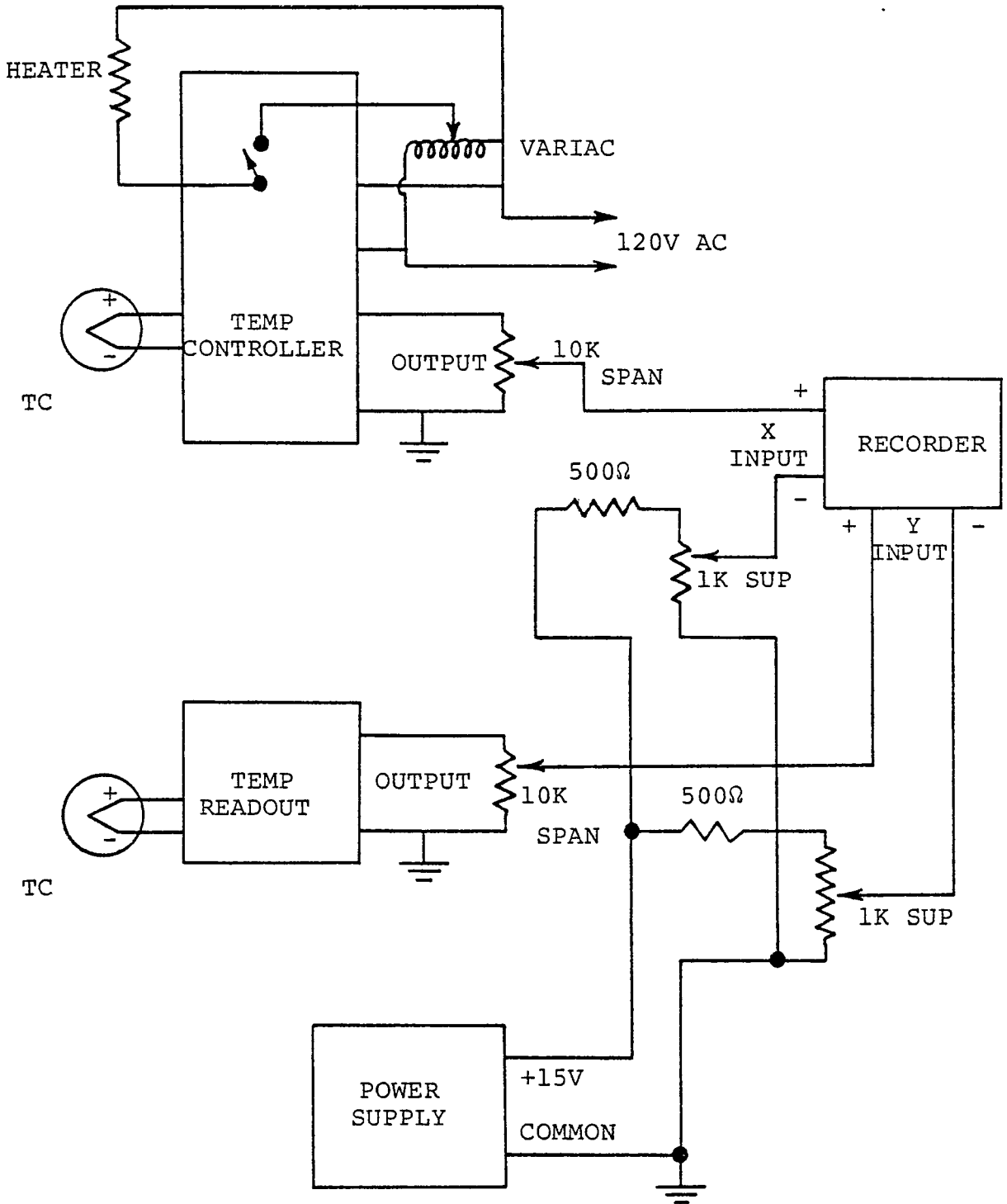


Figure 3.13 Schematic wiring diagram of the temperature controlling and recording system

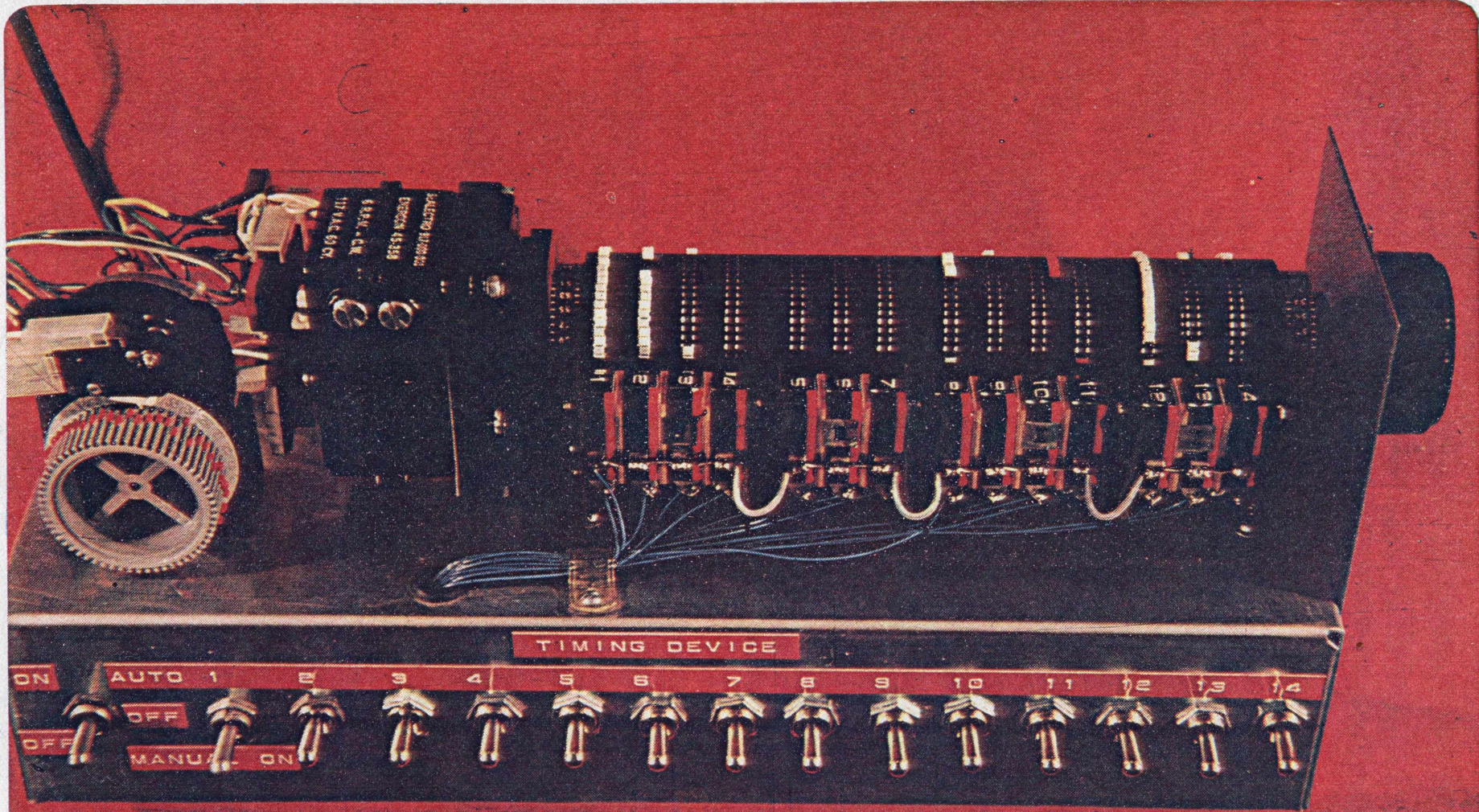


Figure 3.14 View of the assembly of switches, motors and relays constituting the multichannel timer.

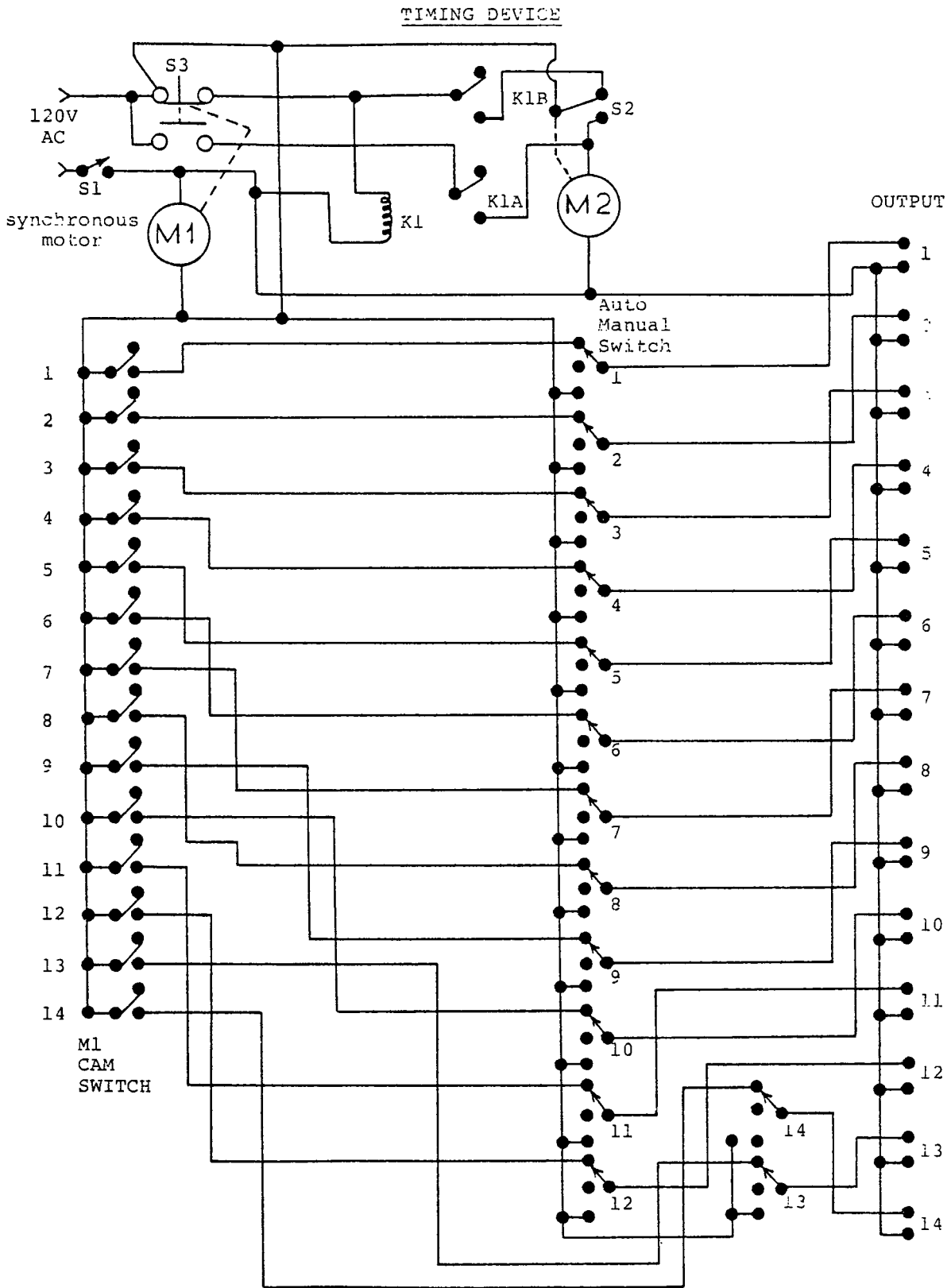


Figure 3.15 Schematic wiring diagram of the timing device

When S3 is released, K1 is pulled in. To continue the stepping action, switch S3 has to be successively actuated and released and the manner in which this is done defines the period of oscillation, τ . (See appendix for a more detailed explanation).

3.6 Product Gas Sampling and Analysis

The system was so designed that during periodic and transient operation the resulting concentration trajectories could be detected by two independent techniques - gas chromatography and infra-red spectrometry.

The Wilkes Miran I variable-filter infra-red analyzer is a single beam instrument equipped with a gold plated flow-through cell with NaCl windows which permit continuous effluent hydrocarbon monitoring with a response time of 1, 4, 10 or 40 seconds. The spectrograms for acetylene, ethylene and ethane are shown in figures 3.16, 3.17 and 3.18 respectively. A permanent record of the concentration trajectories was obtained on a strip-chart recorder (Houston Instruments Omniscrite).

Owing to the time required for elution of the sample, the sampling frequency of the gas chromatographic technique was limited to one every two minutes. However, owing to stable oscillations produced by the well designed reactor, as many as fifteen discrete measurements were made for each period. Injection of the sample was done by a six-port stainless-steel sampling valve (Carle Minivolume #5518) equipped with a 250 microlitre sample loop. Standard 1.5875 mm outside diameter

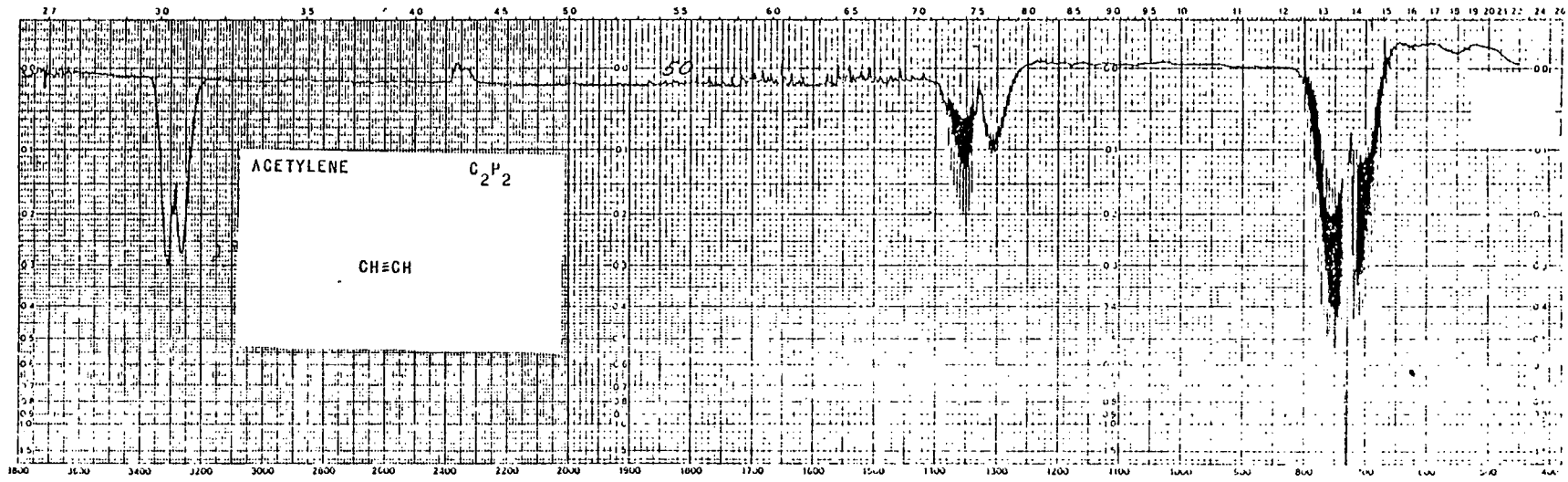


Figure 3.16 Infra-Red Spectrogram for acetylene
(Courtesy of Wilks Scientific)

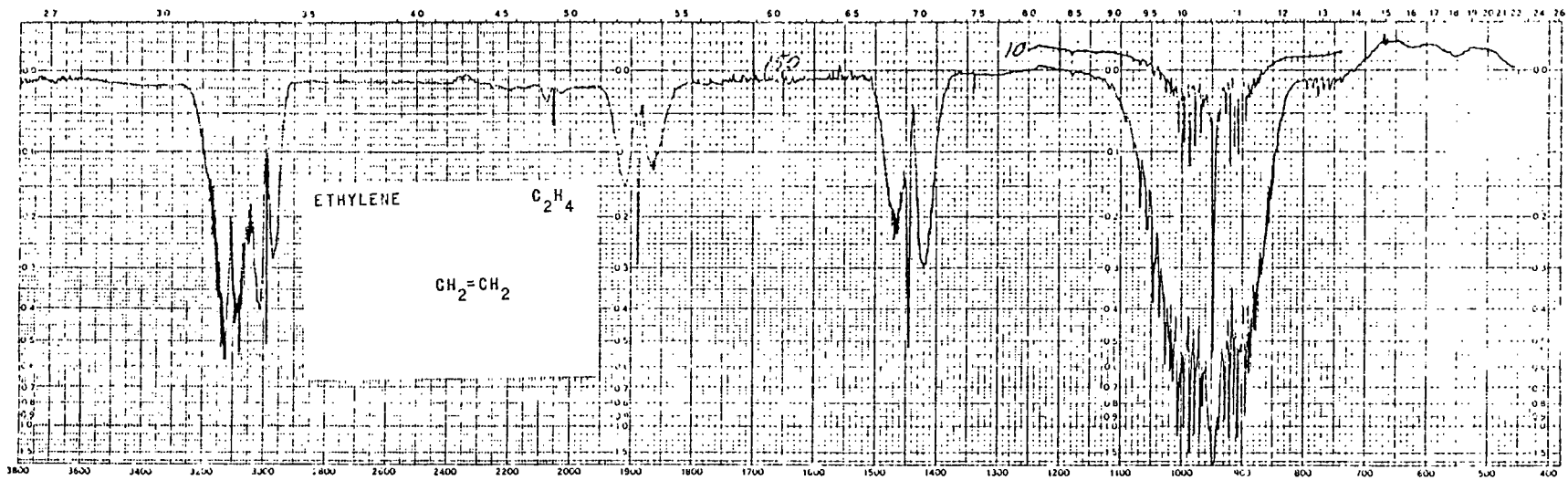


Figure 3.17 Infra-Red Spectrogram for ethylene
(Courtesy of Wilks Scientific)

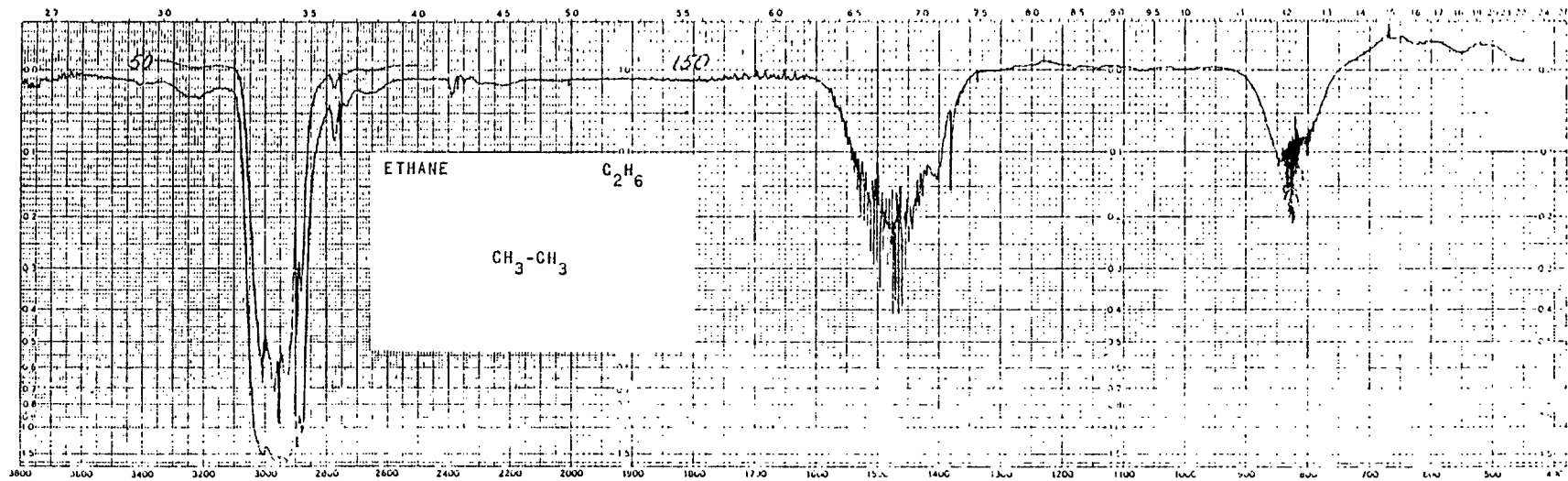


Figure 3.18 Infra-Red Spectrogram for ethane
(Courtesy of Wilks Scientific)

stainless-steel tubing was used to connect the sampling valves in series with the flame-ionization type gas chromatograph (Antek Model 464). The components of the gas sample were separated using a Porapak N column and nitrogen carrier at 313°K. The flame ionization detector operates on the principle that a few hydrocarbon molecules, when introduced into a hydrogen-air flame, produce a large amount of ionization, which is directly proportional to the number of carbon atoms present. All classes of hydrocarbons are detected with equal response as long as they do not contain nitrogen or oxygen atoms in their structure. The resulting peaks from the chromatograph were recorded on a strip-chart (Houston Instruments Omniscribe) and integrated automatically using a digital integrator (Columbia Scientific Model CSI-38).

CHAPTER 4

EXPERIMENTAL PROCEDURES & LIMITATIONS

4.1 System Leak Test

After loading the spinning baskets with the catalyst, the reactor was sealed and inert nitrogen was forced into the system to flush out the trapped air. The effluent line was then shut till the nitrogen pressure in the system reached 5 psig and then the system was sealed. The appropriate Swagelok fittings were then tightened to eliminate any major leaks which were revealed by a hissing sound and by a drop in system pressure. The system was then recharged with nitrogen at 5 psig pressure, sealed and allowed to stand for two hours. During this time any joints suspected of slow leakage were painted with soap water and monitored for any tell-tale bubble formation.

In a similar fashion, the hydrogen and acetylene feed lines were purged of any trapped air and tested for leaks. However, during these flushing and leak-test procedures the acetylene and hydrogen streams were made to by-pass the reactor. Apart from eliminating unstable and inaccurate flow rates, this test is necessitated by safety considerations. Although acetylene is a simple asphyxiant and anaesthetic, experiments have shown that it may be breathed in concentrations as high as 100 mg per litre for up to an hour without chronic harmful effects (Matheson, 1972). However, both hydrogen and acetylene are extremely flammable, so it is imperative that these tests are done before proceeding with further experimentation.

4.2 Catalyst Pretreatment

The nickel catalysts used in the experiments were commercial samples obtained from local manufacturers in the form of reduced and stabilized cylindrical pellets. These pellets were crushed with a mortar and pestle and particles sizes between 0.84 mm and 1.2 mm were separated using standard Tyler wire mesh sieves. As recommended by Komiyama and Inoue (1968), the sieved catalyst particles were prepoisoned by soaking them in a 5% (wt.) solution of sodium thiosulphate ($\text{Na}_2\text{S}_2\text{O}_3$) for 24 hours to reduce their activity. The catalyst particles were then rinsed with deionized water, spread out in a thin layer on aluminum foil and dried in an oven for 24 hours at 343° K.

After the catalyst had been loaded into the reactor and the test described in the previous section had been carried out, the motor was turned on and the catalyst was heated in a nitrogen stream up to 477° K. The nitrogen was then cut off and the heating was continued in a hydrogen stream for 4 hours. The soaking in the thiosulphate solution results in a deposition of sulphur atoms on the catalyst. Any loosely bound sulphur might be removed as H_2S by this initial hydrogen treatment. It should be noted here that the latter part of this procedure was introduced as a precautionary measure after a set of preliminary experiments in which severe catalyst fouling was observed. In an attempt to find possible causes for catalyst poisoning and fouling, a literature search revealed that in the

presence of alumina, at about 675° K, acetylene reacts with H₂S to form thiophene and other by-products (Matheson, 1972). Owing to knowledge of this reaction, the hydrogen treatment was used as standard pretreatment for all subsequent catalysts.

4.3 System Start-up and Shut-down

Unlike the procedures in the last two sections, which were performed once for each set of experiments, the following routine was used in each and every experiment. Before each experiment, the flow of nitrogen carrier to the gas chromatograph was started. Then, the power to the electrometer, the heaters for the injector and detector and column oven switched on, and the instrument was left to stabilize overnight. At the start of each experiment, the electronics were allowed to warm up for about 15 minutes. The water supply to the reactor and the compressed air to the jacket were turned on, and the motor was started. Nitrogen gas was then allowed to flow through the system for half an hour, and, in the meantime, the temperature measuring system and the infra-red analyzer were calibrated as follows. The thermocouple was disconnected from the temperature controller and a standard millivolt source (Chem. Elec. Model S1) was hooked up in its place. After dialing in a voltage corresponding to 300° F, the recorder pen was set at the zero-end of the strip chart by adjusting the zero potentiometer of the suppressor circuit. Then, a new voltage corresponding to 400° F was dialed in and the recorder pen was set at the 100 division mark on the chart paper by adjusting the span potentiometer of the suppression network. These two steps were repeated

several times with simultaneous fine tuning of the corresponding potentiometers until no more adjustment was necessary. A similar procedure was followed for the second thermocouple which was connected to the digital temperature indicator. The thermocouples were re-connected to the respective devices after this procedure.

The infra-red analyzer was then zeroed at each detection wavelength after the slit had been adjusted to 1 mm. using the procedure described in the instrument manual.

After dialing in a set point corresponding to 477° K on the temperature controller, the heater in the reactor was switched on. When the gas phase temperature in the reactor was stable at 477° K the nitrogen was gradually replaced by a hydrogen stream. This "in situ activation" was continued for a period of 6 hours after which the temperature in the reactor was lowered to 439° K. The reaction was then carried out at this temperature, and measurements were made according to one of the procedures described in sections 4.4a, 4.4b, and 4.4c. While the catalyst was being treated with hydrogen, the gas chromatograph was zeroed as described in the instrument manual.

When all the measurements were complete and the data had been recorded, the instruments and the equipment were shut down in the logical sequence stated below. The digital integrator and the infra-red analyzer along with their corresponding strip chart recorders were switched off. Then the acetylene feed to the reactor was stopped, and, after about ten minutes, the

hydrogen feed was also cut off and the heater in the reactor was powered down. Next, the hydrogen and air streams to the gas chromatograph were stopped, and the power to the electrometer and the various heaters in the instrument was switched off. The fan in the column oven was left on, however, and the nitrogen carrier continued to flow through the column till it cooled to room temperature.

In a similar manner the catalyst in the reactor was cooled gradually in a nitrogen stream to room temperature and at this stage all of the remaining instruments and feed streams including the motor, water, and the air were shut off. The above procedure insured a smooth shut-down so that all the instruments were protected from shock and the laboratory was safe.

4.4 Run Procedures

a. Steady State

The reaction was conducted at a temperature of 439° K and a pressure of 108.2 kN/m². The upstream pressure in all the feed lines was maintained at 5 psig and the individual gas flow-rates were set at predetermined values on the rotameter scales with the help of the metering valves. The acetylene flow rate was kept constant at 30 cm³/minute. Since no power was supplied to the solenoid valves during these experiments, hydrogen and nitrogen were metered through the normally open channels, keeping the total gas feed rate to the reactor constant at 300 cm³/minute. The ethylene composition in the exit stream was monitored constantly with the infra-red analyzer. The time required

to reach a steady-state depended on the catalyst and varied from about 15 minutes to as much as two hours. Once the effluent composition for a given steady-state was recorded, the hydrogen and nitrogen flow-rates were reset to a new value. In this manner a whole series of steady states corresponding to different hydrogen/acetylene feed ratios were recorded.

b. Periodic

For a periodic experiment, the period or length of one cycle (τ), had to be set on the multichannel timer. This was done as follows. It was decided that one period would be 15 steps long, so that four periods could be programmed on the big drum, which had a total of 60 slots (each corresponding to one step). The actuator drum, which made one revolution every minute, also had 60 slots which could be programmed to trigger a fixed number of pulses each minute. For example, in order to set a period of 3 minutes, the actuator drum would have to be programmed to emit 5 equally spaced pulses each minute.

Another variable, γ , (defined as the fraction of τ for which the hydrogen flow rate is at the upper level) also had to be set on the big drum. Thus, by varying the number of consecutive steps (out of a total of 15) that the hydrogen solenoid was energised, γ could be changed in increments of $1/15$. It must be noted here that this was only one way of setting τ and γ . This device was built to be flexible enough so that by programming an appropriate combination of the 2 drums, an almost continuous spectrum of τ and γ could be achieved.

After the activation procedure was completed, the hydrogen solenoid was energised with the help of the manual switch on the appropriate channel of the timer. The normally closed inlet was now open, and the hydrogen flow rate through it was set at $1.625 \text{ cm}^3/\text{sec}$. The nitrogen flow rate was correspondingly set at $2.875 \text{ cm}^3/\text{sec}$ through the normally open inlet of the unenergised solenoid. Subsequently, the power to the hydrogen solenoid valve was cut off, and the nitrogen solenoid was energised. In this configuration the alternate inlets for nitrogen and hydrogen were open, and the corresponding flow rates were set at $4.25 \text{ cm}^3/\text{sec}$ and $0.25 \text{ cm}^3/\text{sec}$ respectively. As in the steady state experiments, the acetylene flow rate was set at $0.5 \text{ cm}^3/\text{sec}$.

Once all the settings were complete all the switches on the channels of the timer were flipped to the automatic position, and the reaction was conducted with forced cycling of the hydrogen feed concentration.

Usually after about 8 cycles a stable periodic condition was established and the individual concentration-time profiles were recorded from both infra-red and gas chromatography measurements. After the time invariant effluent concentrations from the surge tanks were recorded, a new γ was set on the timer drum. In this manner, a whole series of time-average compositions and instantaneous concentration profiles were recorded for a fixed value of the period τ .

c. Step Response

In this type of experiment, the hydrogen and nitrogen flow rates were set as described above in the procedure for a periodic experiment, with the aid of the manual switches on the multi-channel timer. However this time, after the settings were complete the channel switches were not flipped to the automatic positions. Instead the nitrogen solenoid was energised manually, the power to the hydrogen solenoid was switched off and the acetylene flow rate was set at the same value as before. When a steady-state had been reached and recorded under those conditions, the hydrogen solenoid was energised and at the same instant the nitrogen solenoid was de-energised. The ethylene concentration was monitored continuously with the infra-red analyzer, and gas chromatograph samples were taken every two minutes until a new steady state was attained. The clock was then restarted and the positions of the switches for the hydrogen and nitrogen channels were reversed simultaneously. Again the compositions were recorded with time until the first steady-state was established once more. In this way the response of a given catalyst to a step increase and a step decrease in hydrogen feed concentration was obtained. The reactor was then shut down according to standard procedure.

4.5 Limitations on the Operating Conditions and Equipment

The experimental system used in this study was designed to meet the objectives stated in section 2.1 and at the same time be flexible enough to be used for the study of other reactions.

Owing to the very diverse nature of these goals, situations sometimes arose when a compromise had to be made between conflicting factors. The values of the various parameters and the operating conditions utilized in the experiments are listed in Table 4.1. Restrictions in the form of upper or lower bounds had to be imposed on some important variables due to various reasons, and these are discussed below.

As stated in an earlier chapter, the presence of oxygen in the reactor is undesirable. In this system the prime source of this impurity was the feed acetylene which contained about 0.03 - 0.3% air. One way of removing oxygen is by hydrogenation in the presence of a catalyst. However this method was not followed because the same catalyst would hydrogenate some of the acetylene and lead to formation of ethylene and ethane and thus complicate matters. Further, in order to ensure that all the oxygen present had indeed been reacted, a quantitative analysis would have to be done. Analysis of traces of oxygen is difficult and requires expensive equipment. Hence the above method was ruled out.

An acetylene cylinder is different from other compressed gas cylinders in that it contains a porous monolithic filler on which the solvent is absorbed. The acetylene is present in a highly dissolved state in this solvent, but the air impurity is relatively insoluble and is present in the small void volume near the neck of the cylinder. By taking advantage of this fact, the impurity was removed almost completely by simply

TABLE 4.1

VALUES OF PARAMETERS AND OPERATING
CONDITIONS USED IN THE EXPERIMENT

Reactor Pressure	108.2 kN/m ² (1 psig)
Activation Temperature	477 ^P K
Reaction Temperature	439 ^O K
Total Feed gas flow-rate	5 cm ³ /s
Hydrogen flow-rate	0.25 to 1.625 cm ³ /s
Nitrogen flow-rate	4.25 to 2.875 cm ³ /s
Acetylene flow rate	0.5 cm ³ /s
Catalyst particle size	0.84 to 1.2 mm
Total volume of catalyst	28 cm ³
Hydrogen/Acetylene ratio	0.5 to 3.25
Speed of rotation of basket	104.7 rad/s (1000 rpm)
Mean residence time	66s
Reactor void volume	330 cm ³
Porapak N column	3.18 mm x 2.44 m
Column temperature	(75 ^O C) 348 ^O K
Flame Ionization Detector Temperature	(125 ^O C) 398 ^O K
Infrared Detection Frequency: C ₂ H ₂	3.05 μm
C ₂ H ₄	5.25 μm
C ₂ H ₆	6.55 μm
Period τ	30s to 450 s
Variable γ	2/15 to 13/15

venting a fresh cylinder containing the gas. After this procedure the oxygen content was analyzed by Linde and found to be less than 2 ppm.

It might be argued that the temperature used for activation was not high enough to ensure complete reduction. Higher temperatures were not used in this study because of several reasons. Preliminary experiments at a temperature of 600° F revealed that some of the seals on the drive shaft of the reactor and the bearings showed signs of rapid wear and tear. Also, a sealing compound used on the mating surfaces of the reactor and jacket was found to decompose at temperatures in excess of 500° F. This decomposed compound was then found to leave an almost insoluble residue which was splattered all over the reactor walls and the catalyst baskets. Apart from interfering with the reaction, this gave rise to a severe cleaning problem.

Komiyama and Inoue (1970) used a temperature of 200° C for activating their nickel catalyst, and this was not very different from the 180° C used by Okazaki et al (1974). In their extensive study on reduction of nickel catalysts, Mark and Low (1973) reported that below 400° C the reduction of nickel by hydrogen is "extensive" but not "complete." However, this deviation from "complete" reduction does not become severe enough to affect results, until reduction temperatures below 100° C are used. Roberts and Sykes (1957) have supported these findings. Since the catalysts used in these experiments were already reduced and stabilized, the activation procedure described earlier was considered adequate, especially in view of

the above remarks.

In this investigation, as well as in Lee's simulations (1972), the ratio of hydrogen to acetylene in the feed stream was the manipulated variable. In Lee's work this ratio varied from 0.010 to 3.00. Since one of the goals of these experiments was to verify Lee's predictions, the entire range of the manipulated variable would have to be investigated in order to make a useful comparison. However, in practice, the lower end of this scale was not utilized and the minimum hydrogen to acetylene feed ratio was limited to 0.5. This was done because, at lower feed ratios, acetylene tends to undergo side reactions, which lead to formation of a yellowish brown liquid and cause very rapid catalyst fouling. On the other end of the scale, the maximum hydrogen to acetylene feed ratio was restricted to 3.25 because it was at the upper end of the hydrogen rotameter scale. Theoretical studies by Bailey (1968) have shown that the maximum benefits of periodic operation are often realised when the amplitude of the forcing function is the largest. In view of this observation it would have been advantageous to push the upper end of the scale even further. Although this was not possible under the current configuration of the system, it could be realised in future with a minimum of pressure fluctuation by utilizing a set of two completely independent feed streams and an electrically operated stream selector valve.

Another limitation of the current system is that the hydrogen concentration was not directly analyzed and was calculated from a mass balance. This was due to the fact that hydrogen,

being a non-polar molecule, could not be detected by infra-red techniques. Also, flame ionization gas chromatography uses a hydrogen-air flame and cannot detect hydrogen. It might have been possible to use another column with a relatively less sensitive thermal conductivity detector along with the existing analysis equipment to detect hydrogen. However, this procedure would have resulted in increasing the time delay between successive samples. Such a reduction in sampling frequency would have been a serious drawback in periodic and step response experiments.

During step response experiments, ethylene was the only component of the product mixture whose concentration was monitored continuously with time by the infra-red detector. The other two hydrocarbons, ethane and acetylene, were sampled every two minutes by gas chromatography. There is an advanced version of our variable-filter infra-red analyzer that would permit almost continuous monitoring of all three hydrocarbons by rapidly switching the filter to preset wavenumbers. However such an instrument is prohibitively expensive and hence not used.

This system does not allow investigation of periodic operation in the relaxed steady-state regime. Periods of less than 20 seconds should not be used. This is recommended because it has been observed, during the bang-bang control strategy with the present configuration, that the flowmeter takes about 2 seconds to stabilize after being switched to a new level. Hence the square-wave type input forcing function would not be sharply defined. It can be readily appreciated, that the

relative deviation between the desired input function and the actual input would become severe in the regime of very rapid cycling.

It would not be inappropriate to mention here that a fundamental limitation of the spinning-basket reactor is that the catalyst temperature is not directly measured. The major problem here was the transfer of a signal from a rotating device to a stationary device. This problem was tackled at considerable length in an attempt to find an acceptable solution. If a slider-brush contact were to be used, the error voltage generated by friction would be at least comparable if not larger than the measured millivolt signal. The only other alternative would be to use a switch in which a rotating contact moves in a pool of mercury. However, owing to the fact that the combination of mercury and acetylene is very dangerous and that the size of the smallest available mercury switch is as large as the reactor itself, this idea was discarded.

CHAPTER 5

PRESENTATION OF RESULTS AND DISCUSSION

5.1 Introduction

Contrary to many previous computational and experimental studies of periodic reactors, in this study, steady states were first evaluated over the entire range of the manipulated variable, namely the hydrogen feed concentration. Subsequently, an attempt was made to obtain via cyclic operation time-average product distributions which were unavailable in any of the steady states considered. Indeed, such selectivity shifts due to cycling were observed with several commercial nickel catalysts. The catalysts used in these experiments were Harshaw Ni-0707T (Catalyst I), Girdler G49A (Catalyst II), Girdler G52 (Catalyst III), Girdler G87RS (Catalyst IV), and modified Harshaw Ni0707T (Catalyst V). Additional information on these catalysts is provided in Appendix 4.

As mentioned earlier, in periodic experiments, the inlet hydrogen flow rate $u(t)$ was varied in a bang-bang fashion as follows:

$$u(t) = \begin{cases} 1.625 \text{ cm}^3/\text{s} & \text{for } 0 \leq t < \gamma\tau \\ 0.250 \text{ cm}^3/\text{s} & \text{for } \gamma\tau \leq t < \tau \end{cases} \quad (5.1)$$

where γ and τ have been defined in an earlier chapter. At subsequent times the manipulated input u was evaluated according to the periodicity rule

$$u(t) = u(t+\tau) \quad \text{for } t \geq 0 \quad (5.2)$$

The mean or time-average hydrogen flow rate was

$$\bar{u} = 0.250 + 1.375\gamma \quad \text{cm}^3/\text{s} \quad (5.3)$$

and the nitrogen feed flow rate $w(t)$ was specified by

$$w(t) = 4.25 - u(t) \quad \text{cm}^3/\text{s} \quad (5.4)$$

The acetylene feed was always constant at $0.5 \text{ cm}^3/\text{s}$.

The reactor was said to be in a periodic state when all the state variables satisfied the condition

$$x_i(t) = x_i(t+\tau) \quad \text{for } t > t_p \quad (5.5)$$

where t_p is defined as the start-up time required to reach periodic conditions. The time-average effluent concentrations were calculated using

$$\bar{x}_i = \frac{1}{\tau} \int_{t_p}^{t_p+\tau} x_i(t) dt \quad (5.6)$$

and sets of instantaneous concentration data which span the period. These computed values were consistently in good agreement with direct surge-tank measurements.

5.2.1 Catalyst I - Experiments

Figure 5.1 presents a comparison of steady-state effluent compositions with time-average values obtained by cycling with different periods for Catalyst I. This catalyst showed negligible fouling with almost constant activity, a result consistent with conventional B. E. T. surface-area measurements

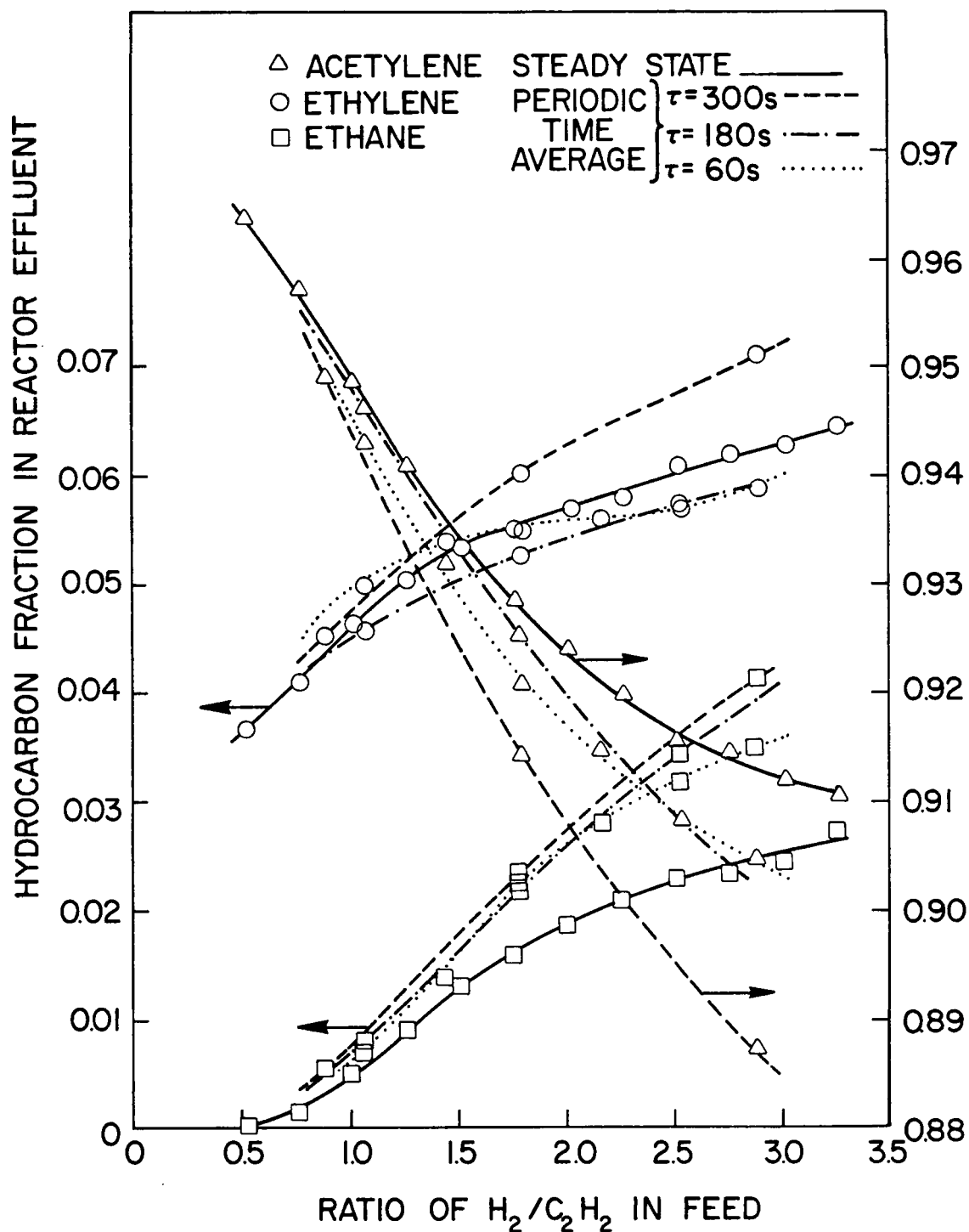


Figure 5.1 Steady-state (solid line) and periodic (broken lines—see legend) effluent hydrocarbon distributions for various time-average hydrogen/acetylene feed ratios for Catalyst I.

which gave values of $\sim 125 - 129 \text{ m}^2/\text{g}$ before and after reaction. The data show that periodic operation results in increased conversion for $\tau = 60 \text{ s}$, $\tau = 180 \text{ s}$, and $\tau = 300 \text{ s}$, with the maximum effect obtained for the longest period. In addition, the data for $\tau = 300 \text{ s}$ show a significant improvement in both ethylene and ethane production. This dependence on cycling period is quite different from Lee's predictions (optimum period $\approx 1/2$ mean residence time = 33 s) and suggests that the catalyst phase dynamics cannot be neglected for this system.

The instantaneous concentration-time profiles obtained during periodic operation with Catalyst I for $\tau = 300 \text{ s}$ are shown in Figure 5.2. All these curves were obtained by making 15 discrete measurements at different times during one period using the gas chromatographic method already described. These data show the effect of varying γ for a constant τ . As expected, the wave-form for each component shows a maximum variation in amplitude for $\gamma \approx 1/2$. The wave-forms for $\gamma = 13/15$ show unusual discontinuities just before the hydrogen is switched to the lower level, and it is this set of operating conditions that gives rise to the largest differences between periodic time-average and steady-state behavior for all three hydrocarbons. For $\gamma = 7/15$ and $\gamma = 2/15$, the profiles indicate that acetylene conversion continues to increase for a short time after the hydrogen feed rate is switched to the lower level. Similar overshoots are also observed for both ethylene and ethane.

These observations reinforce the hypothesis that such phenomena are a direct consequence of capacitances within the

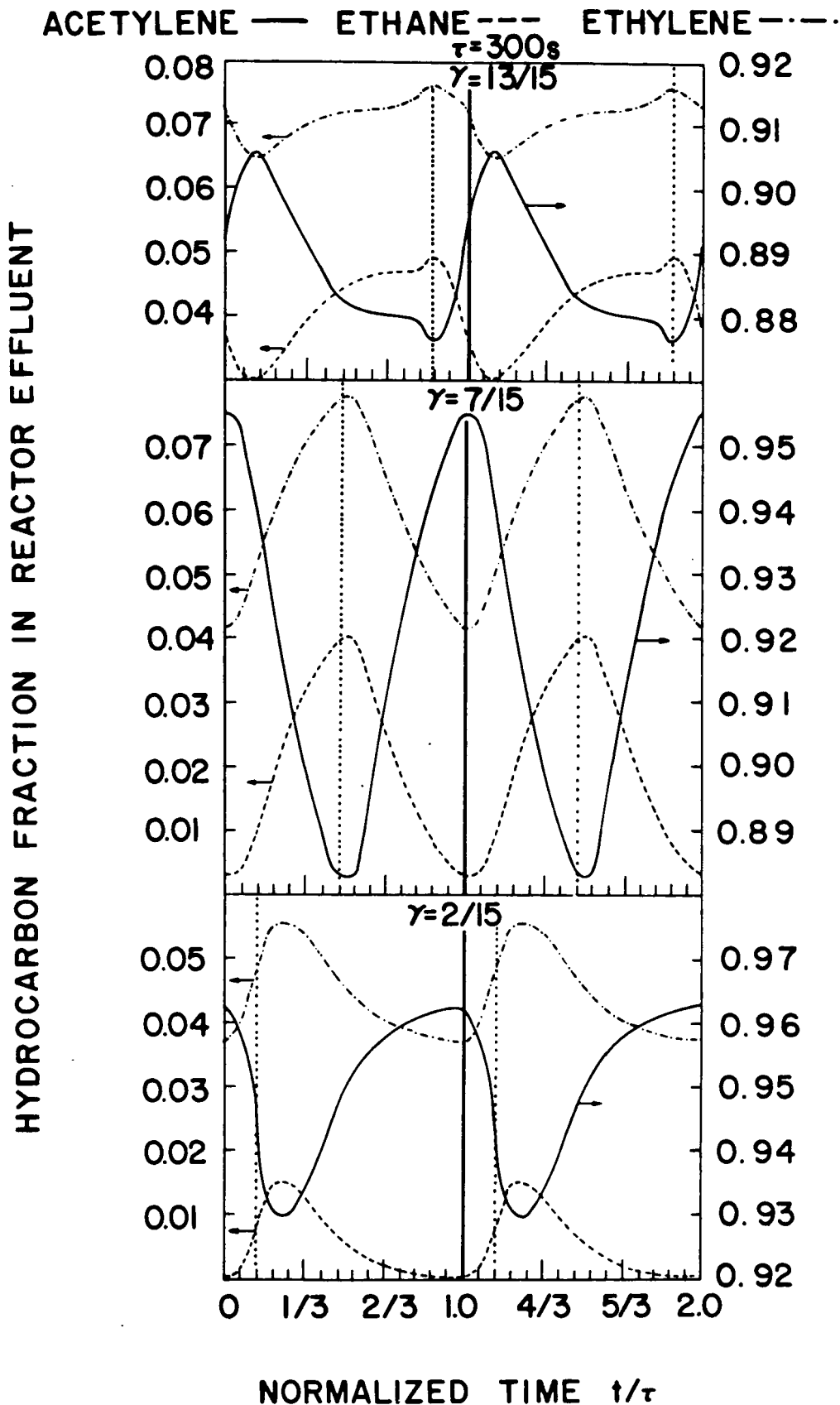


Figure 5.2 Instantaneous effluent compositions for cycling with Catalyst I and a period of 300 s. Different sets of data correspond to different mean hydrogen feed rates.

solid catalyst phase with a response time of the order of several minutes. In an attempt to better understand this unexpected behavior, another series of unsteady-state experiments was conducted. A step increase in hydrogen feed concentration showed an overshoot in the instantaneous ethylene concentration followed by a very slow approach to steady-state (see Figure 5.3). On the other hand, a step decrease in feed hydrogen resulted in a relatively very rapid and monotonic decline to the final steady-state ethylene concentration. It should be noted that the sum of all hydraulic and mixing lags for this system is of the order of 75 s, the diffusional relaxation time (r^2/D_e) is smaller than one second, and the thermal relaxation time ($\rho C_p L^2_{\text{basket}}/k_{\text{eff}}$) is less than 35 seconds. Hence, the extremely slow response observed in the step-up experiment and its asymmetry compared to the step-down result suggest that non-linear dynamics of the gas phase-catalyst surface interaction play a major role in unsteady reactor behavior.

Some interesting pictures of the fractured surface of Catalyst I taken with a scanning electron microscope (SEM) are presented in Figures 5.4 through 5.6 which show the fresh, pre-poisoned and after-reaction stages. All these pictures represent a magnification factor of 900 and 1 mm on the photo represents 1.1 μ . Except for Figure 5.6 which shows evidence of a little more fine debris all three pictures appear to be similar, clearly indicating the absence of any major changes in surface area.

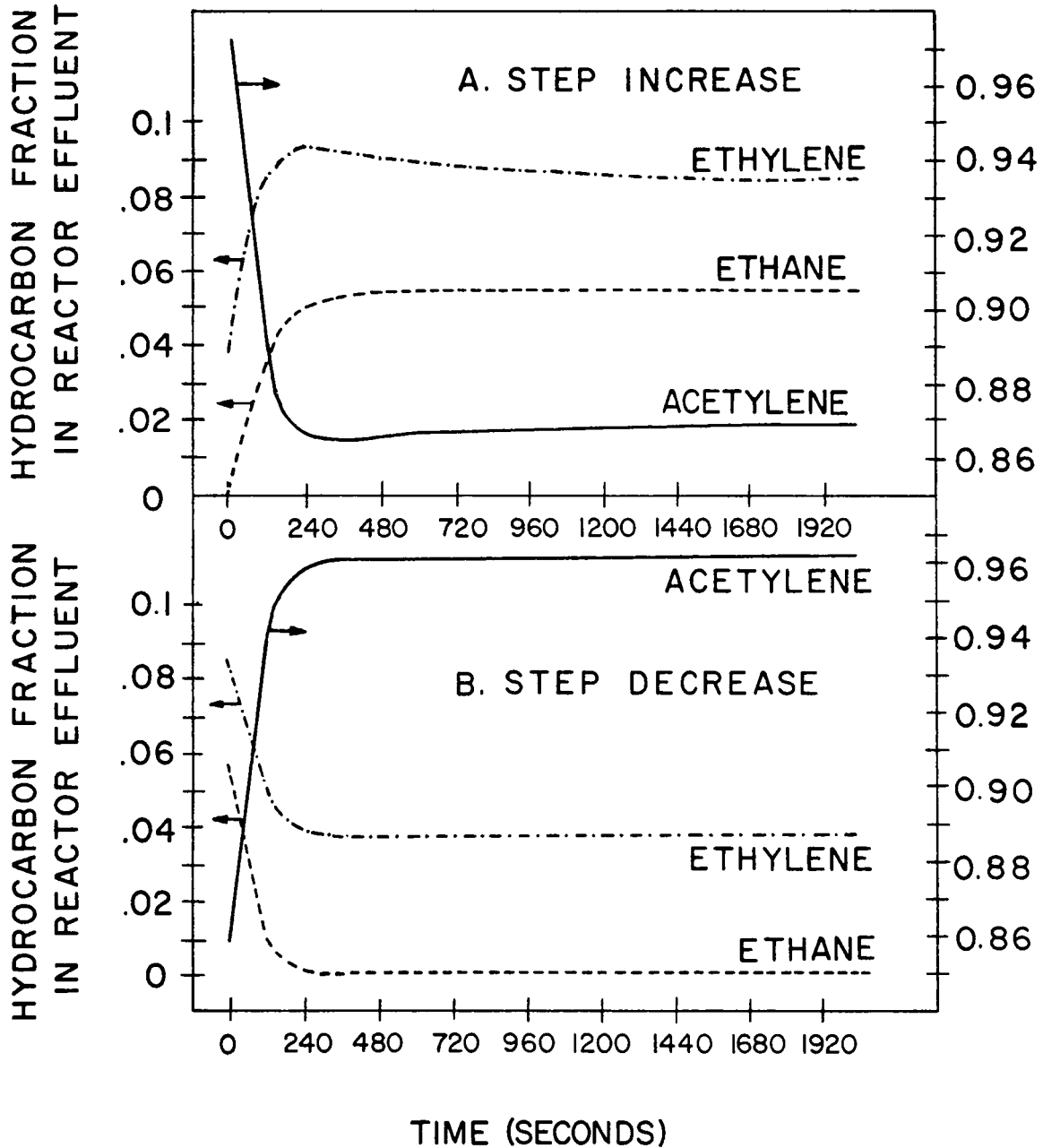


Figure 5.3 The results of a step-up in feed hydrogen mole fraction (A) show overshoots and much longer transients than the reverse step-down experiment (B) for Catalyst I

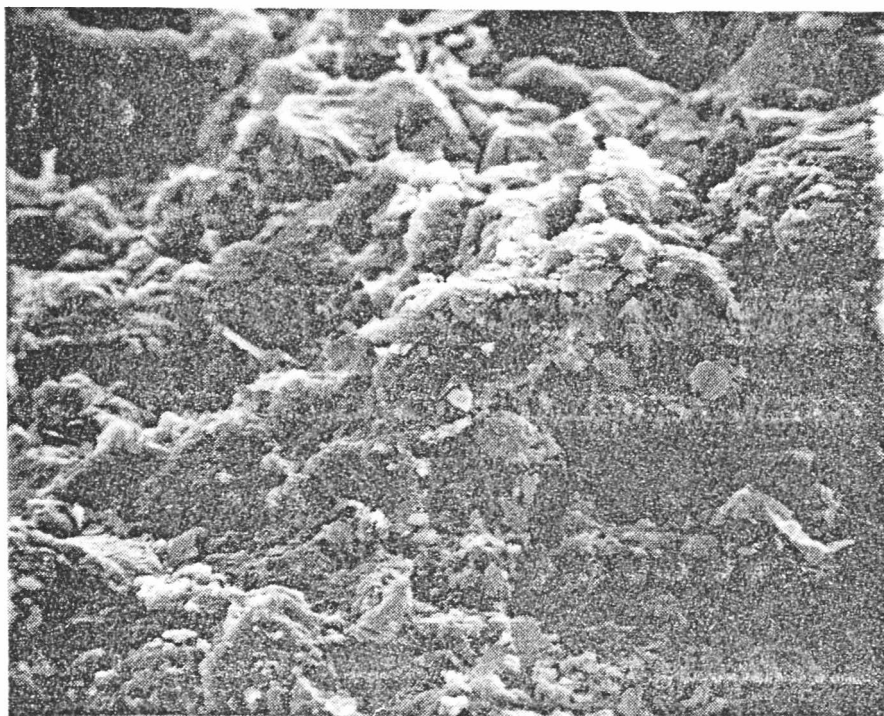


Figure 5.4 SEM photograph of Catalyst I - (fresh sample)

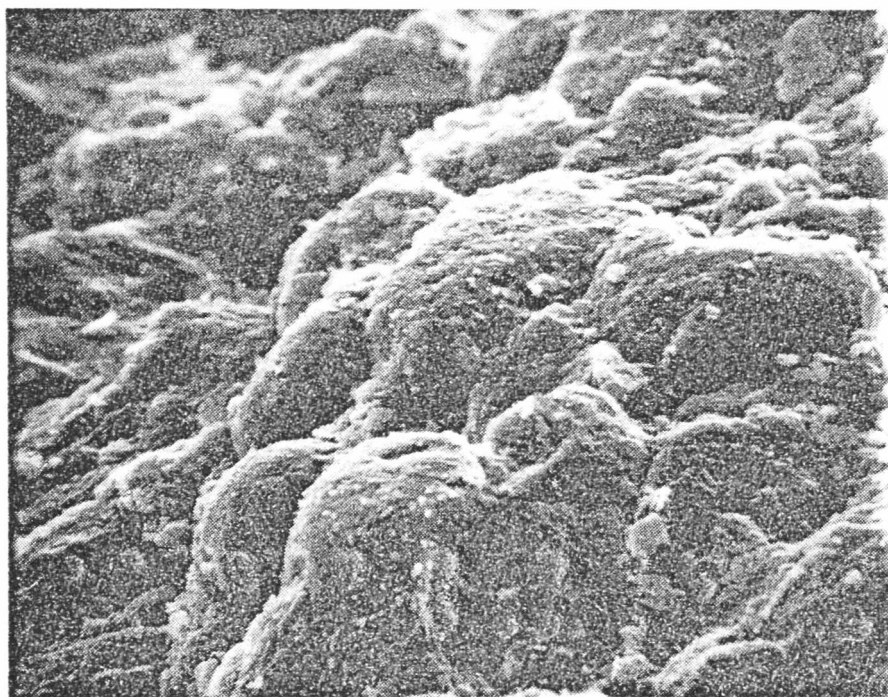


Figure 5.5 SEM photograph of Catalyst I - (prepoisoned sample)

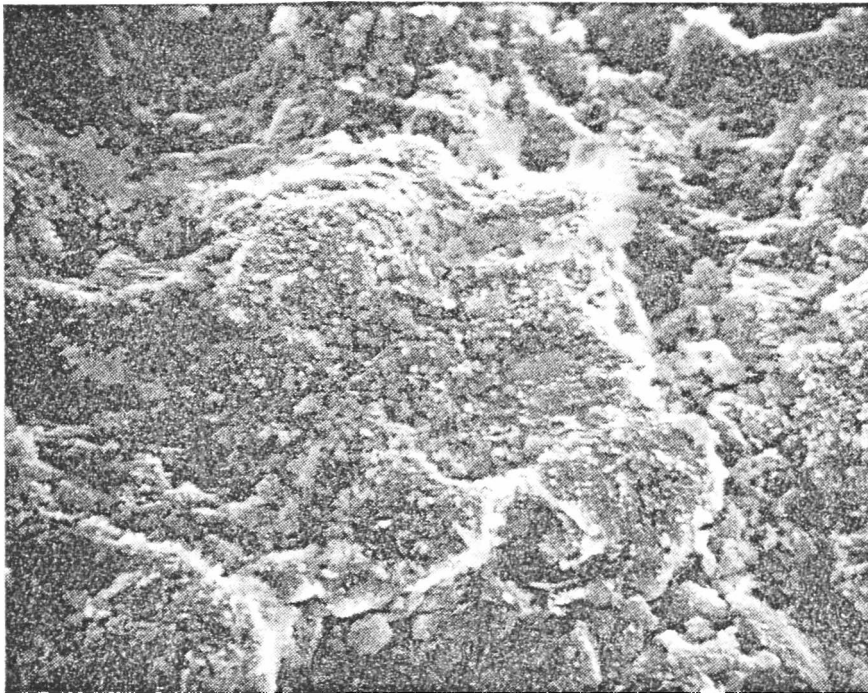


Figure 5.6 SEM photograph of Catalyst I - (after reaction sample)

The response of the spinning basket reactor to a step input of tracer is shown in Figure 5.7. The experimental evidence indicates that the macromixing characteristics are almost identical with those of an ideal CSTR. According to Nauman (1970), if this condition is satisfied, it is very reasonable to assume with a gas phase reaction mixture that micromixing is "perfect;" i.e. the system is in a state of "maximum mixedness."

5.2.2 Catalyst I - Steady State Modeling

Since the spinning-basket reactor was specifically designed to be gradientless, it would be far-fetched to imagine that the experimental measurements for Catalyst I are plagued by the mass and heat transfer disguises discussed in Chapter 2. The dimensionless adiabatic temperature rise β and Weisz's observable modulus ϕ , under the conditions of these experiments, have been estimated (see Appendix for details) to be ≤ 0.001 and ≤ 0.01 respectively. Having established beyond a doubt that diffusion effects are indeed negligible, the steady-state behavior for this catalyst was analyzed as shown below.

Considering the spinning basket reactor to be a pseudo-homogenous stirred tank, the steady-state mass balance equations for the system can be written as follows:

$$\begin{aligned} F_i x_{1i} - F_0 x_1 - r_1 V &= 0 \\ F_i x_{2i} - F_0 x_2 - (r_1 + r_2) V &= 0 \\ -F_0 x_3 + (r_1 - r_2) V &= 0 \\ -F_0 x_4 + r_2 V &= 0 \\ F_i x_{5i} - F_0 x_5 &= 0 \end{aligned} \tag{5.7}$$

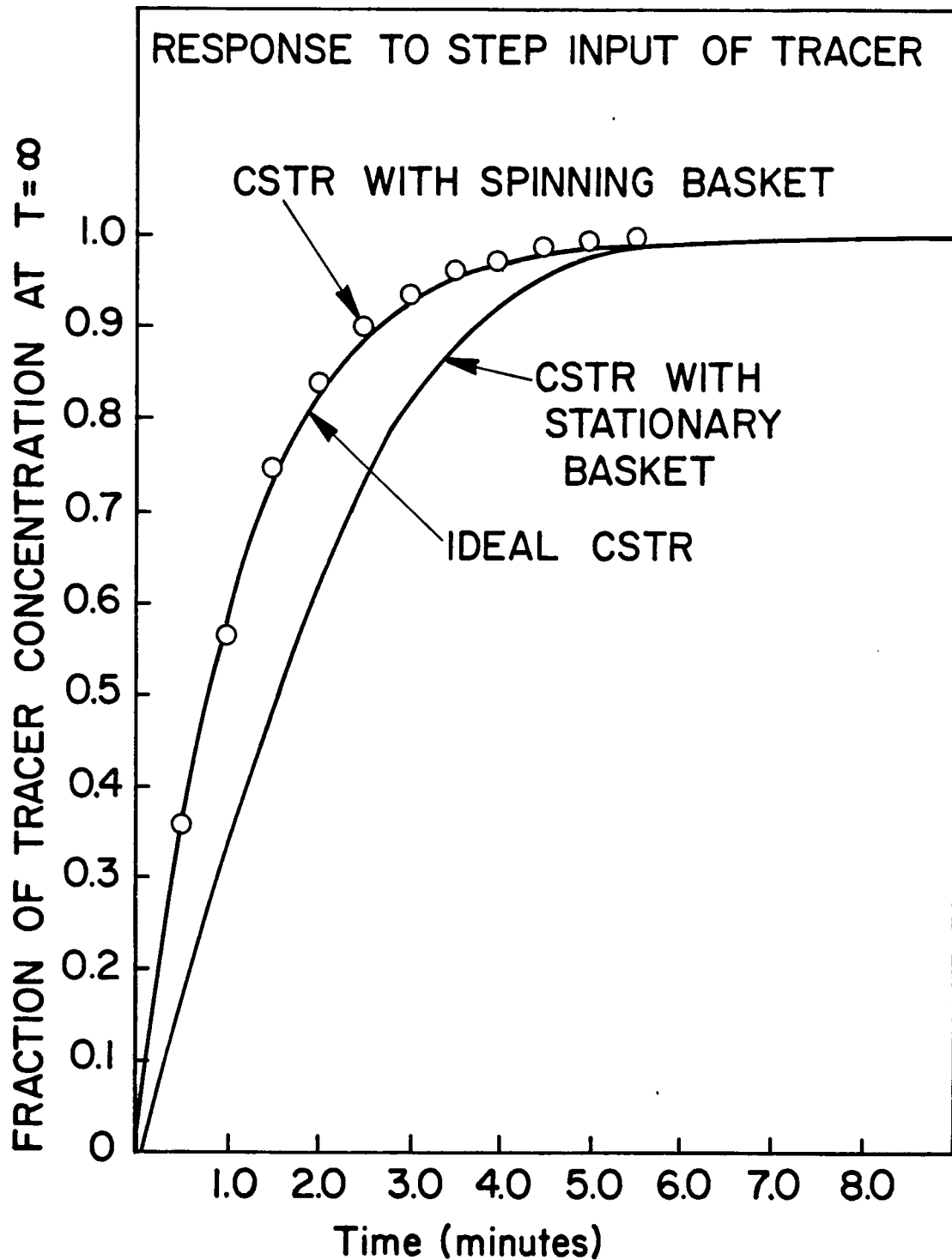


Figure 5.7 Comparison of the spinning basket and stationary basket mixing characteristics to an ideal CSTR

Here F_i and F_0 are inlet and outlet molar flowrates respectively and the x 's denote mole fractions with subscripts 1 through 5 referring to acetylene, hydrogen, ethylene, ethane and inert nitrogen, respectively. The additional suffix i refers to inlet conditions and r_1 and r_2 denote the rates of reactions for the two steps. It should be pointed out that V represents the volume occupied by the gas in the reactor and has been adjusted to include the void fraction in the baskets.

As described in Chapter 4 only the hydrocarbons in the exit stream were analyzed. Convenient effluent composition variables are the hydrocarbon fractions defined as follows:

$$\begin{aligned} A &= \frac{F_0 x_1}{F_0 (x_1 + x_3 + x_4)} \\ B &= \frac{F_0 x_3}{F_0 (x_1 + x_3 + x_4)} \\ C &= \frac{F_0 x_4}{F_0 (x_1 + x_3 + x_4)} \end{aligned} \tag{5.8}$$

In the mass balance equations, the exit flowrate, mole fractions and rates r_1 and r_2 are the only unknowns, the other parameters being predetermined or experimentally measured quantities. The step-wise algebraic solution is given on the following page.

$$F_0 = F_i(1 - (B + 2C)x_{1i})$$

$$x_1 = \frac{F_i x_{1i} A}{F_0}$$

$$x_3 = \frac{Bx_1}{A}$$

$$x_4 = \frac{Cx_1}{A} \tag{5.9}$$

$$x_2 = 1 - \frac{F_i}{F_0} (1 - x_{2i})$$

$$r_1 = (F_i x_{1i} - F_0 x_i) / V$$

$$r_2 = F_0 x_4 / V$$

The last two of the above equations were used to determine the rates of the two reaction steps from the steady-state experimental data. A wide variety of Langmuir-Hinshelwood type rate expressions were fit to the experimental data using the optimization technique recommended by Kuester and Mize (1973). The computation procedure is a slight modification of the algorithm proposed by Powell (1964) to find the minimum of an unconstrained, multivariable, nonlinear function without finding any derivatives. As shown in Table 5.1 the kinetic expressions which gave rise to negative rate constants or negative adsorption equilibrium constants were discarded. The last column in Table 5 shows σ_1 and σ_2 which are the standard

TABLE 5.1

STEADY STATE DATA FIT FOR CATALYST I

MODEL RATE EXPRESSIONS	CONSTANTS	STANDARD DEVIATIONS
1) $r_1 = \frac{k_1 C_1 C_2}{1 + K_2 C_2}$ $r_2 = \frac{k_3 C_3 C_2^{0.5}}{1 + K_2 C_2}$	$k_1 = 21.88 \text{ l}/(\text{mol-min})$ $K_2 = 125.37 \text{ l}/\text{mol}$ $k_3 = 7.19 \text{ l}/(\text{mol-min})$	$\sigma_1 = 0.853 \times 10^{-5}$ $\sigma_2 = 0.127 \times 10^{-4}$
2) $r_1 = \frac{k_1 C_1 C_2}{1 + K_2 C_1}$ $r_2 = \frac{k_3 C_3 C_2^{0.5}}{1 + K_2 C_1}$	$k_1 = 0.743 \text{ l}/(\text{mol-min})$ $K_2 = -343.18 \text{ l}/\text{mol}$ $k_3 = 0.245 \text{ l}/(\text{mol-min})$	$\sigma_1 = 0.138 \times 10^{-4}$ $\sigma_2 = 0.179 \times 10^{-4}$
3) $r_1 = \frac{k_1 C_1 C_2}{1 + K_2 C_1}$ $r_2 = \frac{k_3 C_3 C_2^n}{1 + K_2 C_1}$	$k_1 = 0.764 \text{ l}/(\text{mol-min})$ $K_2 = -342.5 \text{ l}/\text{mol}$ $k_3 = 7.88 \text{ l}/(\text{mol-min})$ $n = 1.192$	$\sigma_1 = 0.125 \times 10^{-4}$ $\sigma_2 = 0.606 \times 10^{-5}$

TABLE 5.1 (continued)

MODEL RATE EXPRESSIONS	CONSTANTS	STANDARD DEVIATIONS
4) $r_1 = \frac{k_1 C_1 C_2}{1 + K_2 C_2}$ $r_2 = \frac{k_3 C_3 C_2^n}{1 + K_2 C_2}$	$k_1 = 27.19 \text{ l}/(\text{mol-min})$ $K_2 = 190.49 \text{ l/mol}$ $k_3 = 319.65 \text{ l}/(\text{mol-min})$ $n = 1.219$	$\sigma_1 = 0.284 \times 10^{-5}$ $\sigma_2 = 0.386 \times 10^{-5}$
5) $r_1 = \frac{k_1 C_1 C_2}{(1+K_3 C_1)(1+K_4 C_2)} + \frac{k_2 C_1 C_2}{(1+K_3 C_1)}$ $r_2 = \frac{k_5 C_3 C_2}{(1+K_7 C_3)(1+K_4 C_2)} + \frac{k_6 C_3 C_2}{(1+K_7 C_3)}$	$k_1 = 111.83 \frac{\text{l}}{(\text{mol-min})} \quad K_3 = -328.35 \frac{\text{l}}{\text{mol}}$ $k_2 = -110.28 \frac{\text{l}}{(\text{mol-min})} \quad K_4 = 0.41 \frac{\text{l}}{\text{mol}}$ $k_5 = 4329.5 \frac{\text{l}}{(\text{mol-min})}$ $k_6 = -4313.35 \frac{\text{l}}{(\text{mol-min})} \quad K_7 = -5204.25 \frac{\text{l}}{\text{mol}}$	$\sigma_1 = 0.562 \times 10^{-5}$ $\sigma_2 = 0.123 \times 10^{-5}$
6) $r_1 = \frac{k_1 C_1 C_2}{1 + K_2 C_2}$ $r_2 = \frac{k_3 C_3 C_2}{1 + K_2 C_2}$	$k_1 = 26.2 \text{ l}/(\text{mol-min})$ $K_2 = 179.0 \text{ l/mol}$ $k_3 = 105.0 \text{ l}/(\text{mol-min})$	$\sigma_1 = 0.329 \times 10^{-5}$ $\sigma_2 = 0.585 \times 10^{-5}$

deviations between the experimentally measured rates and those predicted by the model for the two reaction steps.

The rate expressions which appear to give a superior fit to the experimental data as compared to the others that were tried are given below:

$$\begin{aligned} r_1 &= \frac{k_1 C_1 C_2}{1 + K_2 C_2} \\ r_2 &= \frac{k_3 C_2 C_3}{1 + K_2 C_2} \end{aligned} \tag{5.10}$$

where c_1 , c_2 and c_3 are acetylene, hydrogen and ethylene concentrations respectively and where, at 439°K,

$$k_1 = 26.2 \text{ l}/(\text{mol-min})$$

$$K_2 = 179 \text{ l}/\text{mol}$$

$$k_3 = 105 \text{ l}/(\text{mol-min})$$

It is both interesting and intriguing to note that apparently the hydrogen adsorption appears to be playing a significant role in the reaction, as indicated by the denominator term in the above expressions. No doubt, this is quite different from the Komiyama and Inoue (1968) kinetics which were used by Lee (1972) in his simulations. As indicated in Table 5.1 the use of that model, in which the acetylene concentration term appeared in the denominator, gave rise to negative constants. However, this result is not altogether surprising because the catalyst used in their studies was quite different.

As was pointed out earlier in section 1.2, the studies of this reaction by Bond (1964) have revealed a dependence on complex hydrogen orders for some nickel catalysts. The work of Richardson and Friedrich (1975) cited earlier, on hydrogenation of ethylene over nickel catalysts, concluded that adsorbed hydrogen atoms are relatively strongly held. These results are qualitatively consistent with the steady-state kinetics of equations (5.10).

5.2.3 Catalyst I - Unsteady State Modeling

If the relative time scale for changes in concentration is much larger than the diffusion and conduction relaxation times, the use of a pseudo-homogeneous model to represent the unsteady-state catalytic CSTR is both adequate and justified. It is readily seen that under the conditions used in this experimental study, the above statement is most certainly true for diffusion. Further, the thermal relaxation time reported earlier in this chapter (in a liberal upper bound) strongly suggests that the heat conduction process also meets this criterion. The experimental temperature-versus-time records shown in Figure 5.8 indeed support this claim. It should be pointed out that each major horizontal division on the graph corresponds to 2.5 minutes and that this particular data is for a different catalyst which gave much higher conversions and thus represents the "worst case." The periodic temperature-time profile is for a rapid cycling case with $\tau = 30$ s and

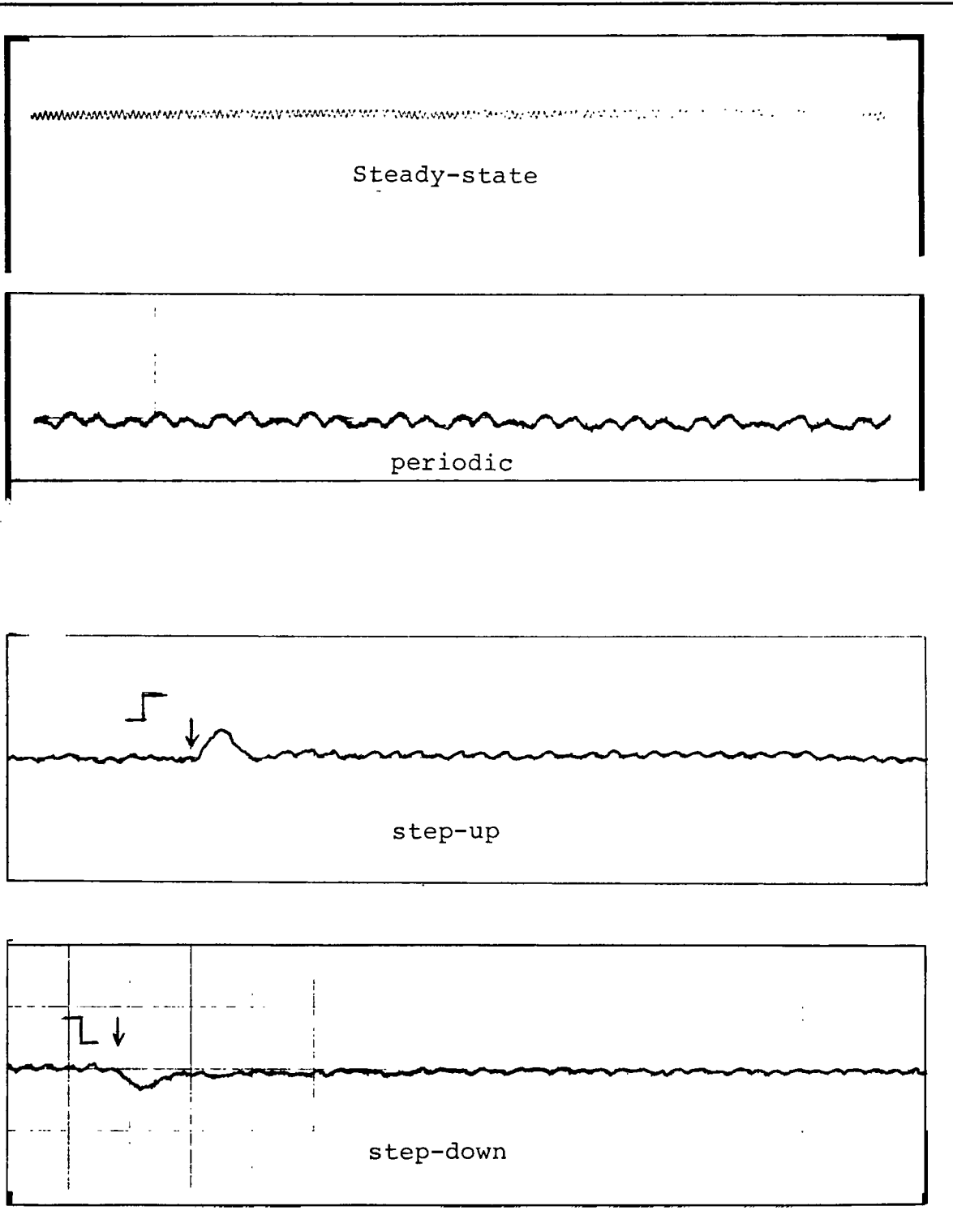


Figure 5.8 Experimental traces of temperature-time profiles for the spinning basket reactor

$\gamma = 7/15$ and in that sense representative of "severe loading" on the temperature control system.

It will be more convenient to write the unsteady-state mass balance equations in terms of volumetric flowrates and concentrations owing to the fact that the rate expressions for the best-fit steady-state kinetics were written that way. These equations for the isothermal, pseudo-homogeneous CSTR are presented below.

$$\begin{aligned}V \frac{dC_1}{dt} &= Q_i C_{1i} - Q_o C_1 - r_1 V \\V \frac{dC_2}{dt} &= Q_i C_{2i} - Q_o C_2 - (r_1 + r_2) V \\V \frac{dC_3}{dt} &= -Q_o C_3 + (r_1 - r_2) V \\V \frac{dC_4}{dt} &= -Q_o C_4 + r_2 V \\V \frac{dC_5}{dt} &= Q_i C_{5i} - Q_o C_5\end{aligned}\tag{5.11}$$

where Q_i and Q_o represent inlet and outlet volumetric flowrates and C_1 through C_5 represent acetylene, hydrogen, ethylene, ethane and inert nitrogen respectively. The other variables have the same definition as stated earlier. Once again the subscript i denotes predetermined inlet conditions.

Assuming the tank pressure to be a constant, the exit volumetric flowrate Q_o can be expressed in terms of known

quantities as

$$Q_o = Q_i - V(r_1+r_2) \left(\frac{RT}{P}\right) \quad (5.12)$$

where P is the total pressure, T is the absolute temperature and R is the universal gas constant. Hence the above equations can be integrated using an explicit method like the fourth order Runge-Kutta with variable step-size. The well known DRKGS subroutine reported by Ralston and Wilf (1960) was used to carry out the computations. These calculations showed that under dilute and low conversion conditions employed in the experiments with Catalyst I, volume change effects were negligible.

Figure 5.9 shows that when the best-fit rate expressions are employed in the steady-state version of the dynamic model, the simulations are in excellent agreement with the experimental data. When the dynamic model was used to simulate the step-response behavior for Catalyst I, a slight discrepancy was observed. As expected, Figures 5.10 and 5.11 indicate that this dynamic model does not predict the overshoots and undershoots which were observed in the experiments. In these figures the simulated response appears to reach the eventual steady-state faster than the experimental response, although in the early stages (up to a time ≈ 300 seconds) a reverse trend is observed. The experimental response to a step-decrease in feed hydrogen resulted in a relatively rapid and monotonic decline to the final steady state and qualitatively, this is correctly

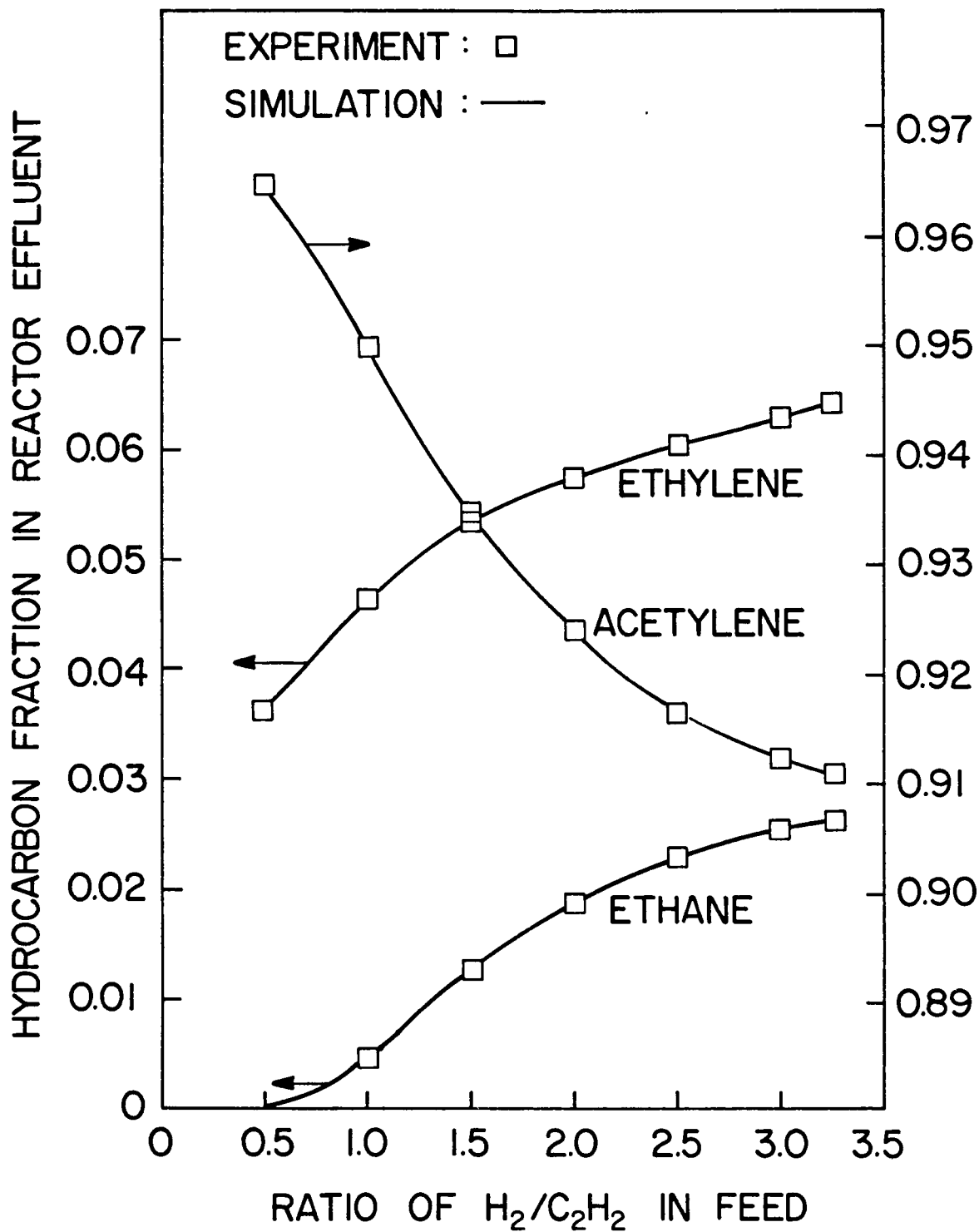


Figure 5.9 Comparisons between experimentally measured effluent compositions and compositions calculated from Equation 5.11 (Steady-state Catalyst I)

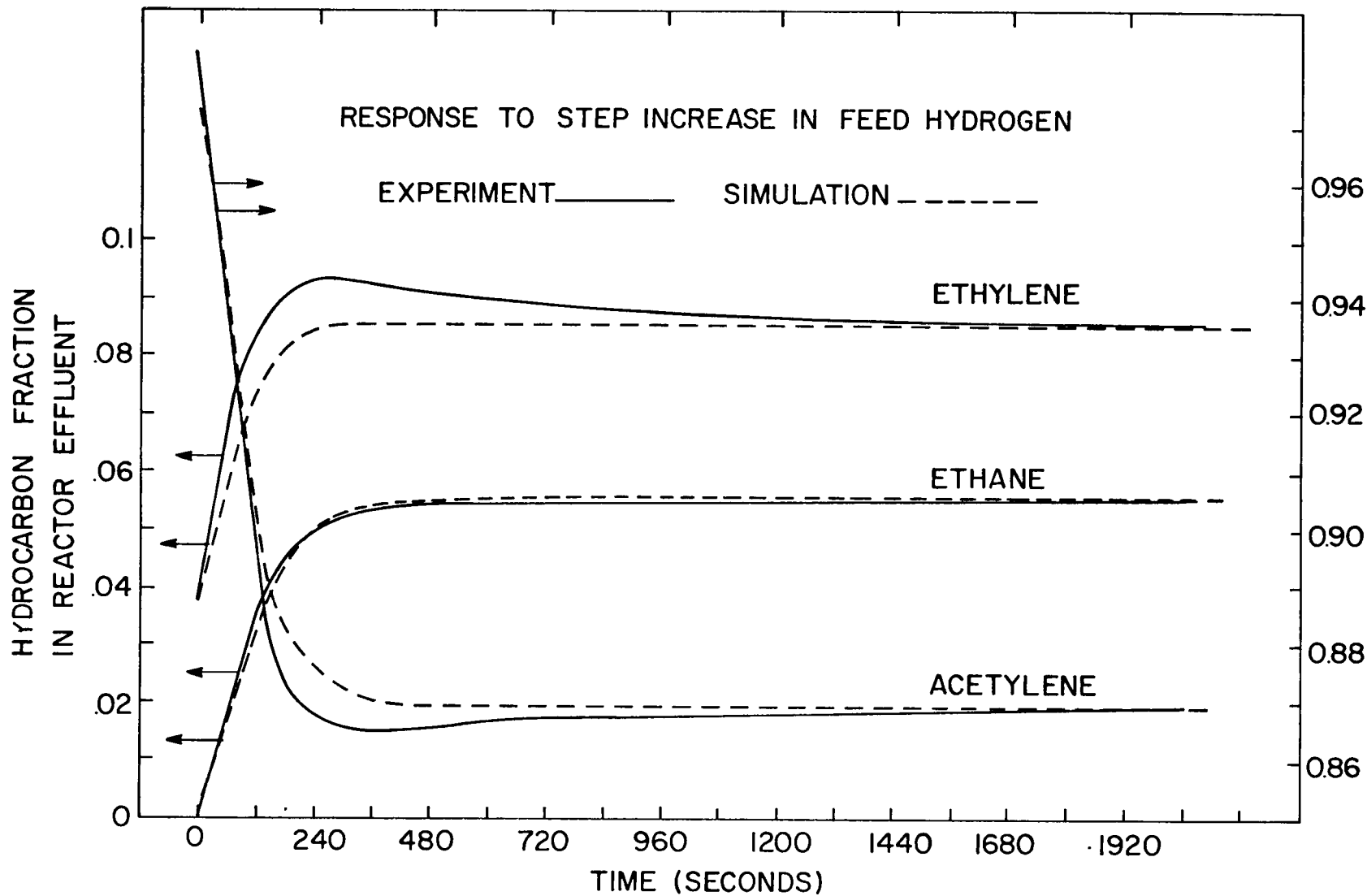


Figure 5.10 Comparisons between experimentally measured effluent compositions and compositions calculated from Equation 5.11 for a step increase in feed hydrogen (Catalyst I)

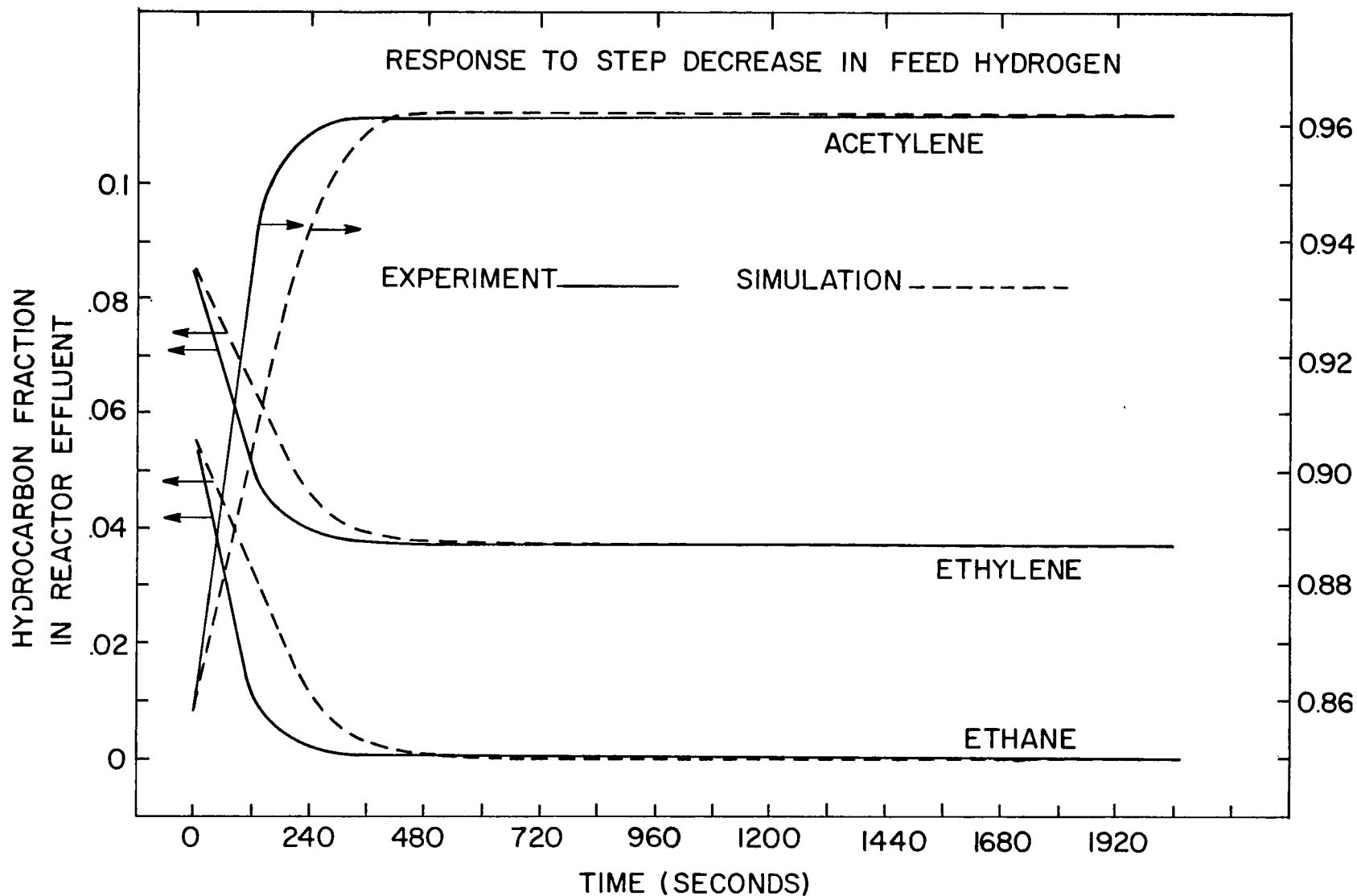


Figure 5.11 Comparisons between experimentally measured effluent compositions and compositions calculated from Equation 5.11 for a step decrease in feed hydrogen (Catalyst I)

predicted by the simulations. However the simulated response lags behind the experimental one, showing the slight inconsistency of the model. By analogy with second-order control systems, it seems that a positive feedback step will have to be incorporated in a reaction mechanism sequence to account for the overshoots observed in the dynamic studies of acetylene hydrogenation.

Step-response techniques have been used to develop dynamic models in heterogeneous catalysis based on experimental data. The experiments of Denis and Kabel (1970) on the vapor phase dehydration of ethanol to diethyl ether catalyzed by cation exchange resin and those of Bennett (1976) on the decomposition of N_2O over silica-supported nickel oxide have shown that surface dynamics effects are important. It is interesting to note that Bennett used a catalytic stirred tank gradientless reactor in his investigations. Kobayashi and Kobayashi (1974) were amongst the first to make extensive use of step-response techniques to elucidate elementary reaction steps for CO oxidation and N_2O decomposition over various metal oxides. It is interesting to note that all these investigators observed these significant overshoots and undershoots in their respective works.

In this work, transient response techniques have been carried one step further in that instantaneous concentration-versus-time trajectories and periodic time average measurements have been recorded during cycling experiments. It is perhaps

here that the inadequacy of steady-state modeling in heterogeneous catalysis becomes glaringly obvious. Figures 5.12, 5.13 and 5.14 show the instantaneous concentration-time curves measured experimentally and those computed from the unsteady-state model with best-fit steady-state kinetics. A similar comparison for the time average behavior is presented in Figure 5.15.

A quick glance at Figure 5.12 shows that for $\gamma = 2/15$, the behavior of ethylene in both the simulation and the experiment is qualitatively fairly consistent. The shapes of the trajectories for acetylene are quite similar but the amplitude of the oscillation is much larger in the experiments as compared to the model predictions. The peaks for ethane in the simulations are not as pronounced as in the actual trajectory.

In Figure 5.13 for $\gamma = 7/15$, as in Figure 5.12 the same behavior pattern emerges for all three hydrocarbon species in that the amplitudes of the experimentally measured oscillations are much larger. This discrepancy is most dramatic for acetylene. In spite of these differences, a significant point in favor of this particular pseudo-homogeneous dynamic model is that qualitatively it predicts these almost symmetric waveforms very well. Further the changes in the direction of the trajectories are very faithfully followed at every instant in the time-span of a single cycle.

In his simulations based on the Komiyama and Inoue (1968) kinetics, Lee (1972) found that the period of the oscillations

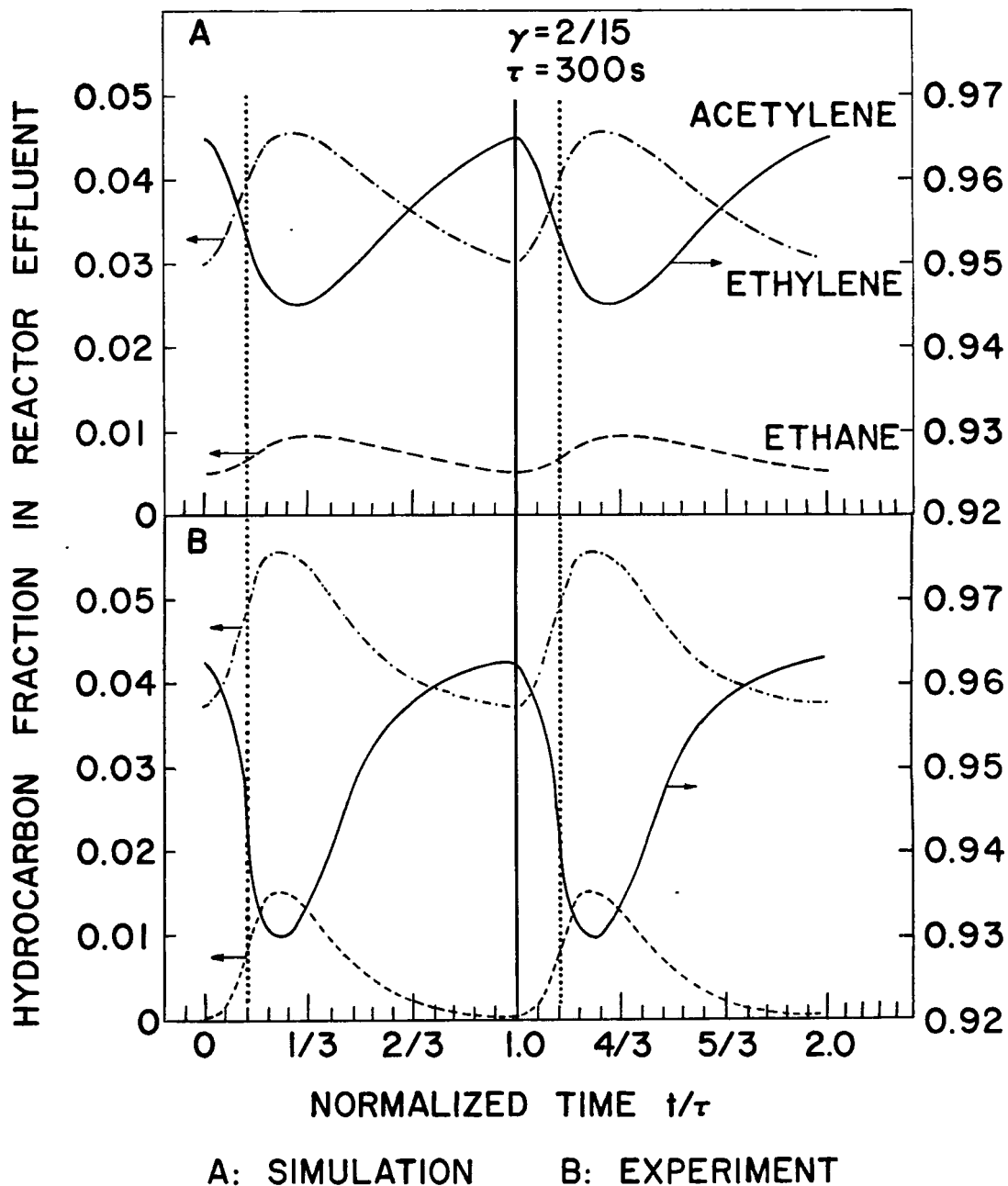


Figure 5.12 Comparison of the instantaneous concentration trajectories for (A) Simulations with the dynamic model and (B) Experiments (Catalyst I)

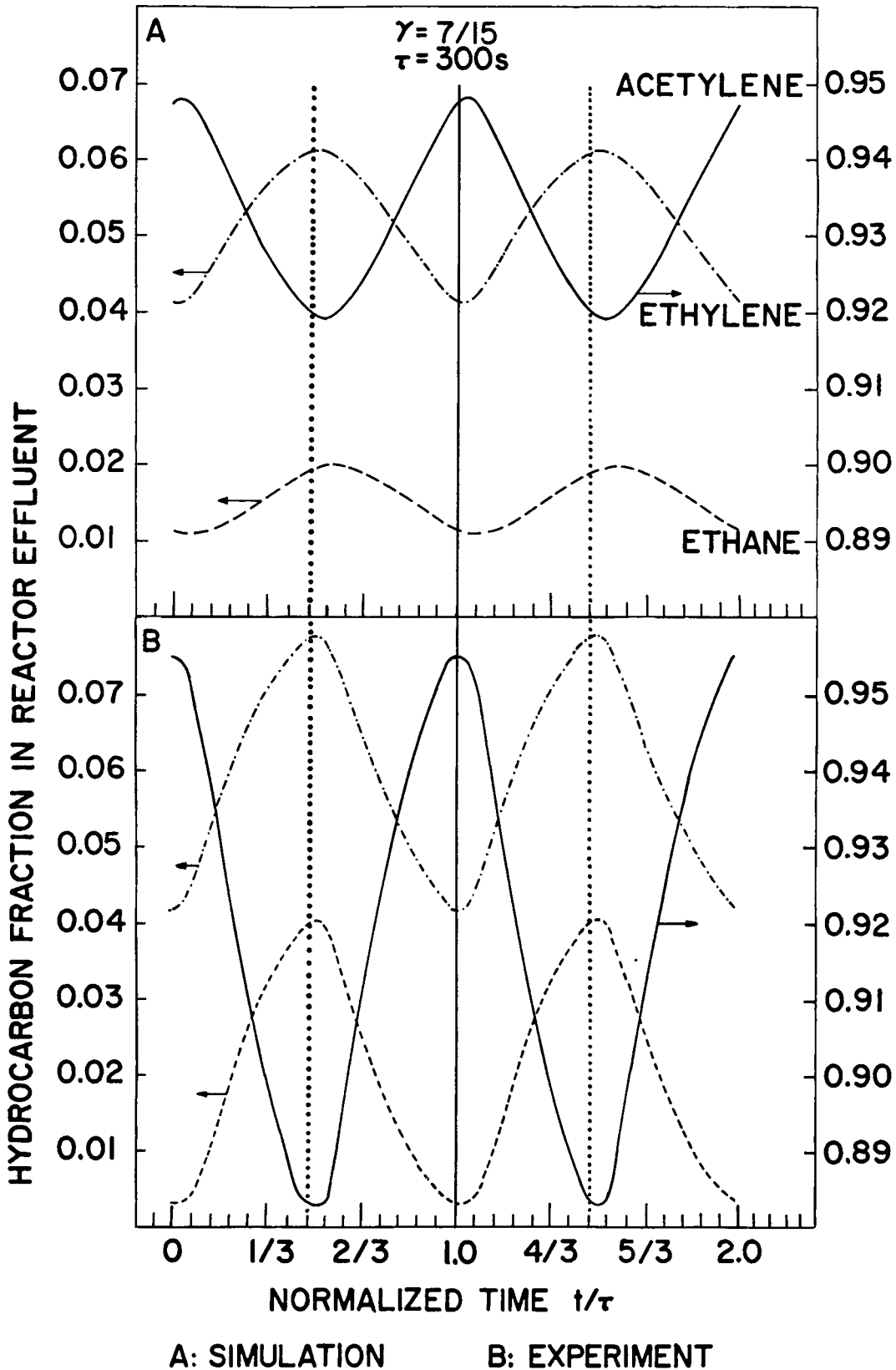


Figure 5.13 Comparison of the instantaneous concentration trajectories for (A) Simulations with the dynamic model and (B) Experiments (Catalyst I)

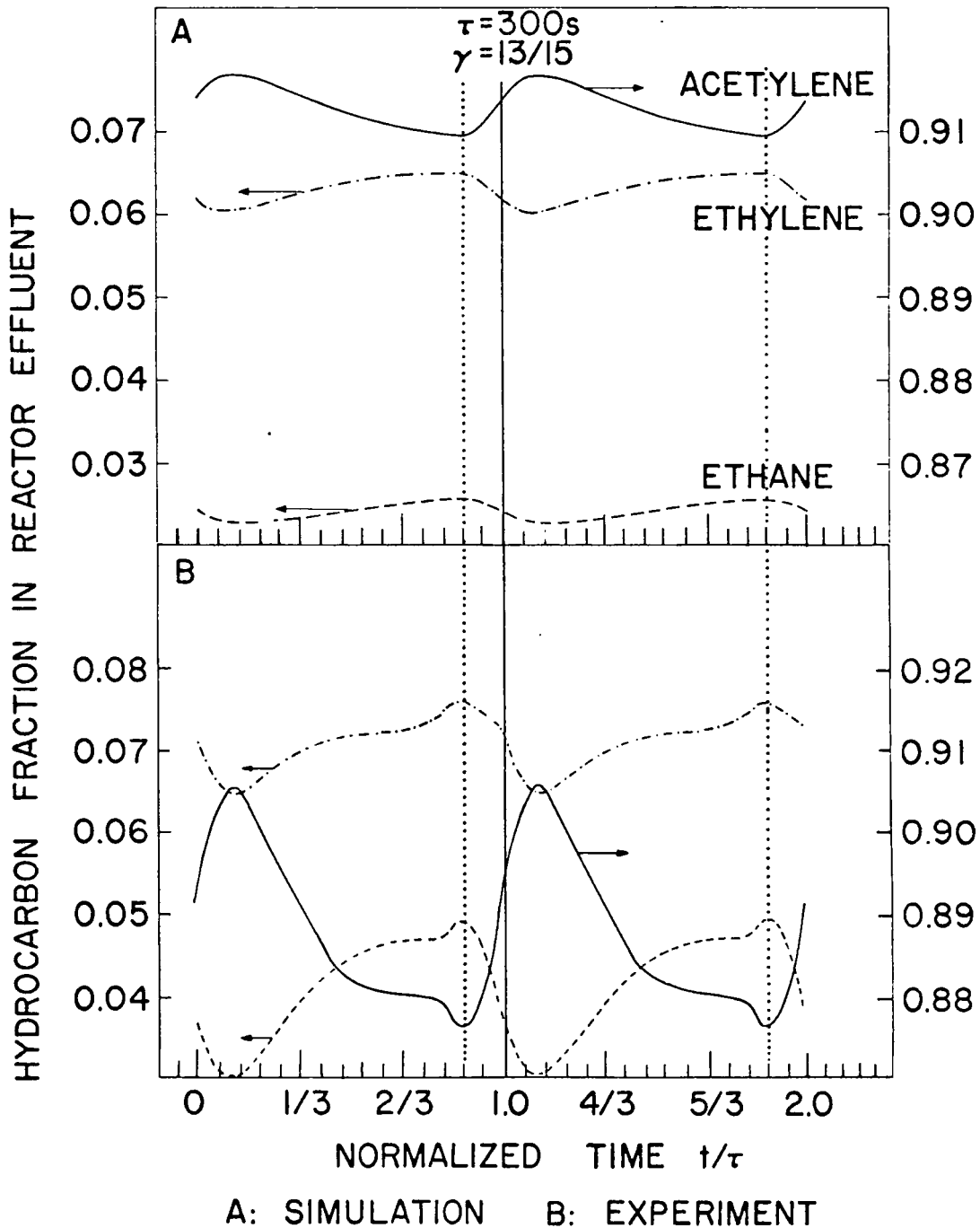


Figure 5.14 Comparison of the instantaneous concentration trajectories for (A) Simulations with the dynamic model and (B) Experiments (Catalyst I)

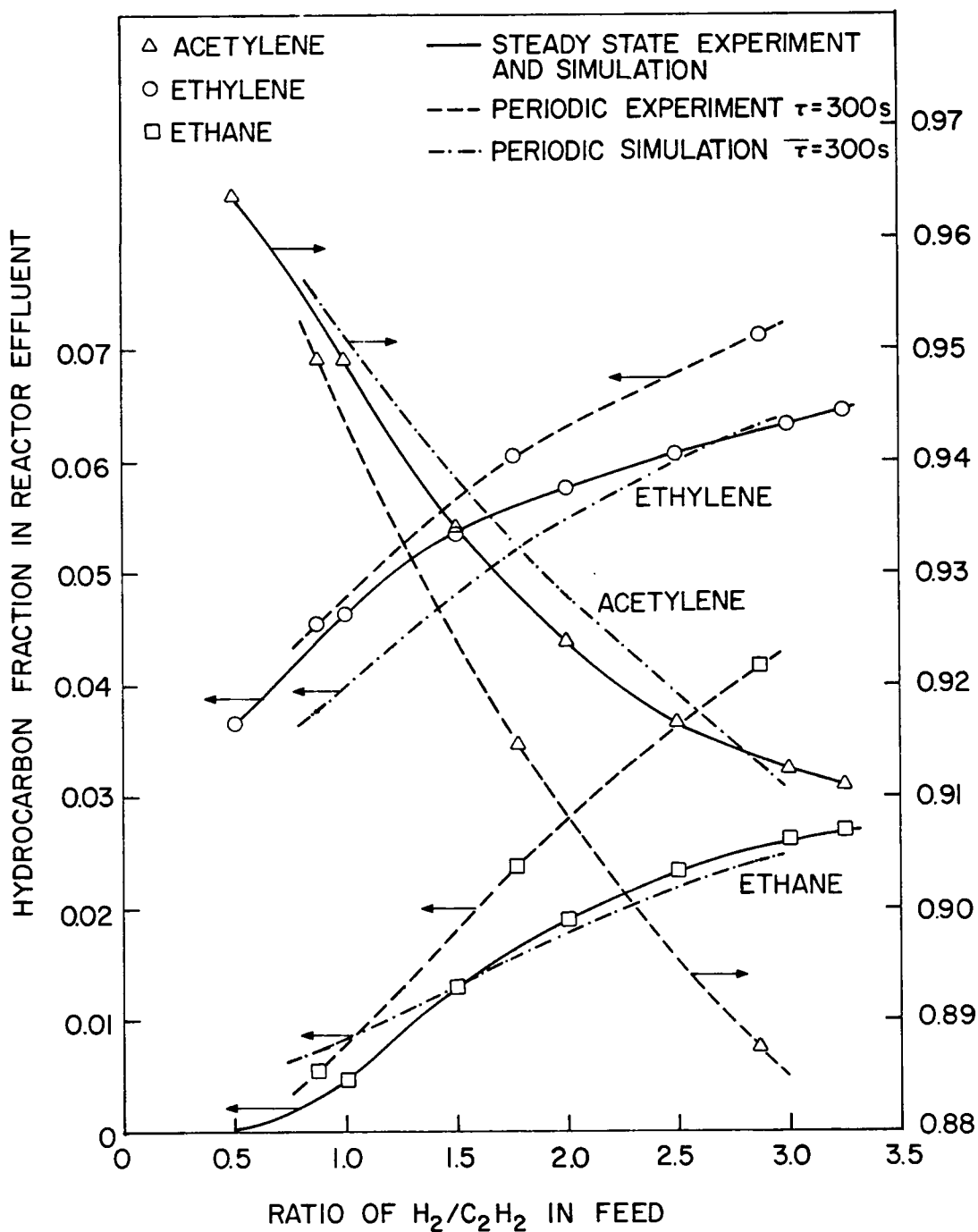


Figure 5.15 Comparison of periodic time-average and steady-state effluent compositions obtained by simulation with the dynamic model to the corresponding compositions measured experimentally (Catalyst I)

is identical to the period of the forcing function. Later studies by Sincić (1974) showed that this was not always necessarily true for all reaction systems. However, experimental results reported here demonstrate that the dynamics of acetylene hydrogenation do follow the forcing function and offer experimental evidence in support of Lee's assumption.

In Figure 5.2 the unusual discontinuities for $\gamma = 13/15$ were pointed out. It is only in Figure 5.14 that these discontinuities play a very significant role in bringing about the downfall of this dynamic model. Here the model completely breaks down in that it is totally unable to match the experimental trajectories even qualitatively, let alone quantitatively. Evidently some kind of limiting condition must have been reached under this experimental configuration so that the non-linear dynamics of the gas phase-catalyst surface interaction become magnified. It could be argued by someone who did not know better that this unusual discontinuity is not a discontinuity at all but an error in experimental measurement, and then the dynamic model would not appear to fail so miserably. In such a case, in view of the qualitative agreement discussed above, this pseudo-homogeneous dynamic model based on best-fit steady state rate expressions may even appear to be a successful first approximation. However, such thoughts are totally misleading and self-deceptive and are a manifestation of the easy way out of an apparent controversy. These unusual behavior patterns were observed experimentally for several different catalysts

and confirmed independently by both gas chromatography and infra-red measurements.

In his theoretical simulations of consecutive-competitive reactions, Renken (1972) used symmetric input forcing functions. While these do produce the largest amplitudes of oscillation, as was pointed out in an earlier chapter, a study of periodic reactor behavior is not complete without varying γ (i.e. relaxing the symmetry condition). The importance of this variable was dramatically demonstrated in the comparisons made in Figures 5.12 through 5.14.

Manifestations of alteration in time-average behavior are apparent in Figure 5.15 which reveals that the direction as well as the magnitudes of the shifts in effluent compositions produced by forced cycling are incorrectly predicted by the dynamic model. Hence, as pointed out in Chapter 1, under applications of forced cycling, the nonlinear interactions produced in a periodic reactor appear to be a very sensitive and valuable tool to obtain a better understanding of heterogeneous catalysis.

5.2.4 Catalyst I - Plug Flow Simulations

In order to find out how the conventional plug-flow reactor would behave, another set of simulations was done using the same kinetic rate expressions in a very simple pseudo-homogeneous plug-flow reactor model. The complete step-wise sequence of simple equations required to simulate a steady-

state experiment is given below.

$$F_5 = \text{known constant}$$

$$F_3 = F_2 - F_{2i} + 2(F_{1i} - F_1)$$

$$F_4 = F_{2i} - F_2 - (F_{1i} - F_1)$$

$$v = \frac{RT}{P} \sum_{j=1}^5 F_j \quad (5.13)$$

$$C_j = F_j/v$$

$$\frac{dF_1}{dV_R} = -r_1$$

$$\frac{dF_2}{dV_R} = -(r_1 + r_2)$$

where F_1 through F_5 represent acetylene, hydrogen, ethylene, ethane and nitrogen molar flowrates respectively and v is the volumetric flowrate. As is well known, V_R , the volume of the reactor, is the counterpart of time t and is the independent variable in the simulations. The above equations were written in the form of a Fortran subroutine which was used in conjunction with the DRKGS subroutine described earlier.

The results of the simulations are plotted using the attainable set concept as was done by Horn and Bailey (1968) and are presented in Figure 5.16. It should be pointed out that the volume of the plug-flow reactor was allowed to vary

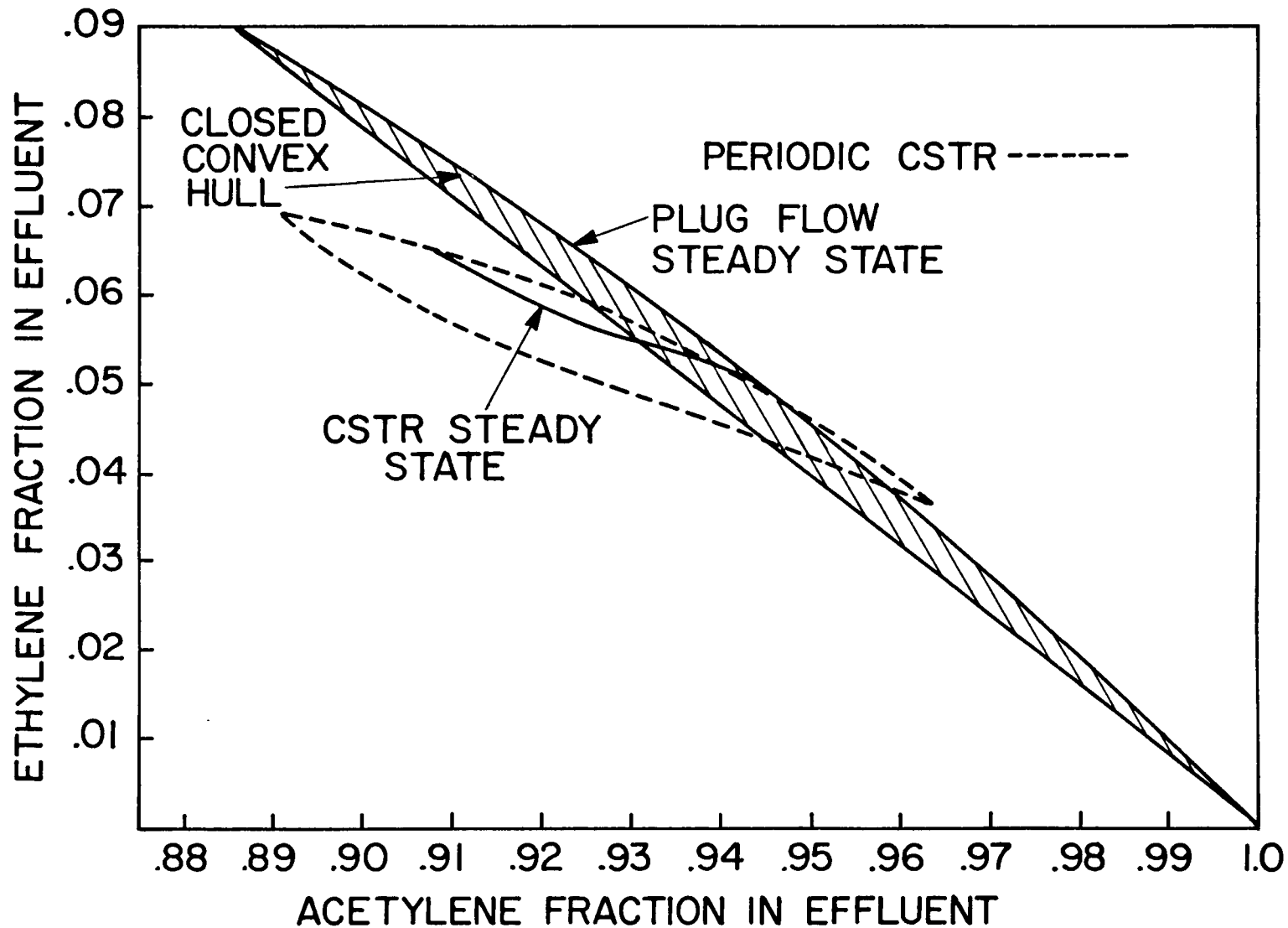


Figure 5.16 "Attainable Sets" of effluent compositions obtained by simulations of a plug-flow reactor and from cyclic experiments with the spinning basket reactor (Catalyst I)

indefinitely so that the entire plotted range of the two variables shown in the figure was covered. The result of this procedure is that the attainable set for the plug-flow model plotted in Figure 5.16 contains effluent compositions for cases in which the mean residence time was much greater than that used in actual experiments with the spinning-basket reactor. As indicated by Bailey (1972) imposing forced cycles on this oversimplified reactor model gives only points within the closed convex hull of the steady-state attainable set. This attainable set for periodic operation is the closed region shown in the figure. The sole purpose of this computational exercise with the ideal plug-flow model was to illustrate the fact (proved earlier by Horn and several other investigators of periodic reactors) that forced cycling of a CSTR gives rise to compositions which are unavailable by any policy of cycling a plug-flow reactor, over the entire range of the manipulated variable.

Having discussed Catalyst I at considerable length, only the interesting and significant results obtained with the other catalysts will be presented below. At the same time, attention will be given to important similarities and differences among them.

5.3 Catalyst II

Catalyst II contained about 60% nickel on a kieselguhr. This catalyst was used mainly in preliminary experiments to learn about the behavior of the reaction and the experimental

system. The initial steady-state data for Catalyst II is shown in Figure 5.17. As compared to Catalyst I the conversion of acetylene to products is much higher and the steady-state ethylene curve passes through a maximum. This maximum is similar to the one in Lee's study and as shown in Table 5.2 a Komiyama and Inoue type Langmuir-Hinshelwood rate expression pair appears to be the best fit for this catalyst. Since this catalyst had caused severe fouling and cleaning problems in the preliminary stages and evidence of similar fouling was present after the first three experiments, further study of Catalyst II was discontinued.

5.4 Catalyst III

A more complete set of experiments was done with Catalyst III which gave higher absolute conversions than Catalyst I for the same feed conditions. However, this catalyst, which had a higher nickel content and more acid sites than Catalyst I, was found to be subject to severe fouling. In order to keep track of the gradual decline in catalyst activity, the sequence of experiments was modified in such a way that periodic experiments were sandwiched in between steady-state experiments. Figure 5.18 shows a comparison of steady-state and periodic time-average data for ethane on Catalyst III. The results show an increasing trend in ethane selectivity due to cycling which was counter to the gradual decline in catalyst activity due to drastic fouling. The steady-state region shown on this figure indicates the attainable set of ethane compositions by steady-

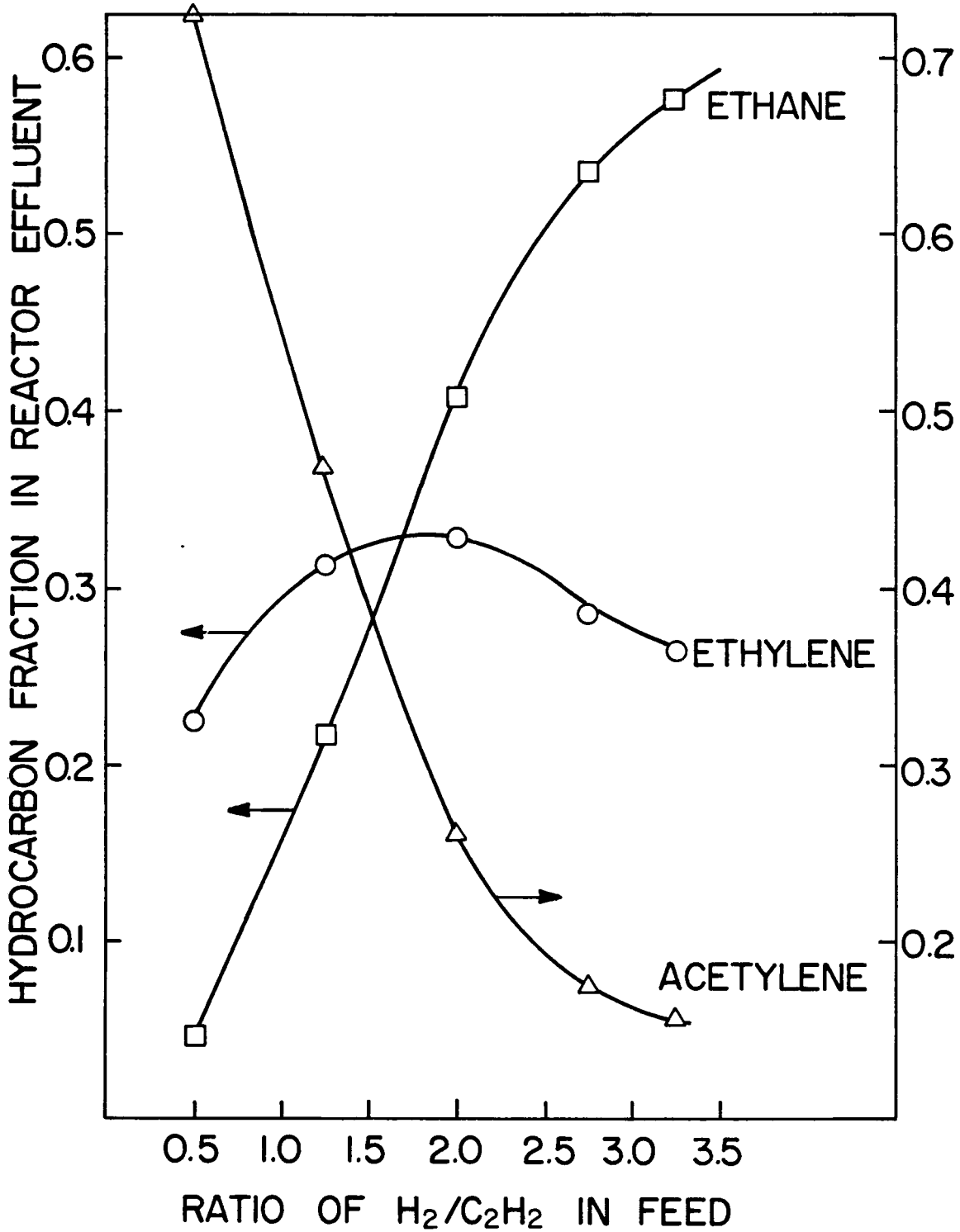


Figure 5.17 Steady-state effluent compositions obtained by experiments with Catalyst II

TABLE 5.2

STEADY STATE DATA FIT FOR CATALYST II

MODEL RATE EXPRESSIONS	CONSTANTS	STANDARD DEVIATIONS
1) $r_1 = \frac{k_1 C_1 C_2}{1 + K_2 C_2}$ $r_2 = \frac{k_3 C_3 C_2^{0.5}}{1 + K_2 C_2}$	$k_1 = 681.53 \text{ l}/(\text{mol-min})$ $K_2 = -65.08 \text{ l/mol}$ $k_3 = 17.64 \text{ l}/(\text{mol-min})$	$\sigma_1 = 0.31724 \times 10^{-3}$ $\sigma_2 = 0.11919 \times 10^{-3}$
2) $r_1 = \frac{k_1 C_1 C_2}{1 + K_2 C_1}$ $r_2 = \frac{k_3 C_3 C_2^n}{1 + K_2 C_1}$	$k_1 = 1115.85 \text{ l}/(\text{mol-min})$ $K_2 = 326.56 \text{ l/mol}$ $k_3 = 95.76 \text{ l}/(\text{mol-min})$ $n = 0.712$	$\sigma_1 = 0.19809 \times 10^{-3}$ $\sigma_2 = 0.44768 \times 10^{-4}$
3) $r_1 = \frac{k_1 C_1 C_2}{1 + K_2 C_2}$ $r_2 = \frac{k_3 C_3 C_2}{1 + K_2 C_2}$	$k_1 = 741.37 \text{ l}/(\text{mol-min})$ $K_2 = -46.44 \text{ l/mol}$ $k_3 = 315.29 \text{ l}/(\text{mol-min})$	$\sigma_1 = 0.28230 \times 10^{-3}$ $\sigma_2 = 0.18164 \times 10^{-3}$

TABLE 5.2 (continued)

MODEL RATE EXPRESSIONS	CONSTANTS	STANDARD DEVIATIONS
4) $r_1 = \frac{k_1 C_1 C_2}{1 + K_2 C_1}$ $r_2 = \frac{k_3 C_1 C_2^{0.5}}{1 + K_2 C_1}$	$k_1 = 1153.18$ $K_2 = 380.63$ $k_3 = 29.69$	$\sigma_1 = 0.19612 \times 10^{-3}$ $\sigma_2 = 0.10334 \times 10^{-3}$
5) $r_1 = \frac{k_1 C_1 C_2}{(1+K_3 C_1)(1+K_4 C_2)} + \frac{k_2 C_1 C_2}{(1+K_3 C_1)}$ $r_2 = \frac{k_5 C_3 C_2}{(1+K_7 C_3)(1+K_4 C_2)} + \frac{k_6 C_3 C_2}{1+K_7 C_3}$	$k_1 = -6.60 \frac{\ell}{\text{mol-min}} \quad K_3 = 264.92 \frac{\ell}{\text{mol}}$ $k_2 = 1007.70 \frac{\ell}{\text{mol-min}} \quad K_4 = -305.02 \frac{\ell}{\text{mol}}$ $k_5 = -1.72 \frac{\ell}{\text{mol-min}} \quad K_7 = -618.52 \frac{\ell}{\text{mol}}$ $k_6 = 1.82.94 \frac{\ell}{\text{mol-min}}$	$\sigma_1 = 0.24831 \times 10^{-3}$ $\sigma_2 = 0.14615 \times 10^{-4}$
6) $r_1 = \frac{k_1 C_1 C_2}{1 + K_2 C_1}$ $r_2 = \frac{k_3 C_3 C_2}{1 + K_2 C_1}$	$k_1 = 1038.22 \ell/(\text{mol-min})$ $K_2 = 214.12 \ell/\text{mol}$ $k_3 = 443.01 \ell/(\text{mol-min})$	$\sigma_1 = 0.21559 \times 10^{-3}$ $\sigma_2 = 0.13340 \times 10^{-3}$

state operation throughout the entire useful life of this catalyst and hence includes effects which are a direct consequence of the fouling. Figure 5.18 clearly demonstrates that in spite of fouling, periodic operation of chemical reactors gives rise to product compositions which are unavailable in any steady-state operation. The steady-state data showing deactivation trends is presented in Figure 5.19. As the deactivation proceeds, the maximum in the ethylene steady-state curve appears to disappear. The ethane production also declines from experiment 1 to experiment 2 and then appears to pick up again in the next experiment. Owing to the presence of variations in kinetic behavior among experiments and possible mass transfer disguises caused by residue deposited on this catalyst, modeling was not attempted in this case.

Step response experiments for this catalyst show that when the reactor is subjected to a step increase in feed hydrogen, the ethylene concentration profile exhibits damped oscillations, while ethane and acetylene show an overshoot and an undershoot, respectively, followed by a slow monotonic approach to the final steady-state value. On the other hand, an asymmetric response was again observed for a step decrease in feed hydrogen (Figure 5.20).

Figure 5.21 shows the results of a parametric study of the instantaneous concentration-time profiles obtained by cyclic operation with Catalyst III for different τ 's and γ 's. All these curves were obtained from gas chromatographic

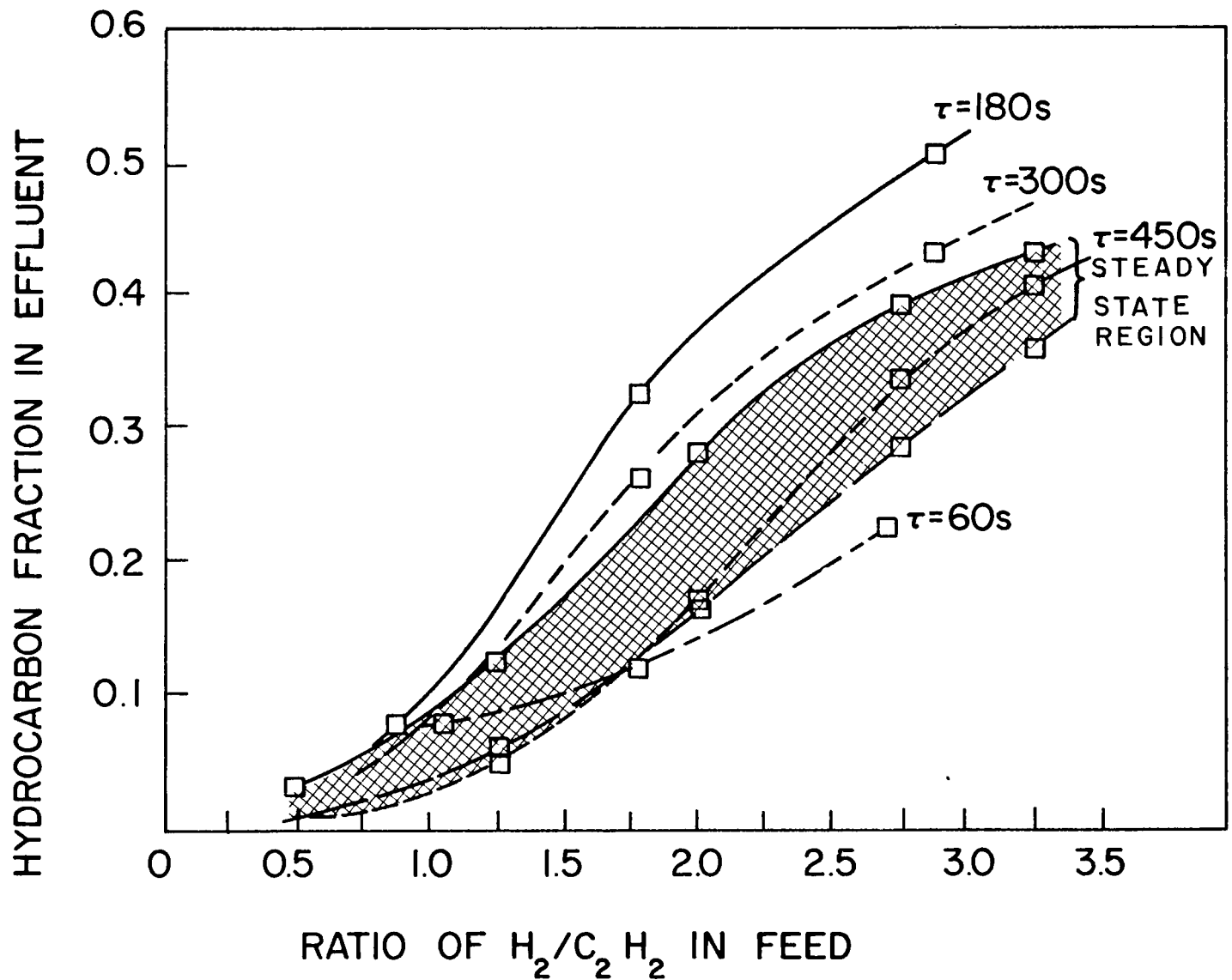


Figure 5.18 The shaded region shows the domain of ethane yields obtained in several different steady-state experiments at different stages of deactivation of Catalyst III. The curves show ethane yields obtained by cycling feed hydrogen concentration with different periods

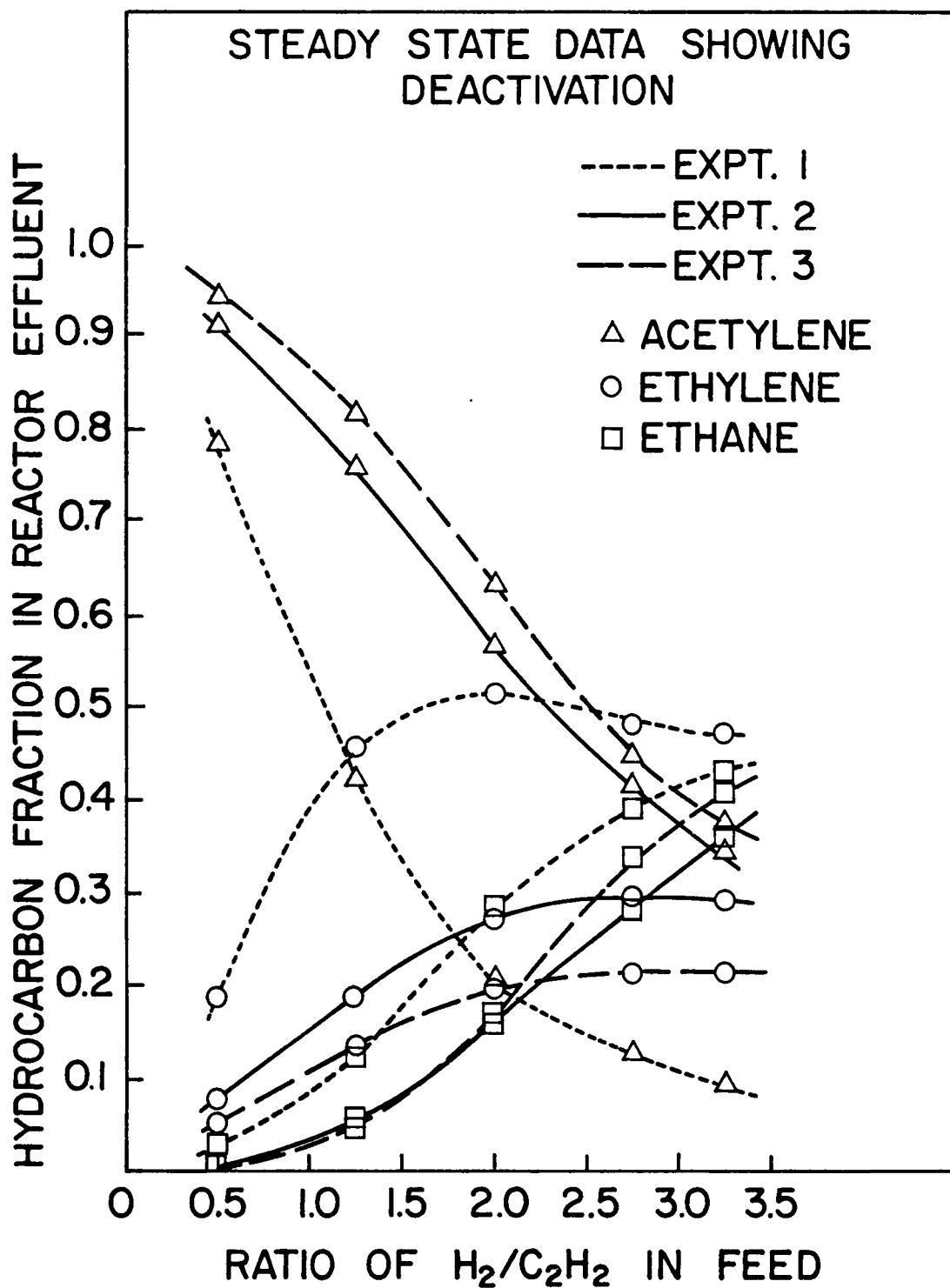


Figure 5.19 Effect of fouling on steady-state effluent compositions for Catalyst III

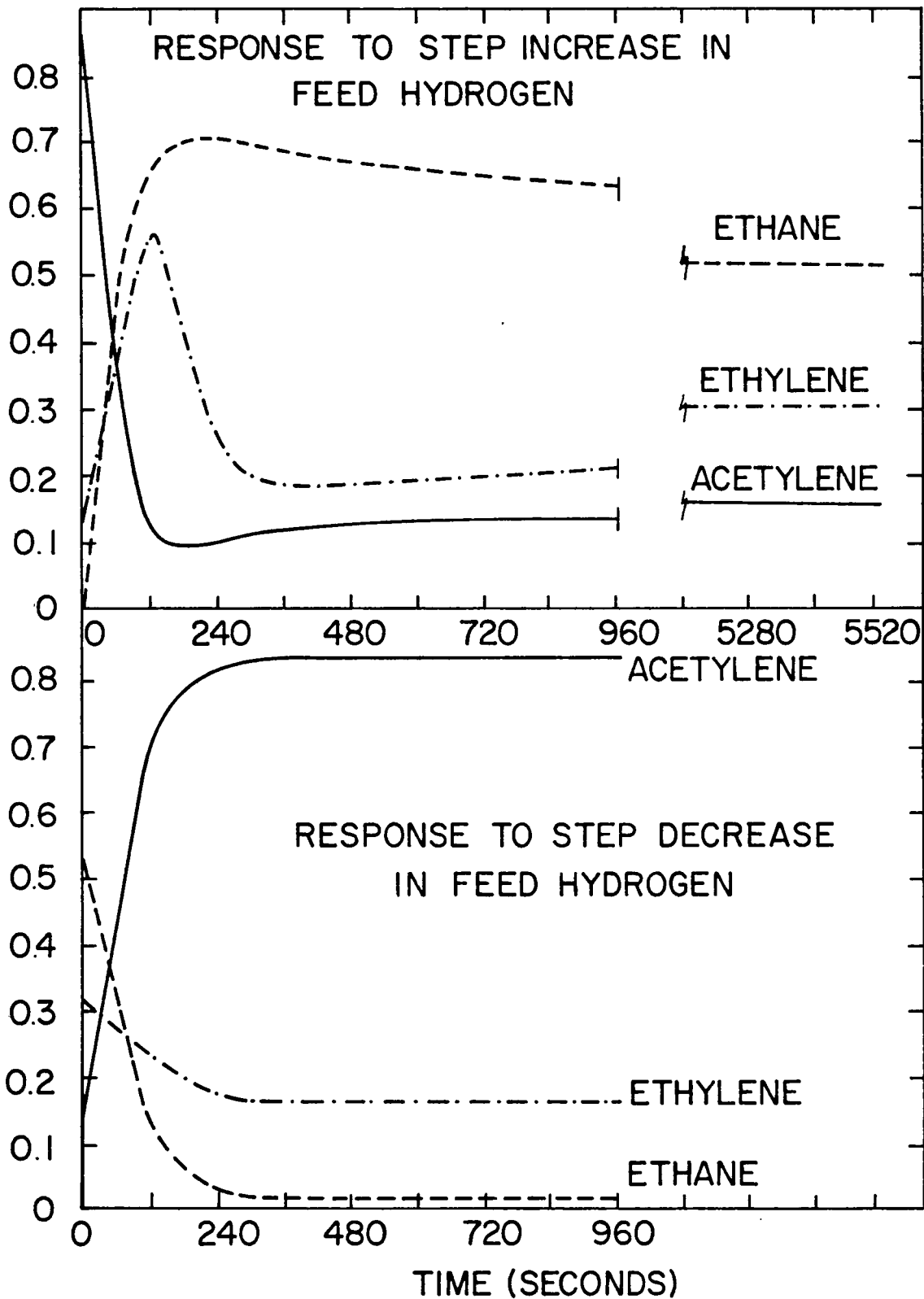


Figure 5.20 Feed hydrogen step-up (A) for Catalyst III produces a damped oscillation in effluent ethylene in contrast to a step-down in feed hydrogen (B)

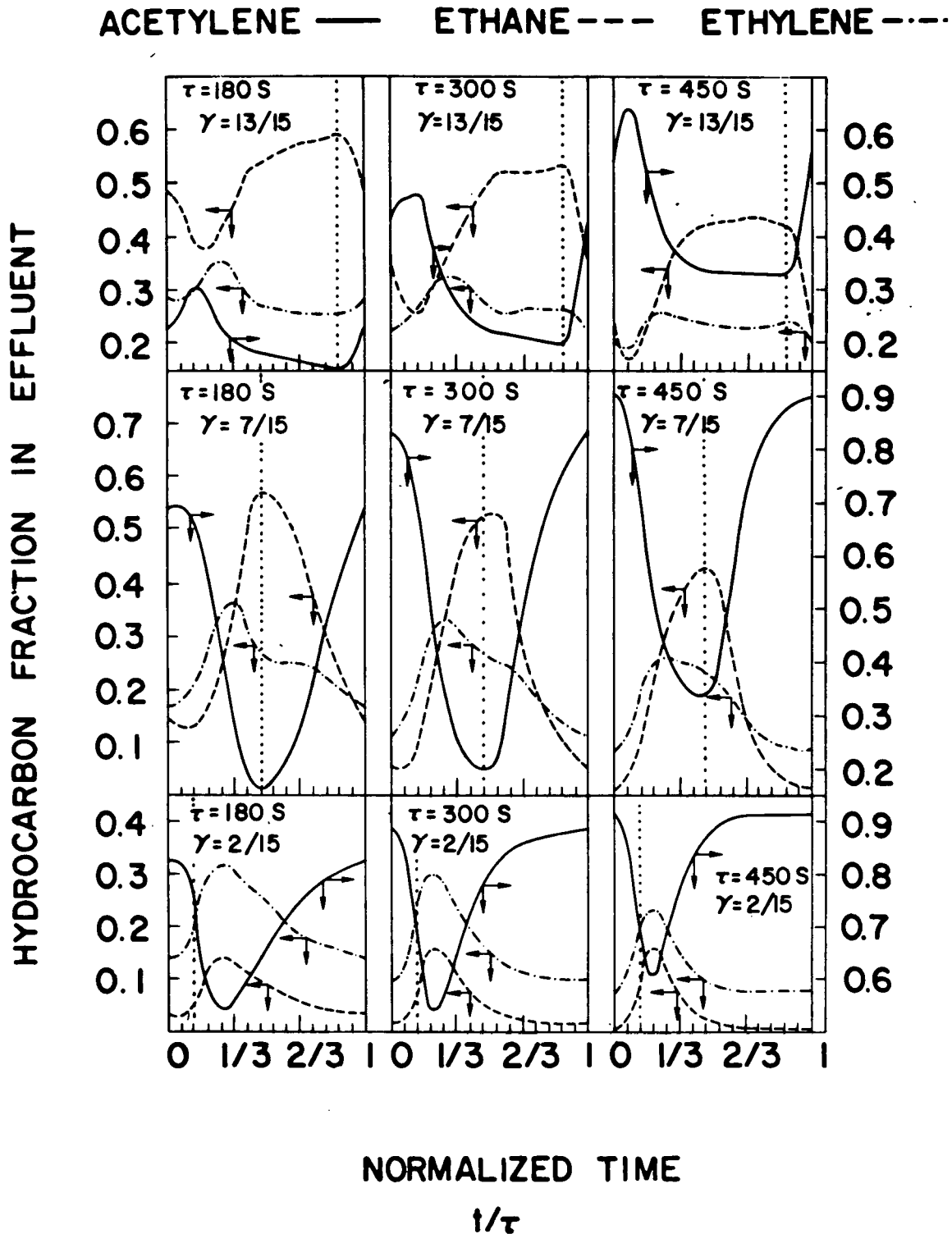


Figure 5.21 Instantaneous effluent compositions for feed hydrogen cycling with Catalyst III for nine sets of periods (τ) and mean hydrogen feed rates (directly related to γ : See Equation 5.3)

measurements. Once more, as with Catalyst I, for $\gamma = 2/15$ and all three τ 's the profiles tend to overshoot the switching point. As expected, for a fixed value of γ , the peaks in the wave-forms tend to become sharper as τ increases, and this effect is most clearly seen in the bottom row of diagrams. The curves for $\gamma = 7/15$ are different in that acetylene and ethane seem to follow the switch from high to low hydrogen feed rate fairly well although they tend to overshoot the reverse switching point. The behavior of ethylene for these cases is dramatically different. In the case of $\gamma = 13/15$ all three components follow the high to low hydrogen switch very well, but show a considerable lag for the reverse operation. These rather unusual response patterns have been confirmed by continuous infra-red measurements (see Figure 5.22).

The SEM pictures for Catalyst III are very striking in that the appearance of the surfaces of the fresh and fouled catalyst are dramatically different. These are shown in Figures 5.23 and 5.24, respectively. The surface of the fresh catalyst looks like a garbage heap whereas the thick coating of residue makes the fouled catalyst look like a chocolate covered peanut bar. The next two pictures of the prepoisoned catalyst are even more interesting because of the presence of regular crystalline structures on the fractured surface. The dark rod-like split plates of alumina are shown in Figure 5.25. When the typical prepoisoned particle was further magnified (x 18,500 where 1mm on photo represents 540 \AA) tiny face-

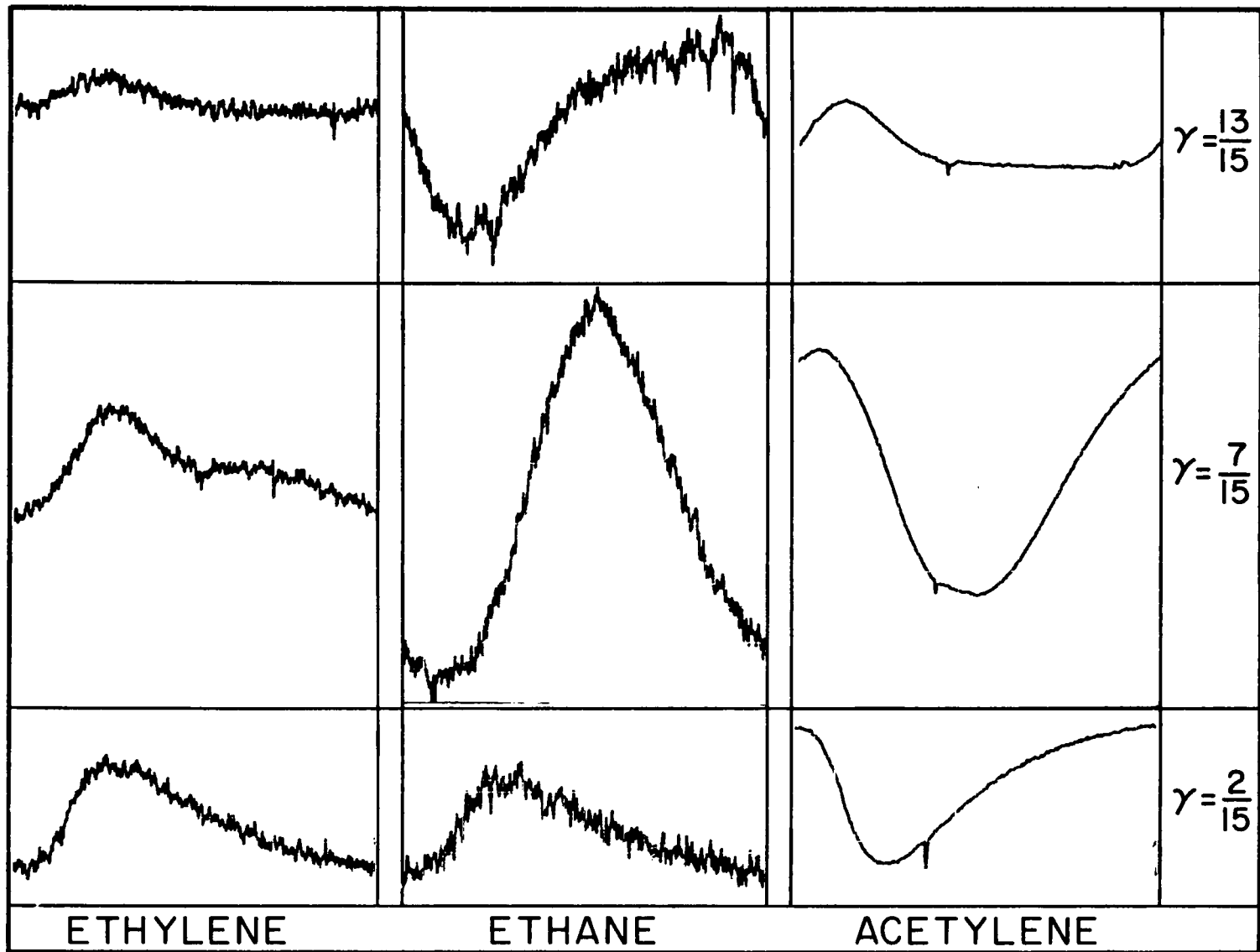


Figure 5.22 Periodic effluent concentrations for three different switching fractions as measured continuously using the ir analyzer ($\tau = 180$ s, Catalyst III)

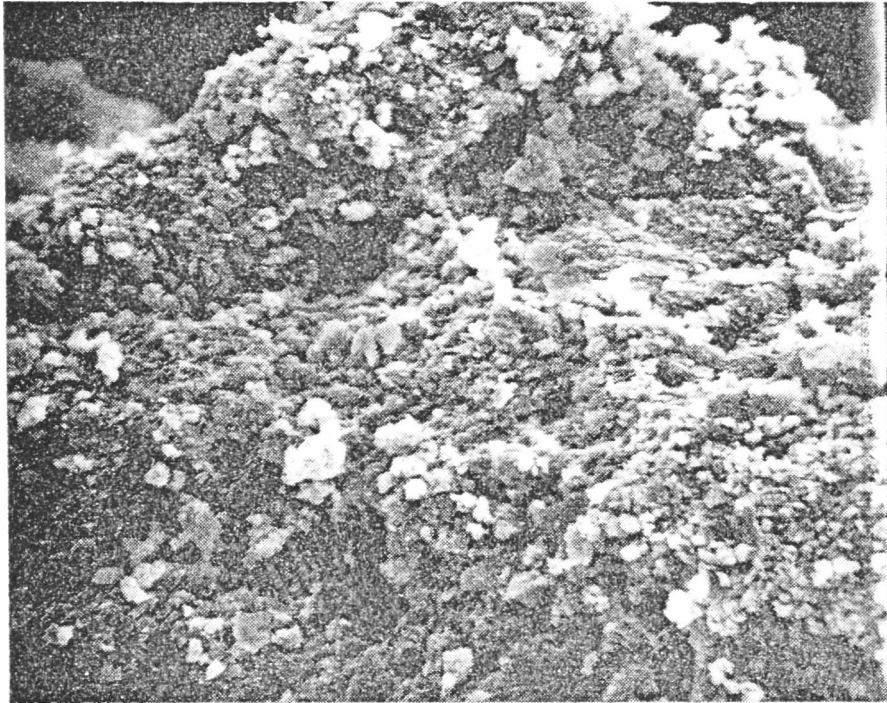


Figure 5.23 SEM photograph of Catalyst III - (fresh sample)

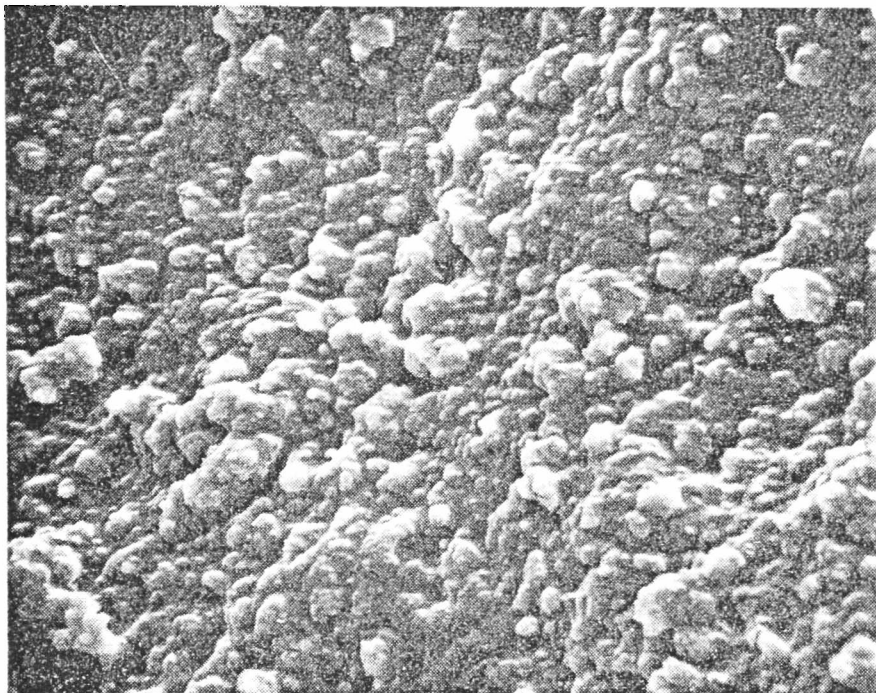


Figure 5.24 SEM photograph of Catalyst III - (fouled sample)

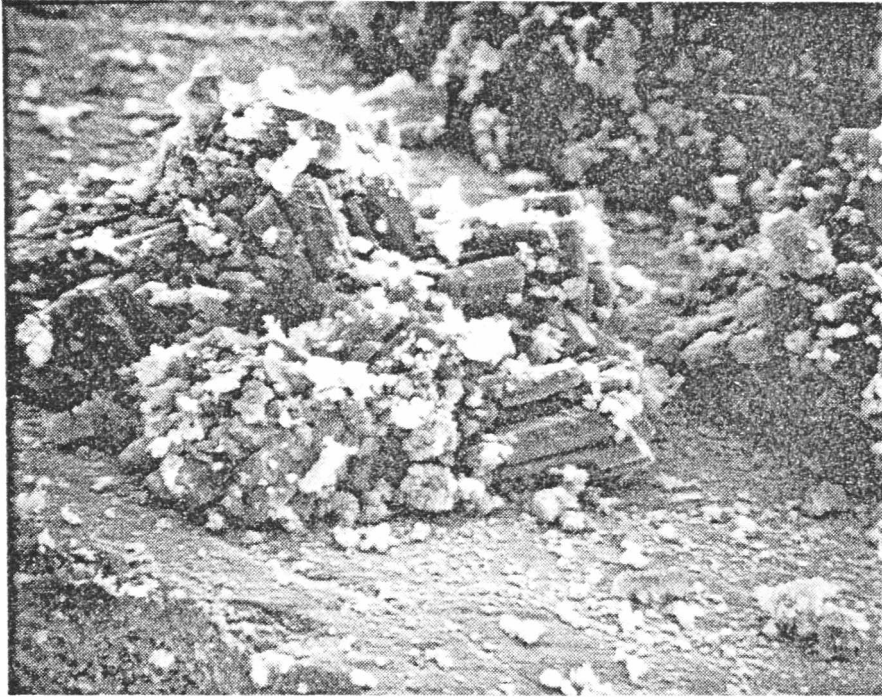


Figure 5.25 SEM photograph of Catalyst III - (prepoisoned sample)

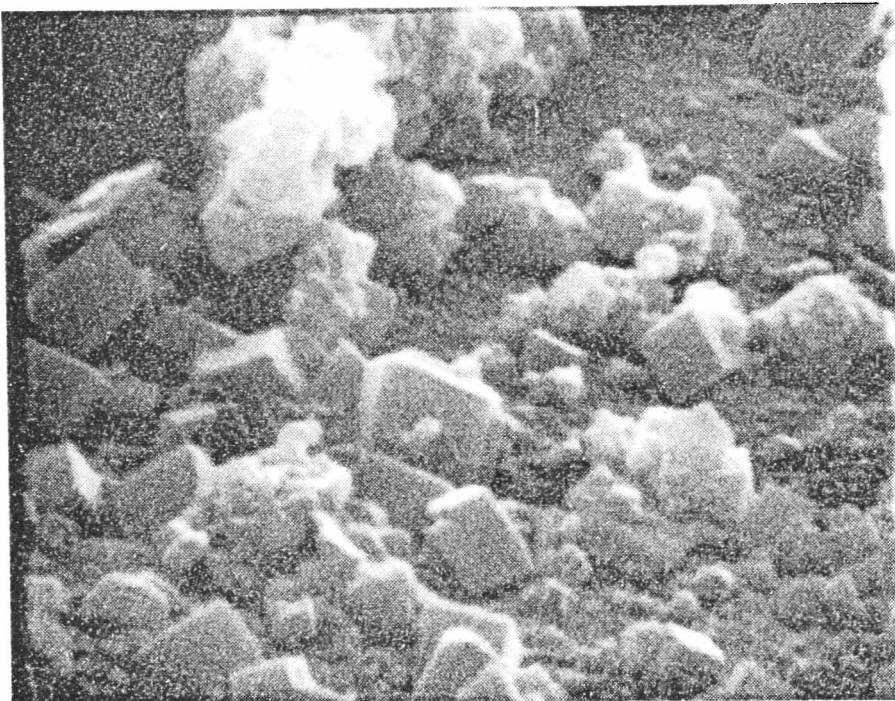


Figure 5.26 SEM photograph of Catalyst III (magnified view of a small region of Figure 5.25)

centered-cubic crystals of nickel became visible. (See Figure 5.26) The popcorn-like particles near the cubes are clusters of sulphur. As was the case with Catalyst I, the other three pictures of Catalyst III are for a magnification factor of 900.

5.5 Catalyst IV

Another set of intriguing results was shown by Catalyst IV. Studies with this catalyst indicate that, apart from changing steady-state behavior, the deactivation caused by fouling can completely change the dynamic characteristics of the stirred tank. The experimental data for a response to identical step increases in feed hydrogen for fresh and fouled catalyst are presented in Figures 5.27 and 5.28 respectively. These figures reveal a lot of interesting features. The change in steady-state behavior is manifested by the shifts in the initial and final values of the concentrations of all three hydrocarbon species. While the ethylene profile for the fresh catalyst is very intriguing by itself, the major changes in both acetylene and ethylene profiles for the fresh and fouled catalysts are even more dramatic. For the fresh catalyst, the ethylene concentration exhibits a wrong-way behavior, increasing sharply at first and then rapidly declining to the final steady-state value corresponding to the higher input hydrogen concentration. This kind of anomalous behavior is absent for the fouled catalyst which, however, does exhibit a slower broader peak in the ethylene profile. On the other hand, the acetylene trajectory

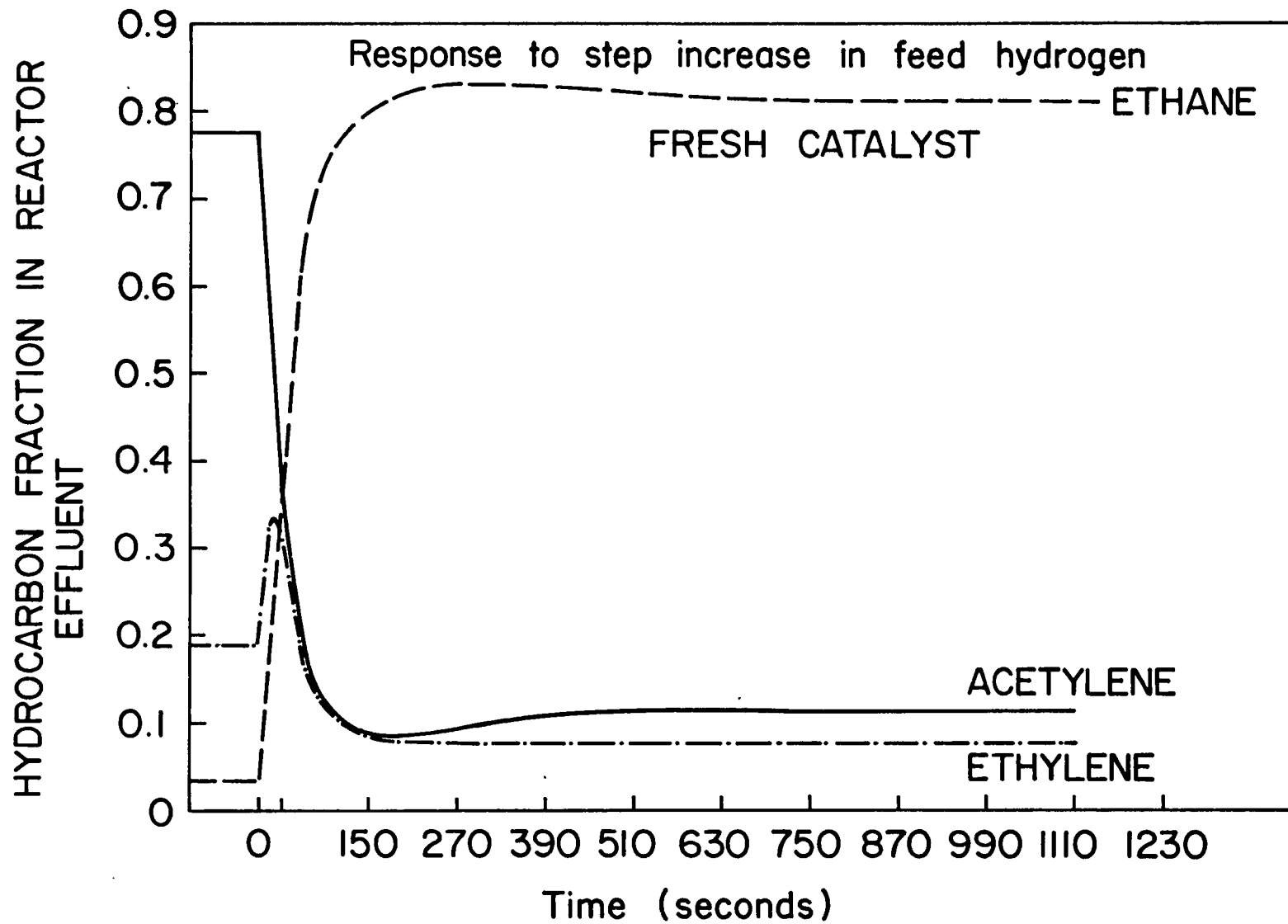


Figure 5.27 Experimental step-response data for Catalyst IV

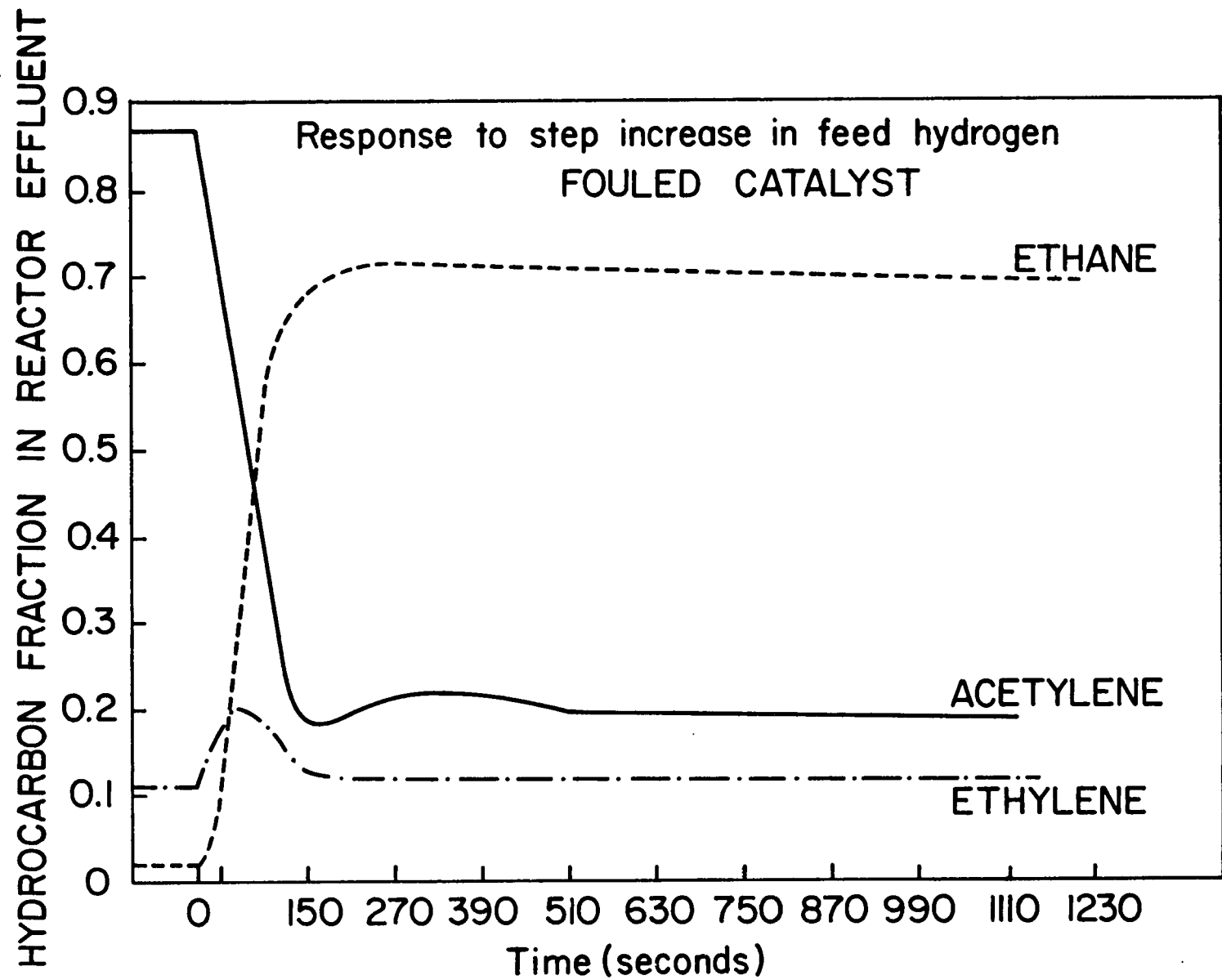


Figure 5.28 Experimental step-response data for Catalyst IV

for fresh catalyst reveals a single undershoot, and damped oscillations are seen for the poisoned catalyst sample.

The response to a step decrease in feed hydrogen is shown next in Figures 5.29 and 5.30. Once again the ethylene profile reveals major changes due to deactivation and the presence of the wrong-way phenomenon (see Mehta's study (1978) for a detailed mathematical analysis and explanation of wrong-way behavior). It appears that the poisoning affects different elementary reaction steps differently and needs to be investigated more thoroughly in the future. Clearly, the effect of poisoning is more complex than is often assumed conventionally in writing kinetic expressions in which a factor less than unity is used as a multiplier. The importance of such drastic changes in behavior on the stability and control of chemical reactors cannot be over emphasized.

Owing to fairly rapid fouling of Catalyst IV, one set of steady-state and periodic time-average measurements ($\tau = 30$ s) were made in the same run, followed by another set of periodic time-average measurements ($\tau = 60$ s) the next day. Figure 5.31 shows the results of this series of experiments. The periodic time-average data show that even for the poisoned catalyst the acetylene conversion is higher and ethane production is up. However, the ethylene production progressively declined with each successive experiment even though all the measurements were made in the relatively short time-span indicated above. This behavior of ethylene is not unreasonable, considering the

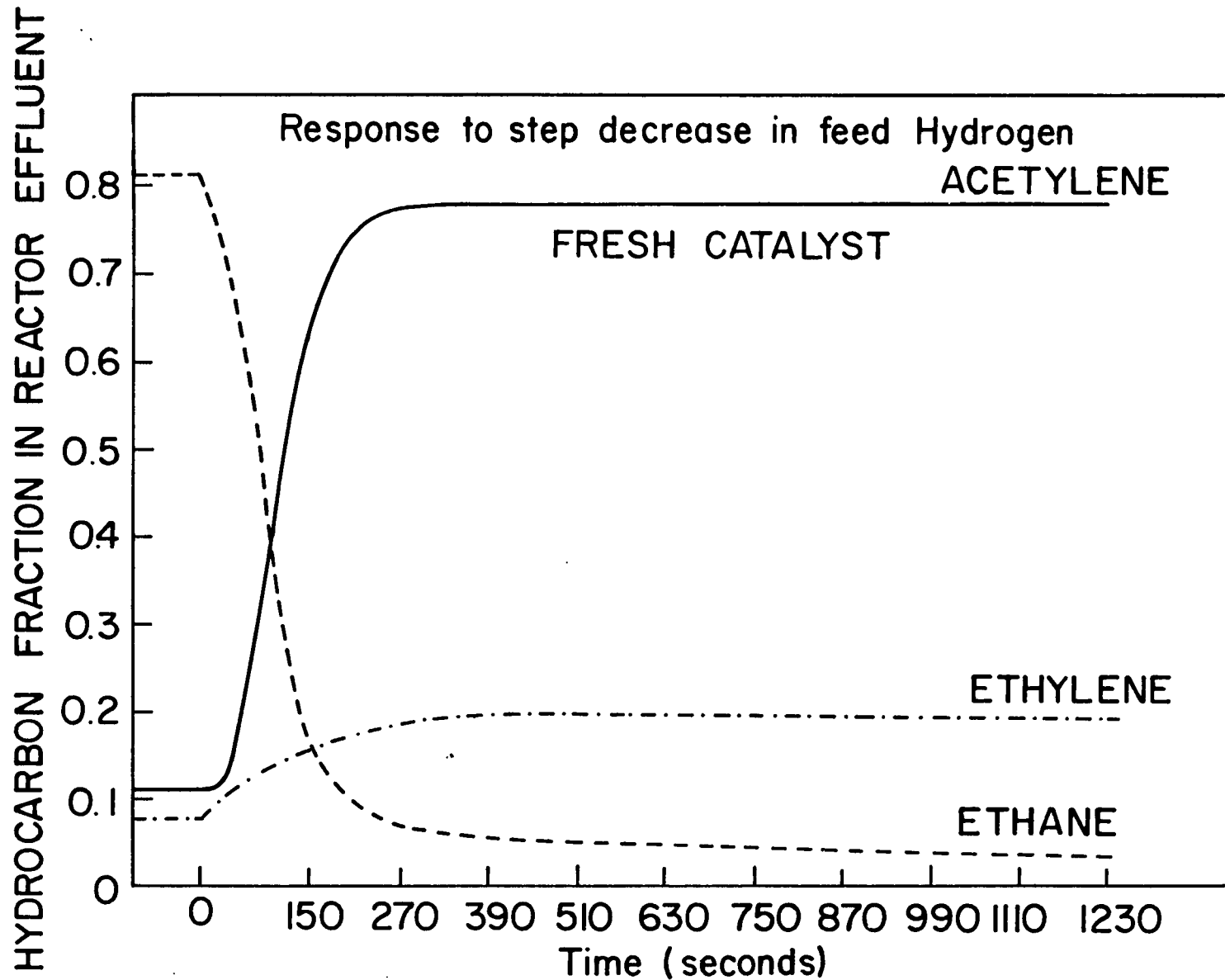


Figure 5.29 Experimental step-response data for Catalyst IV

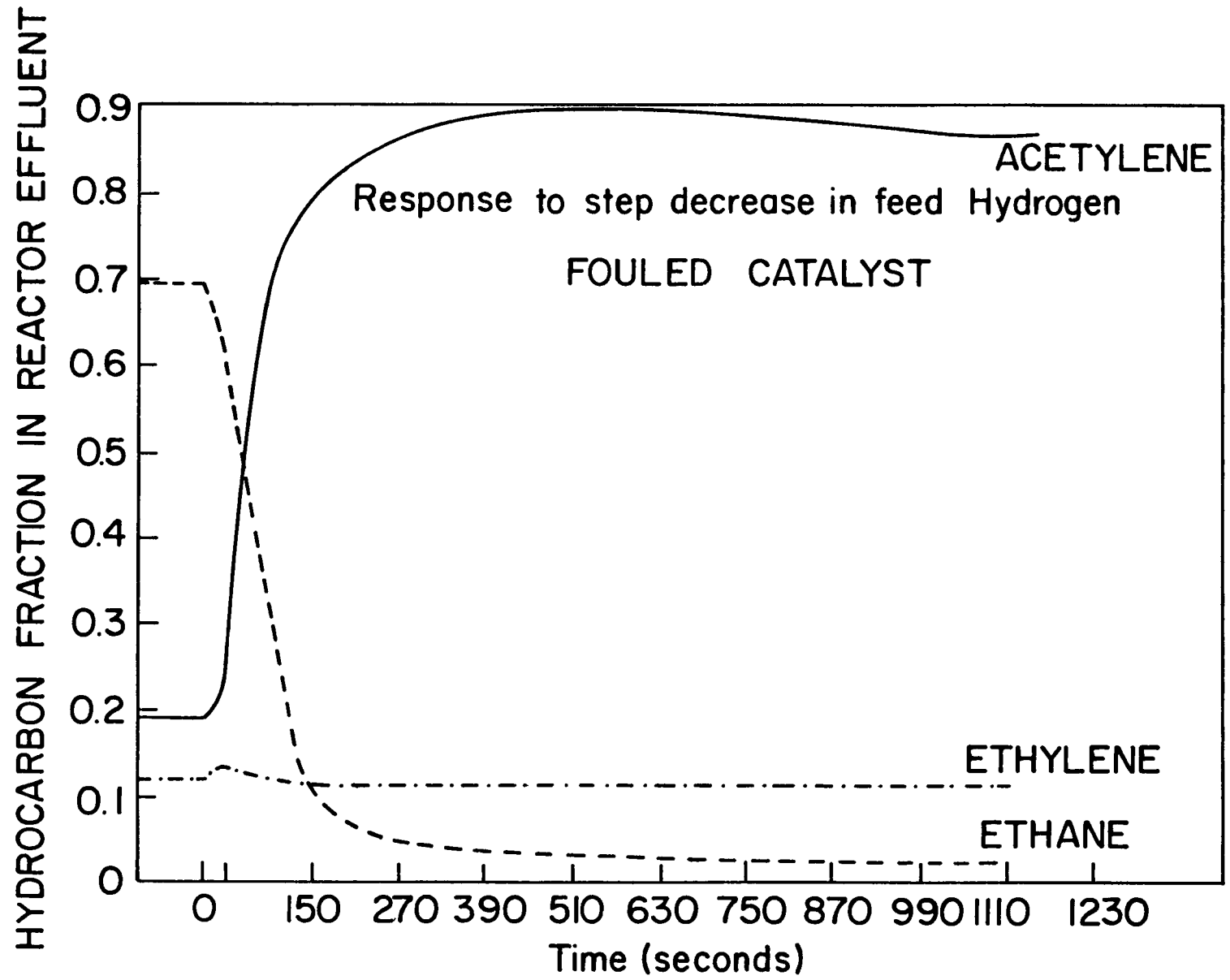


Figure 5.30 Experimental step-response data for Catalyst IV

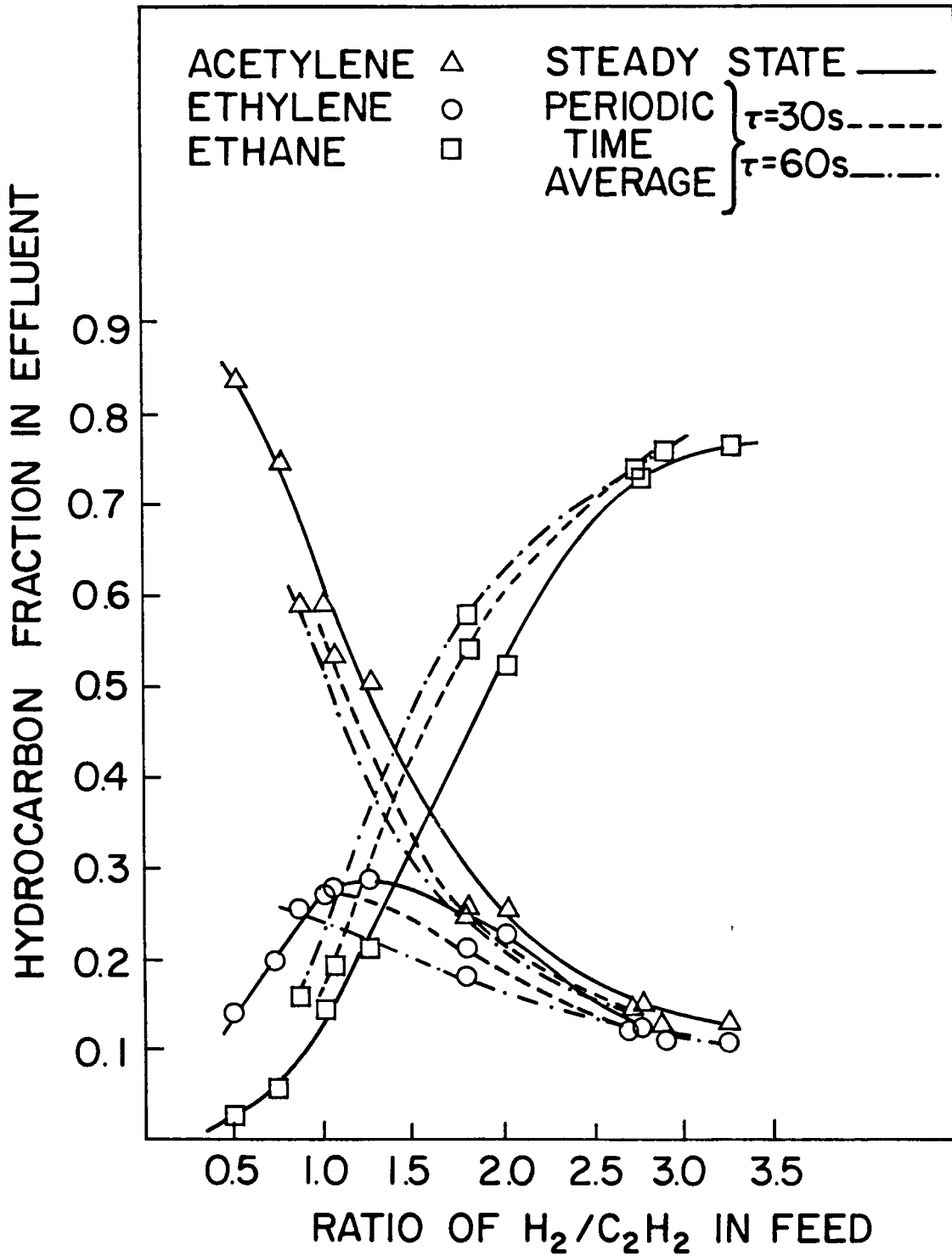


Figure 5.31 Steady-state (solid line) and periodic (broken lines—see legend) effluent hydrocarbon distributions for various time-average hydrogen/acetylene ratios for Catalyst IV

observations made with step-response measurements which clearly indicate that it is this hydrocarbon that is affected the most by fouling. Viewing periodic operation as a repetitive step-change operation, the periodic experiments with $\tau = 30$ s and $\tau = 60$ s were carried out with the intention of exploiting the ethylene peak of Figure 5.27. However, this strategy to improve time-average production of ethylene which had worked successfully with Catalyst I and in experiments on propylene oxidation by Renken (1974), misfired in this case. Although it is very difficult to pinpoint the reason for this failure, it is very likely that the wrong-way phenomenon played a significant role. As expected from earlier experience with Catalyst III the SEM pictures for Catalyst IV, shown in Figures 5.32 through 5.35 do reveal drastic fouling, Although they do not disclose any new information, these photos were included to complete the overall story on this catalyst and because the view of the residue-coated macro pore is simply spectacular.

5.6 Catalyst V

In order to overcome the single drawback of the spinning-basket reactor (the inability to measure catalyst temperature directly) a limited set of experiments was done with the stationary basket reactor. To avoid the problems associated with poisoning it was decided that Catalyst I would be used for these experiments.

A new sample of pellets was ground and treated as described in section 4.2. However, during the prepoisoning stage,

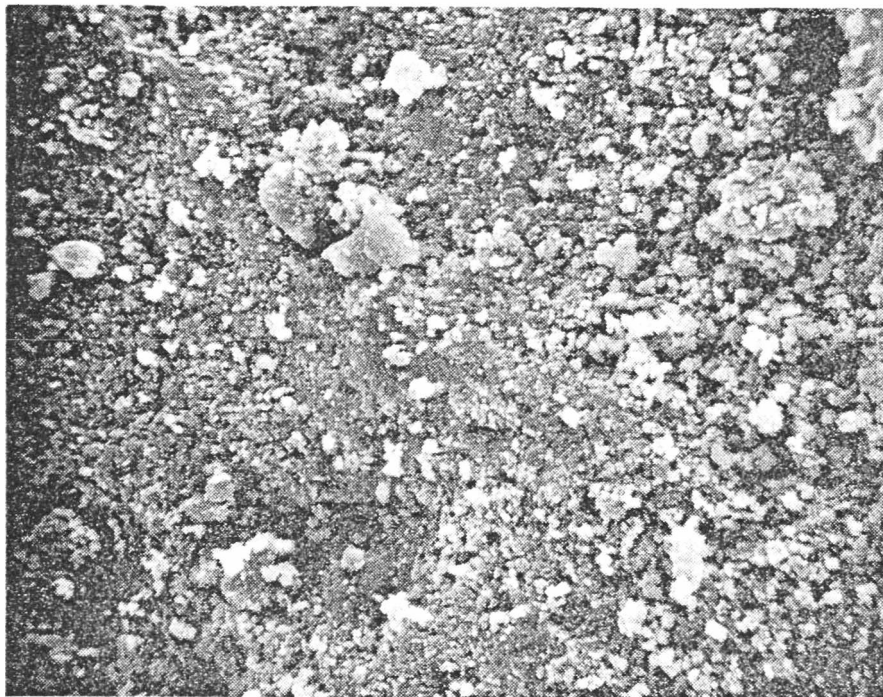


Figure 5.32 SEM photograph of Catalyst IV - (fresh sample)

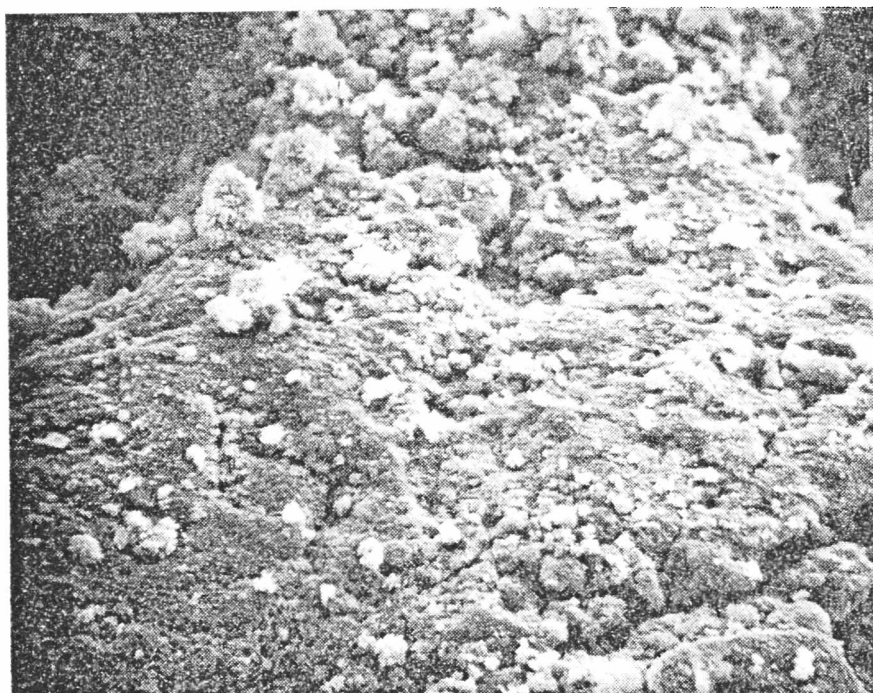


Figure 5.33 SEM photograph of Catalyst IV - (prepoisoned sample)

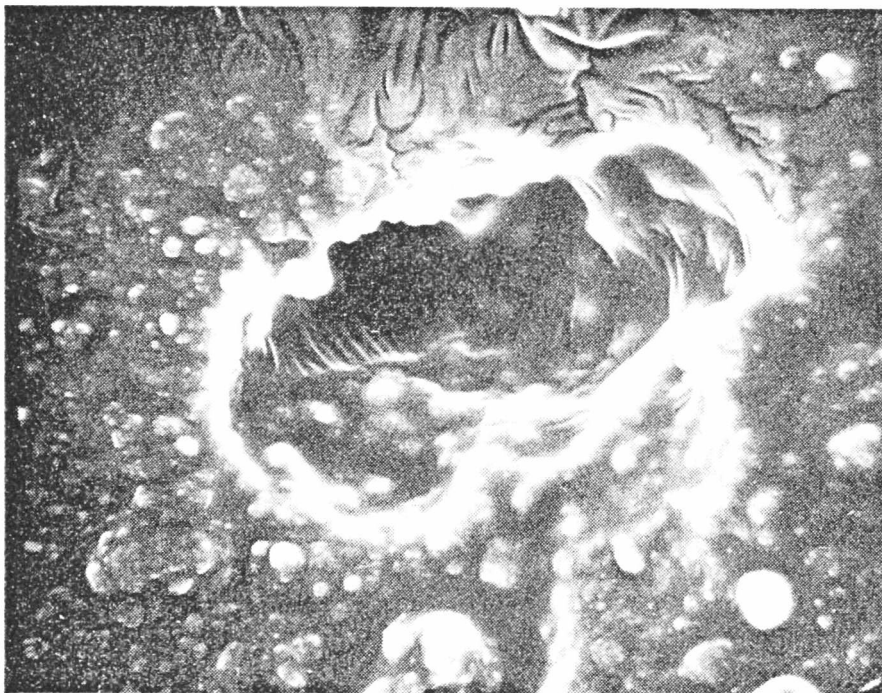


Figure 5.34 SEM photograph of Catalyst IV - (fouled sample)



Figure 5.35 SEM photograph of Catalyst IV - (enlarged view of portion of Figure 5.34)

the catalyst slurry was continuously stirred with a propeller-type agitator. This catalyst will henceforth be referred to as Catalyst V, and the significance of this will become self-evident later. The experimental results for Catalyst V are presented in Figures 5.36 and 5.37. The main purpose of these experiments was to monitor the catalyst bed temperature during dynamic operation and to verify that transient thermal effects are relatively unimportant. It can be concluded that this is indeed the case because the bandwidth of the measured catalyst temperature fluctuations did not exceed 2.5°C. Figure 5.36 shows the comparison between the steady-state and periodic time-average compositions obtained in the stationary basket reactor whereas Figure 5.37 shows similar data for Catalyst V in the spinning basket reactor. The stationary basket reactor data show that periodic operation does enhance the reactor performance for $\tau = 300$ and $\tau = 450$ s, the longer period showing the greatest improvement. It was assumed at first that this was Catalyst I, and so the differences in the shapes of the curves between Figures 5.1 and 5.36 caused considerable concern. When this catalyst (which did show slight discoloration caused by poisoning) was transferred to the spinning-basket, curves similar to those in Figure 5.36 were obtained and these have been presented in Figure 5.37. Similar shaped curves for both reactors point to the fact that the measured data for this set of experiments is internally consistent and is a property of the catalyst. However, for the spinning basket reactor,

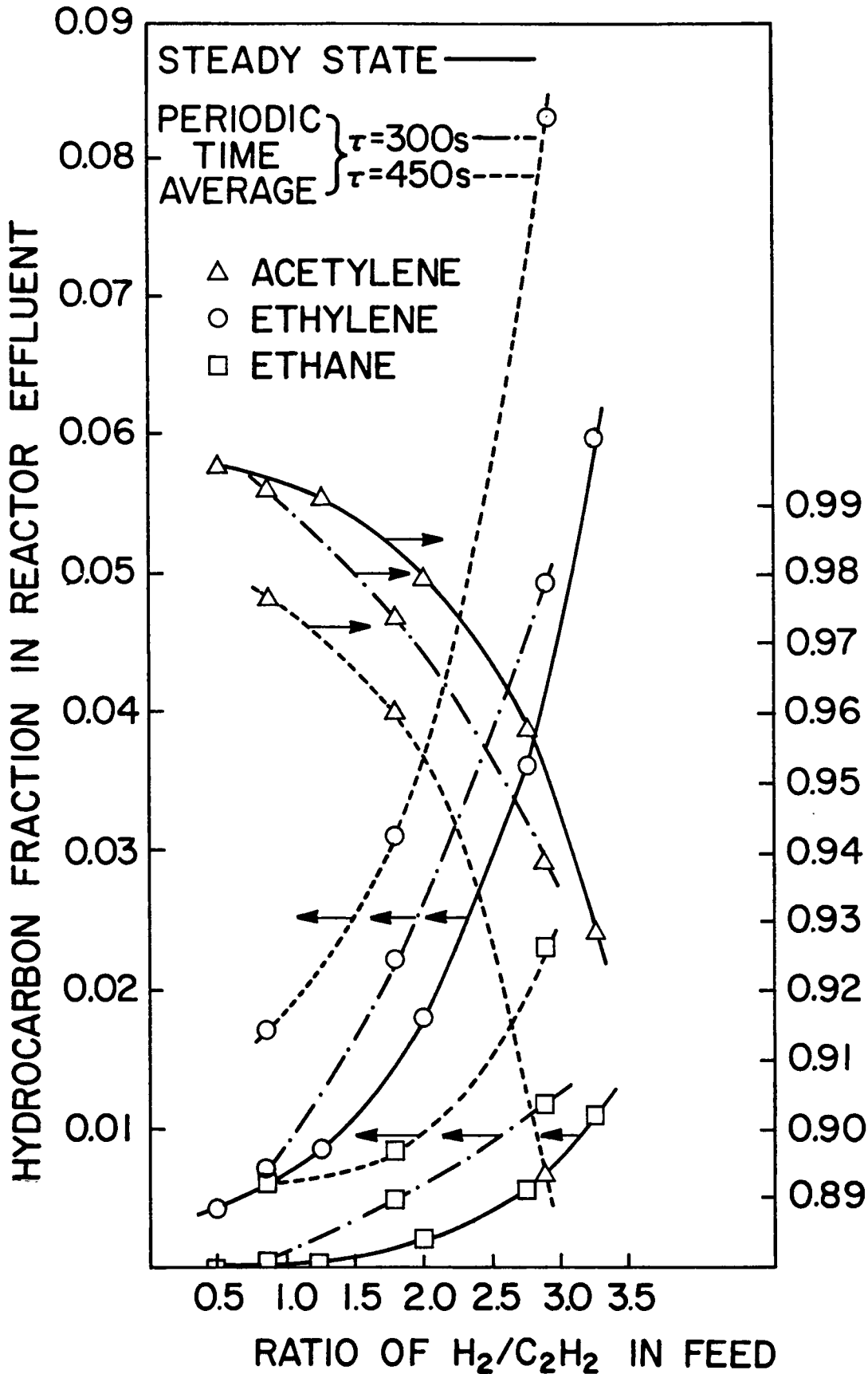


Figure 5.36 Steady-state (solid line) and periodic (broken lines—see legend) effluent hydrocarbon distributions for various time-average hydrogen/acetylene ratios for Catalyst V (stationary basket)

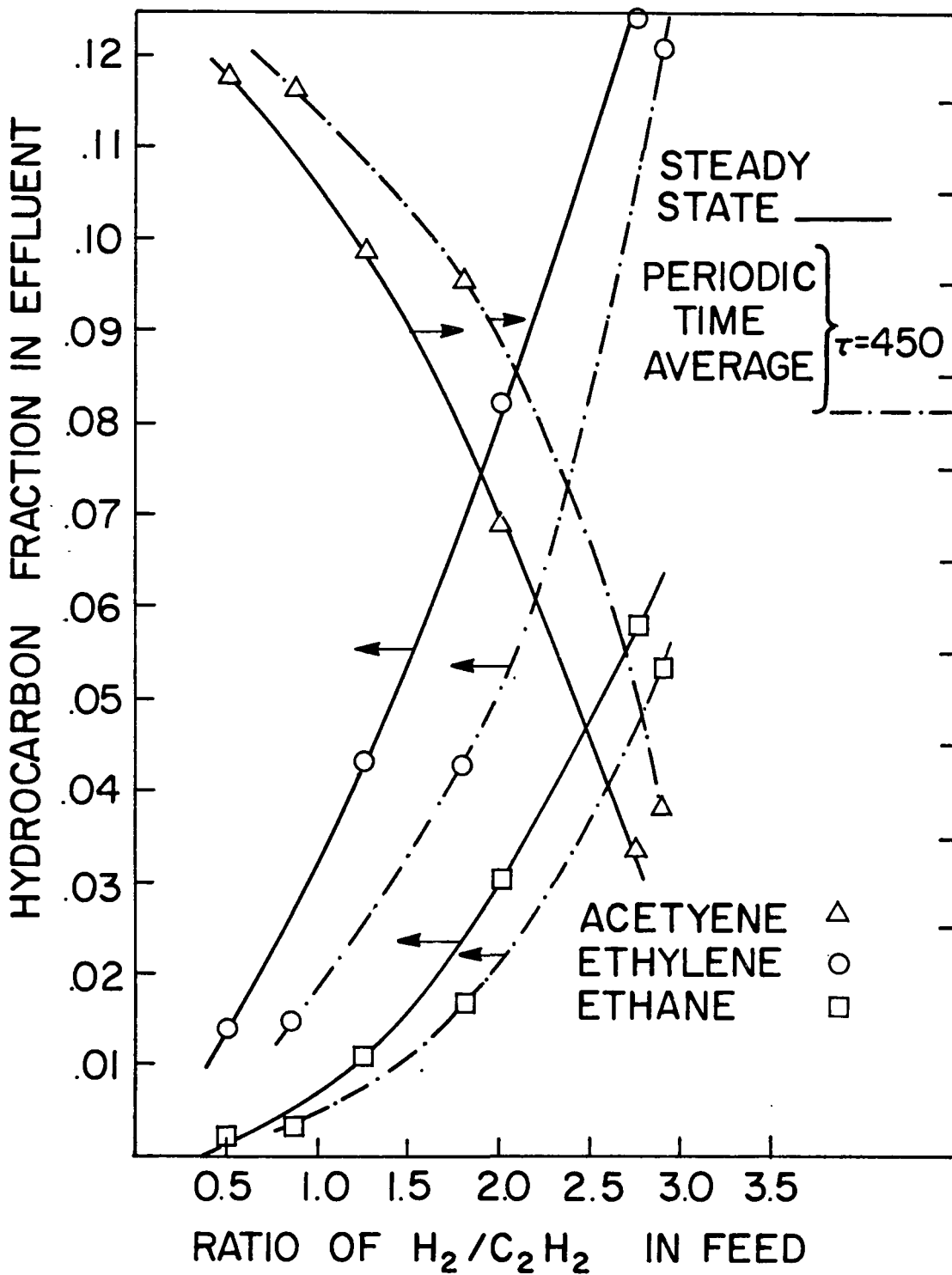


Figure 5.37 Steady-state (solid line) and periodic (broken lines—see legend) effluent hydrocarbon distributions for various time-average hydrogen/acetylene ratios for Catalyst V (spinning basket)

periodic operation with $\tau = 450$ s does not give any improvement over the steady-state which again is different from that of the stationary basket reactor.

Clearly at this stage there is an apparent controversy and two major questions may be posed:

1) Why have the characteristics of Catalyst I changed from the earlier set of experiments?

and 2) Why is there is discrepancy between the steady-states for the two reactors even though the very same catalyst was used?

It was hypothesized that the answers to these questions were:

1) The continuous stirring during the prepoisoning step caused a more uniform deposition of a large amount of sulphur on the particles, giving rise to an essentially "modified catalyst".

2) The stationary basket reactor does not provide as good a mixing as the spinning basket reactor.

Indeed, the additional experiments done to verify these hypotheses confirm the validity of the above statements. The results of the mixing tests are shown in Figure 5.7 presented earlier, and in Figure 5.38 which shows the actual infra-red response to a step feed of tracer. Additional comparison between the two reactors is shown in Table 5.3. Conventional B. E. T. measurements on prepoisoned samples of the two catalysts show a difference of $15 \text{ m}^2/\text{g}$ in total surface area.

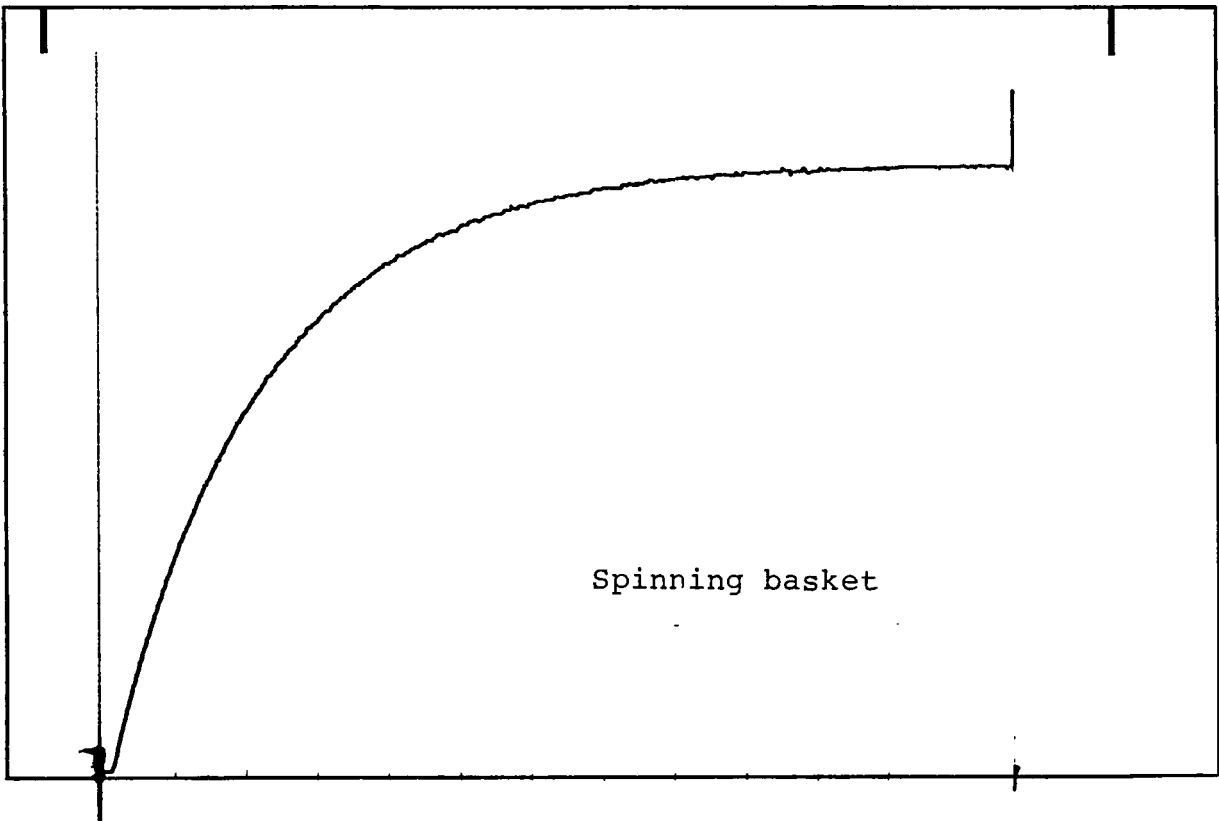
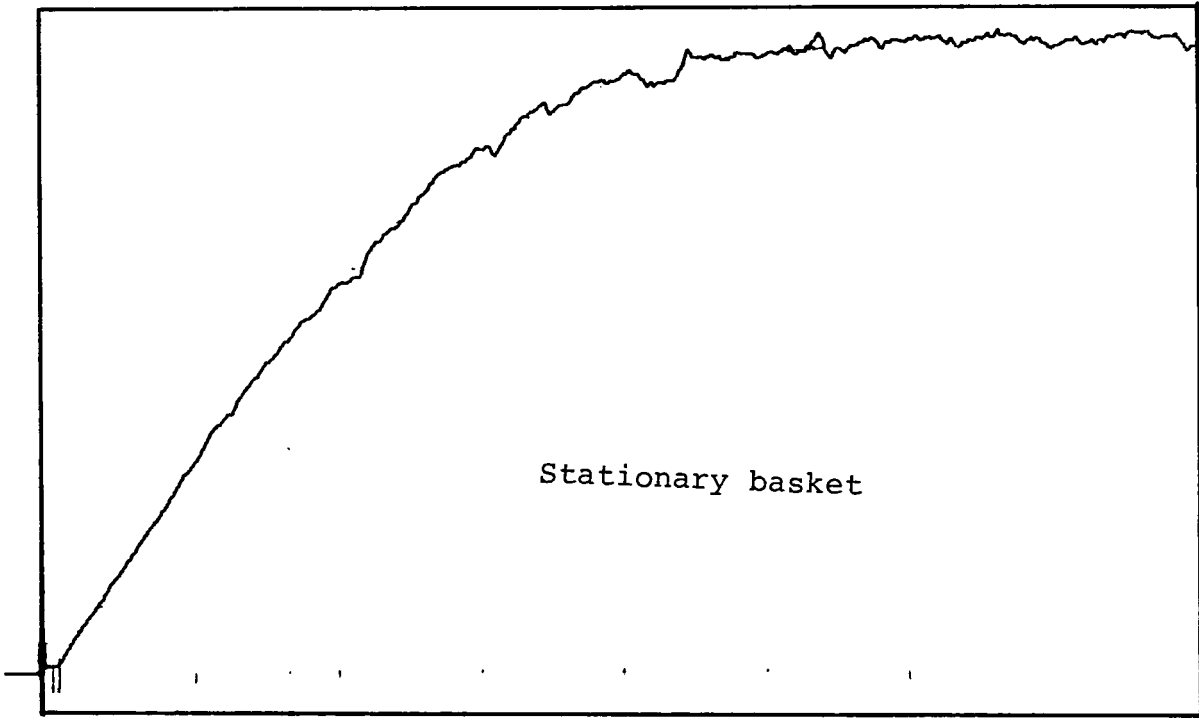


Figure 5.38 Experimental Infra-Red records of response to step feed of tracer

TABLE 5.3

COMPARISON BETWEEN THE TWO REACTORS

PARAMETER	STATIONARY BASKET REACTOR	SPINNING BASKET REACTOR
CATALYST VOLUME	28.0 cm ³	28.0 cm ³
EXPOSED WIRE-MESH AREA	81.0 cm ²	121.0 cm ²
VOID VOLUME	318 cm ³	330 cm ³
MEAN RESIDENCE TIME	63.6 s	66 s

TABLE 5.4

COMPARISON BETWEEN CATALYST I AND CATALYST V

PROPERTY	PREPOISONED CATALYST I	PREPOISONED CATALYST V
B.E.T. SURFACE AREA	129.17 m ² /g	113.89 m ² /g
TOTAL SULPHUR CONTENT	SAMPLE 1 = 0.0430 g-S/g-catalyst	SAMPLE 1 = 0.0943 g-S/g-catalyst
	SAMPLE 2 = 0.0453 g-S/g-catalyst	SAMPLE 2 = 0.0941 g-S/g-catalyst

These and the results of the sulphur content analysis using a modified version of the UOP method 357-76 (1976) are presented in Table 5.4. These results are consistent with other observations that the ratio of the sulphur and the nickel content does have a significant effect on this reaction (Takeuchi et al., 1975).

CHAPTER 6

CONCLUSIONS AND RECOMMENDATIONS

6.1 Conclusions

If the events of the past decade are viewed in an historical sequence, it may be concluded that these dynamic studies of acetylene hydrogenation on nickel catalysts constitute the logical completion of the first cycle in a long term iterative process of the modeling of and experimentation with periodic chemical reactors. This cycle began when Horn introduced the concept of the attainable set. Utilizing this concept, Bailey introduced a mathematical definition of selectivity which is compatible with past usage of the term and which provides a basis for a less ambiguous discussion of the performance of chemical reactors in which a complex reaction is occurring. Lee identified acetylene hydrogenation as a reaction system of practical interest and showed with the help of computer simulations that improvements in ethylene selectivity could be realized by forced cycling of the feed to a catalytic CSTR. The results of these experiments with a spinning-basket reactor demonstrate that indeed such selectivity modifications and improvement in both ethylene and ethane yields can be achieved by periodic operation.

The results obtained in these unsteady-state studies clearly show that the dynamics of the gas phase-catalyst surface interactions cannot be neglected when determining a periodic control strategy. Although intrapellet diffusional effects were considered

by Lee, it is important to note that other dynamic phenomena which might occur within the porous catalytic solid were totally neglected in his model which was based on published steady-state kinetics for a different catalyst. It is not at all surprising that these findings are considerably different from Lee's predictions, because, as pointed out in the discussion for Catalyst I, the steady-state kinetics and the observed dependence on cycling period are distinctly dissimilar from Lee's results. Further, the experiments with the five different catalysts in this work unequivocally point to the fact that the dynamics of the reaction are very strongly dependent on the nature of the surface of the individual catalyst.

A major contribution of this study is the experimental demonstration of the hypothesis that steady-state modeling does not reveal all the information necessary to obtain a better understanding of heterogeneous catalyst dynamics. Furthermore, step response experiments, do not provide nearly as rigorous a test for the catalyst dynamics model as do periodic experiments.

As stated in section 2.1, the principal objective of this investigation was to experimentally demonstrate the benefits of cyclic operation for consecutive-competitive reactions and thereby lend credence to earlier modeling studies, illustrate successful utilization of the available theory, and to spur the development of other applications. Undoubtedly, the results presented and discussed in Chapter 5 indicate that these benefits are realized in some cases and clearly reveal the partial

inadequacy of the earlier models for this particular system. Indeed, these findings do illustrate successful utilization of the available theory and will definitely lead to the development of improved models which will hopefully explain at least some of these interesting phenomena.

Other significant conclusions which may be drawn here are that catalyst surface capacitance should not generally be neglected when investigating stability and control of catalytic reactors and that improved reactor performance due to cycling can be realized even when deviations from ideal mixing are present. The former conclusion is also evident in recent studies by Sheintuch and Schmitz (1977) and Pikios and Luss (1977) of self-oscillating isothermal catalytic reactions, whereas, the latter one agrees with the observations of Claybaugh et al. cited earlier. It is interesting and significant to note that the experimental studies of Unni (1972), Renken (1974, 1976) and Al-Taie (1978) have all led to the conclusion that the dynamics of fundamental surface rate processes such as adsorption, surface reaction, and desorption of the system species appear to have a considerable influence on forced periodic operation of chemical reactors.

6.2 Recommendations for Future Work

It is difficult if not impossible to make an a priori categorical statement about the direction of future cyclic reactor experiments and simulations at this stage. Clearly, this decision depends on several factors and significant among these are the

availability and extent of research grants and the interest and the expertise of the principal investigator and coworkers.

However, some possibilities have been suggested below in brief:

1) In the future, direct experimental measurements of hydrogen trajectories will significantly enhance the ability to understand and compare the results of experiments and simulations. The apparent dependence of the kinetics on hydrogen concentration, as indicated by the best-fit model for Catalyst I clearly demonstrate the importance of such a modification to the current experimental system.

2) In view of the practical importance of acetylene hydrogenation in ethylene purification processes, it would be more meaningful to better represent the industrial situation by introducing relatively large amounts of ethylene in the reactor feed. Such changes would be relatively simple to implement and should not introduce very many additional complications.

3) Another useful strategy would be to oscillate both hydrogen and acetylene feed concentrations, both in phase and out of phase with each other. Theoretical simulations by Sincić (1976) have shown that additional improvement in time-average behavior can be obtained by such a policy.

4) The present reactor could be replaced by an entirely new gradientless stationary basket design or by a recycle reactor.

Such a change would allow direct catalyst temperature measurements and investigation of more rapid cyclic oscillations, respectively.

5) A process control computer and electronic flowmeters could be used to achieve very rapid switching between several concentrations and to introduce more exotic input waveforms.

6) Theoretically, new models must be developed which can reproduce and explain both steady-state and transient and oscillatory experimental results.

7) Such a refined model could be used in conjunction with optimization programs to search for a new optimal cycling strategy.

REFERENCES

- Al-Taie, A. K. S. M., Ph.D. Thesis, University of London, 1977.
- Al-Taie, A. K. S. M. and L. S. Kershenbaum, "Chemical Reaction Engineering - Houston" (V. W. Weekman, Jr. and D. Luss, eds.) ACS Symposium Ser. 65, 512 (1978).
- Anderson, J. R., "Structure of Metallic Catalysts," Academic Press, New York, 1975.
- Aris, R. and N. R. Amundson, Chem. Eng. Sci., 7, 132 (1958).
- Bailey, J. E., Ph.D. Thesis, Rice University, 1968.
- Bailey, J. E., Automatica, 8, 451 (1972a).
- Bailey, J. E., Int. J. Control, 16(2), 311 (1972b).
- Bailey, J. E., AIChE J., 18(2), 459 (1972c).
- Bailey, J. E., Canad. J. Chem. Eng., 50, 108 (1972d).
- Bailey, J. E., Chem. Eng. Commun., 1, 111 (1973).
- Bailey, J. E., Chem. Eng. Sci., 29, 767 (1974).
- Bailey, J. E., "Periodic Phenomena in Chemical Reactors", in Chemical Reactor Theory: A Review (L. Lapidus and N. R. Amundson, eds.) Prentice Hall, New Jersey, 1977.
- Bailey, J. E. and F. J. M. Horn, J. Opt. Theory & Appl., 2(6), 441 (1968).
- Bailey, J. E. and F. J. M. Horn, Ber. Bunsenges. Phys. Chem., 73, 274 (1969).
- Bailey, J. E. and F. J. M. Horn, Ber. Bunsenges. Phys. Chem., 74, 611 (1970a).
- Bailey, J. E. and F. J. M. Horn, I&EC Fundam., 9(2), 299 (1970b).
- Bailey, J. E. and F. J. M. Horn, J. Opt. Theory & Appl., 7(5), 378 (1971a).

- Bailey, J. E. and F. J. M. Horn, *AIChE J.*, 17(3), 550 (1971b).
- Bailey, J. E. and F. J. M. Horn, *Chem. Eng. Sci.*, 27, 109 (1972).
- Bennett, C. O., *Cat. Rev. - Sci. & Eng.*, 13, 121 (1976).
- Bennett, C. O., M. B. Cutlip and C. C. Yang, *Chem. Eng. Sci.*, 27, 2255 (1972).
- Bernardo, C. A. and L. S. Lobo, *J. Catal.*, 37, 267 (1975).
- Bianchi, D., G. E. E. Gardes, G. M. Pojonk, and S. J. Teichner, *J. Catal.*, 38, 135 (1975).
- Bilimoria, M. R. and J. E. Bailey, "Chemical Reaction Engineering - Houston" (V. W. Weekman, Jr. and D. Luss, eds.) *ACS Symposium Ser.* 65, 526, 1978.
- Bird, R. B., W. E. Stewart and E. N. Lightfoot, "Transport Phenomena", John Wiley & Sons, New York, 1960.
- Bittanti, S., G. Fronza and G. Guardabassi, *IEEE Trans. Auto. Cont.*, AC-18, 33 (1973).
- Bond, G. C., "Catalysis By Metals", Chapters 11 and 12, Academic Press, New York, 1962.
- Bond, G. C. and P. B. Wells, "Proc. Int. Congr. Catal. - Paris," 1, 1135 (1961).
- Bond, G. C. and P. B. Wells, *Adv. in Catalysis*, 15, 155 (1964).
- Briggs, J. P., R. R. Hudgins and P. L. Silveston, *Chem. Eng. Sci.*, 32, 1087 (1977).
- Brisk, M. L., R. L. Day, M. Jones and J. B. Warren, *Trans. Instn. Chem. Engrs.*, 46, T3 (1968).
- Bruns, D. D. and J. E. Bailey, *Chem. Eng. Sci.*, 32, 257 (1977).
- Cannon, M. R., *Oil & Gas J.*, 51, 268 (1952).
- Cannon, M. R., *Oil & Gas J.*, 55, 68 (1956).
- Cannon, M. R., *I&EC*, 53, 639 (1961a).

- Cannon, M. R. and R. A. Gaska, I&EC, 53, 630 (1961b).
- Cannon, M. R. and J. R. McWhirter, I&EC, 53, 631 (1961c).
- Carberry, J. J., I&EC, 56(11), 39 (1964).
- Choudhary, V. R. and L. K. Doraiswamy, I&EC Proc. Des. Develop., 11(3), 420 (1972).
- Claybaugh, B. E., J. R. Griffin and A. T. Watson, U. S. Pat. #3,472, 829, Oct. 14, 1969.
- Codell, R. B. and A. J. Engel, AIChE J., 17, 220 (1971).
- Denis, G. H. and R. L. Kabel, Chem. Eng. Sci., 25, 1057 (1970).
- Denis, G. H. and R. L. Kabel, Chem. Eng. Sci., AIChE J., 16, 972 (1970).
- Doraiswamy, L. K. and D. G. Tajbl, Cat. Rev. - Sci. & Eng., 10(2), 177 (1974).
- Doraiswamy, L. K. and R. A. Rajadhyaksha, Cat. Rev. - Sci. & Eng., 13, 209 (1976).
- Dorawala, T. G., Ph.D. Thesis, University of Rochester, 1969.
- Dorawala, T. G. and J. M. Douglas, AIChE J., 17, 974 (1971).
- Douglas, J. M., "Chemical Process Dynamics and Control," Prentice Hall, New Jersey, 1972.
- Douglas, J. M. and D. W. T. Rippin, Chem. Eng. Sci., 21, 305 (1966).
- Douglas, J. M. and N. Y. Gaitonde, I&EC Fundam., 6, 265 (1967).
- Duffy, G. J. and I. A. Furzer, AIChE J., 24(4), 588 (1978).
- Edwards, W. M., J. E. Zuniga-Chaves, F. L. Worley, Jr. and D. Luss, AIChE J., 20, 571 (1974).
- Farhadpour, F. A. and L. G. Gibilaro, Chem. Eng. Sci., 30, 735 (1975).

Farhadpour, F. A. and L. G. Gibilaro, Chem. Eng. Sci., 30, 997 (1975).

Fjeld, M., Ph.D. Thesis, The Technical University of Norway, 1971.

Fjeld, M., "Asynchronous Quenching" in Periodic Optimization (A. Marzollo, ed.), Vol. II, Springer Verlag/CISM, Wien (1972).

Fjeld, M., Chem. Eng. Sci., 29, 921 (1974).

Guardabassi, G. and N. Schiavoni, Sixth IFAC Triennial World Congr., Boston, Paper #22.2, (1975).

Gutmann, H. and H. Lindlar, "Partial Catalytic Hydrogenation of Acetylenes" in Chemistry of Acetylenes (H. G. Viehe, ed.), Marcel Dekker, New York, 1969.

Halladay, J. B. and R. V. Mrazek, J. Catal., 28, 221 (1973).

Horn, F. J. M., Chem. Ing. Tech., 36, 99 (1964).

Horn, F. J. M., I&EC Proc. Des. Develop., 6, 31 (1967).

Horn, F. J. M. and R. C. Lin, I&EC Proc. Des. Develop., 6, 21 (1967).

Kilpatrick, J. E., E. J. Prosen, K. S. Pitzer and F. D. Rossini, J. Res. Nat. Bur. Standards, 36:599-612, (1946).

Kobayashi, M. and H. Kobayashi, Cat. Rev. - Sci. & Eng., 10, 139 (1974).

Komiyama, H. and H. Inoue, J. Chem. Eng. Japan, 1, 142 (1968).

Komiyama, H. and H. Inoue, J. Chem. Eng. Japan, 3, 206 (1970).

Kothandaraman, C. P. and S. Subramanyan, "Heat and Mass Transfer Data Book," John Wiley & Sons, New York, 1975.

Krupiczka, R., Chem. Stosow, B., III-183 (1966).

Kuester, J. L. and J. H. Mize, "Optimization Techniques with Fortran," McGraw Hill, New York, 1973.

- Lee, C. K., M. S. Thesis, University of Houston, 1972.
- Linde Specialty Gas Division - Personal Commun. (1975).
- Luss, D., Chem. Eng. J., 1, 311 (1970).
- Mark, H. and M. J. D. Low, J. Catal., 30, 40 (1973).
- Mars, P. and M. J. Gorgels, "Proc. Third Europ. Symp. Chem. React. Eng. - Amsterdam," 55 (1964).
- Matheson Gas Data Book, Matheson Publications, New Jersey (1972).
- Mears, D. E., I&EC Proc. Des. Develop., 10(4), 541 (1971).
- Mehta, P. S., Ph. D. Thesis, University of Houston, 1978.
- Nauman, E. B., Chem. Eng. Sci., 25, 1595 (1970).
- Ogunye, A. F. and W. H. Ray, AIChE J. 17, 365 (1971).
- Pareja, P., A. Amariglio and H. Amariglio, J. Catal., 36, 379 (1975).
- Perry, J. H., "Chemical Engineers' Handbook," 4th ed., McGraw Hill, New York (1963).
- Pikios, C. A. and D. Luss, Chem. Eng. Sci., 32, 191 (1977).
- Powell, M. J. D., Computer J. 7, 155 (1964).
- Prosen, E. J., K. S. Pitzer and F. D. Rossini, J. Res. Nat. Bur. Standards, 34:403-411 (1945).
- Ralson, A. and H. S. Wilf, "Mathematical Methods for Digital Computers," John Wiley & Sons, New York, 1960.
- Ray, W. H., I&EC Proc. Des. Develop., 7, 422 (1968).
- Reid, R. C. and T. K. Sherwood, "The Properties of Gases and Liquids," 2nd ed., McGraw Hill, New York (1966).
- Renken, A., Chem. Eng. Sci., 27, 1925 (1972).
- Renken, A., Chem. Ing. Techn., 46, 113 (1974).

- Renken, A., H. Helmrich and M. Lenthe, "Proc. AIChE/GVC Joint Meeting - Munich," A3-1 (1974).
- Renken, A., M. Müller and C. Wandrey, "Proc. Fourth ISCRE, Heidelberg, III-107 (1976).
- Richardson, J. T. and H. Friedrich, J. Catal., 37, 8 (1975).
- Roberts, M. W. and K. W. Sykes, Proc. Roy. Soc., A242, 534 (1957).
- Schrodt, V. N., I&EC Fundam., 4, 108 (1965).
- Schrodt, V. N., H. H. Chien, J. T. Sommerfeld, and P. E. Parisot, Sep. Sci., 1, 245 (1966a).
- Schrodt, V. N., J. T. Sommerfeld, P. E. Parisot and H. H. Chien, Sep. Sci., 1, 281 (1966b).
- Schrodt, V. N., J. T. Sommerfeld, O. R. Martin, P. E. Parisot and H. H. Chien, Chem. Eng. Sci., 22, 759 (1967a).
- Schrodt, V. N., I&EC, 59, 58 (1967b).
- Sehr, R. A., Chem. Eng. Sci., 9, 145 (1958).
- Sheintuch, M. and R. A. Schmitz, Cat. Rev. - Sci. & Eng., 15, 107 (1977).
- Sheridan, J., J. Chem. Soc. (London), p. 133 (1944).
- Sheridan, J., J. Chem. Soc. (London), p. 301, 305, 470 (1945).
- Simons, J. B., D. G. Tajbl and J. J. Carberry, I&EC Fundam., 5, 171 (1966).
- Sinčić, D., M. S. Thesis, University of Houston, 1974.
- Sinčić, D., Ph.D. Thesis, University of Houston, 1976.
- Smith, W. D., "AIChE Ann. Meeting - Chicago," (1970).
- Tajbl, D. G., Canad. J. Chem. Eng., 47, 154 (1969a).
- Tajbl, D. G., I&EC Proc. Des. Develop., 8, 364 (1969b).

- Tajbl, D. G., H. L. Feldkirchner and A. L. Lee, Adv. Chem. Ser., 69, 166 (1967).
- Takeuchi, A., K. I. Tanaka, I. Toyoshima and K. Miyahara, J. Catal., 40, 94 (1975).
- Tellis, C. B. and H. M. Hulburt, "AIChE Ann. Meeting - Los Angeles," (1975).
- Thomas, C. L., "Catalytic Processes and Proven Catalysts," Academic Press, New York, 1970.
- Toei, R., K. Nakanishi and M. Okazaki, J. Chem. Eng. Japan, 7(3), 193 (1974).
- Trifiro, F., C. Banfi, G. Caputo, P. Forzatti and I. Pasquon, J. Catal., 30, 393 (1973).
- Unger, B. D. and R. G. Rinker, I&EC Fundam., 15, 225 (1976).
- Unni, M. P., R. R. Hudgins and P. L. Silveston, Canad. J. Chem. Eng., 51, 623 (1973).
- UOP Method 357-76, "Traces of Sulfur in Petroleum Distillates by the Nickel Reduction Method," (1976).
- Van Dijck, W. J. D., U.S. Pat. #2,011,186 (1935).
- Wagman, D. D., J. E. Kilpatrick, K. S. Pitzer, and F. D. Rossini, J. Res. Nat. Bur. Standards, 35:467-496 (1945).
- Wandrey, C. and A. Renken, Chem. Ing. Techn., 45, 854 (1973).
- Wandrey, C. and A. Renken, "Proc. AIChE/GVC Joint Meeting - Munich," p. A3-3 (1974).
- Wandrey, C. and A. Renken, Chem. Eng. Sci, 32, 448 (1977).
- Wankat, P. C., Sep. Sci., 9, 85 (1974).
- Weekman, V. W., Jr., "AIChE Ann. Meeting - Philadelphia," (1973).
- Weisz, P. B. and C. D. Prater, Adv. Catal., Vol. III, p. 143, Academic Press, New York (1954).
- Wheeler, A., "Catalysis" (P. H. Emmett, ed.) Vol. II, Reinhold, New York (1955).

Young, K. H. and O. A. Hougen, Chem. Eng. Progress,
46(3), 146 (1950).

APPENDIX 1

FLOWMETER CALIBRATIONS

Al.1 Nitrogen Flowmeter Calibration

A Fischer and Porter #10A1460 Lab Crest Low Flow rotameter was used in this investigation to measure the rate of inert nitrogen gas flow to the reactor. A standard soap-film bubble meter was used for the calibration. The elapsed time was measured with an electronic digital clock with a least count of 0.1s. The measurements were made at a temperature of 74°F (23.3°C) and a constant inlet pressure of 5 psig. The calibration curve for the glass tube #FP1/8-038-G-6/443U381U18 and a tantalum float is presented in Figure Al.1.

Al.2 Acetylene Flowmeter Calibration

The measurements were done in the same manner as described for nitrogen under identical conditions of temperature and pressure. The calibration curve for the glass tube #FP1/8-034-G-6/443U381U09 and a constant density black-glass float is shown in Figure Al.2.

Al.3 Hydrogen Flowmeter Calibration

Once again, the same procedure described for the other gases was used under identical conditions of temperature and pressure. The corresponding calibration curve for the glass tube #FP1/8-034-G-6/443U381U09 and a constant density black glass float is shown in Figure Al.3.

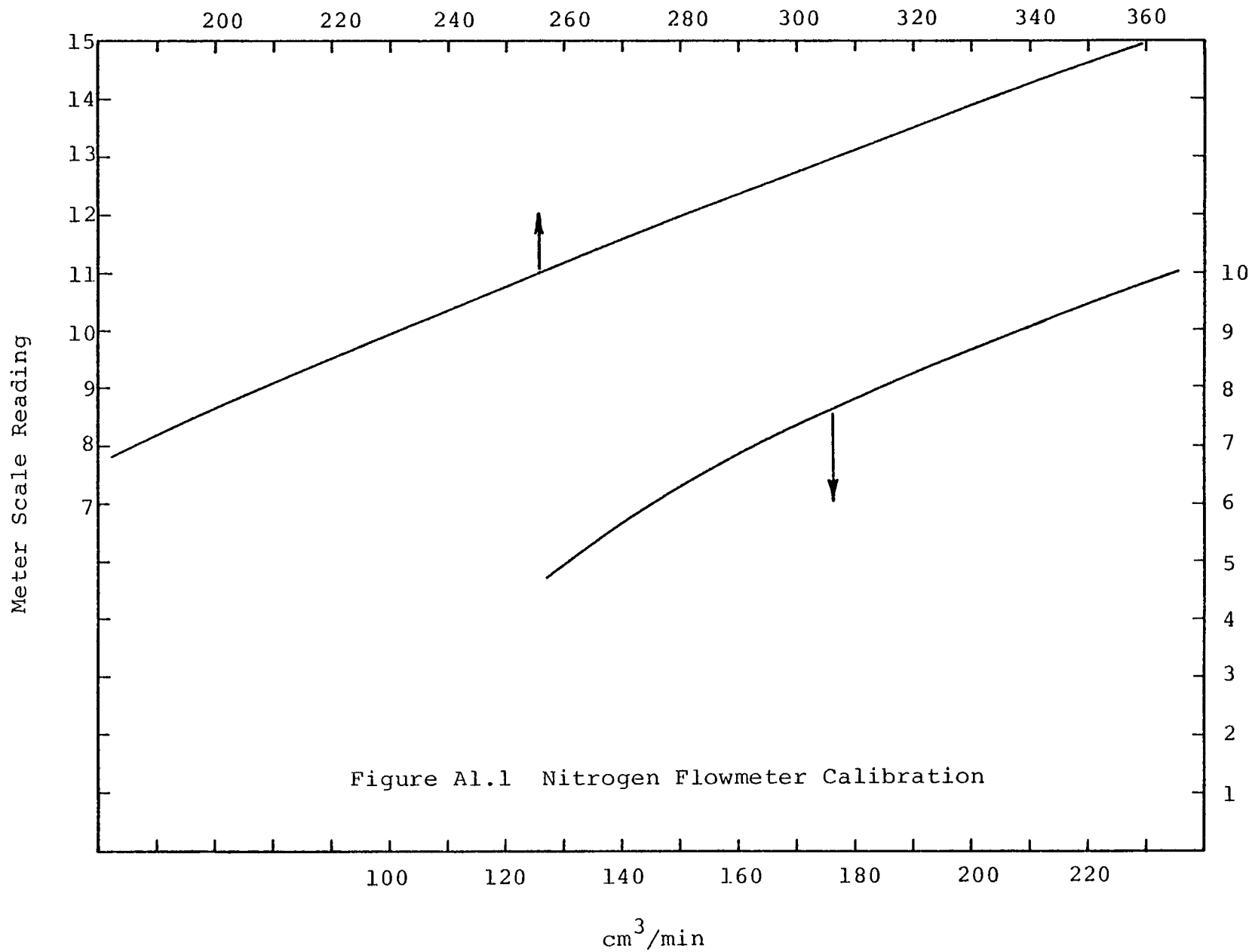


Figure A1.1 Nitrogen Flowmeter Calibration

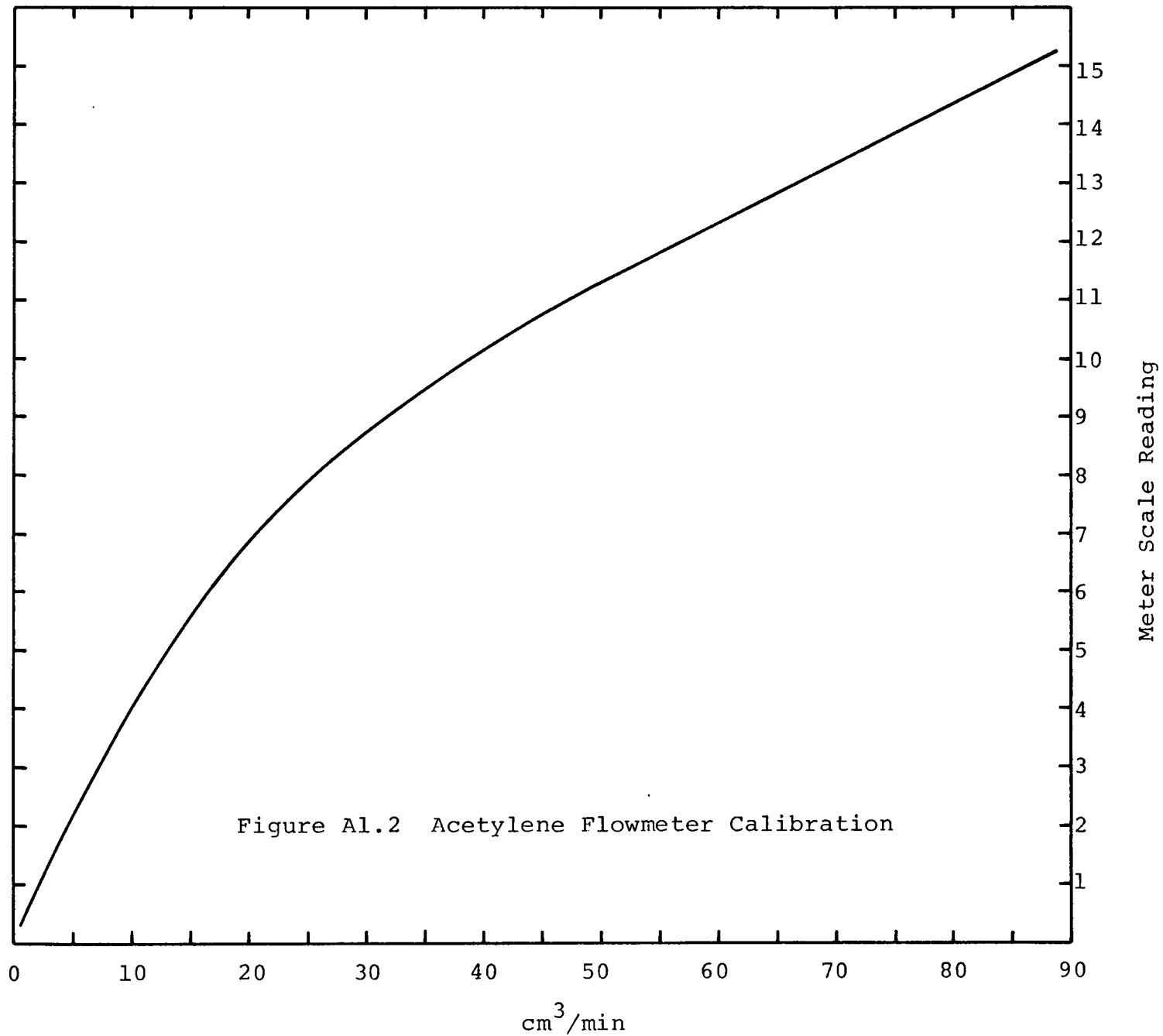


Figure A1.2 Acetylene Flowmeter Calibration

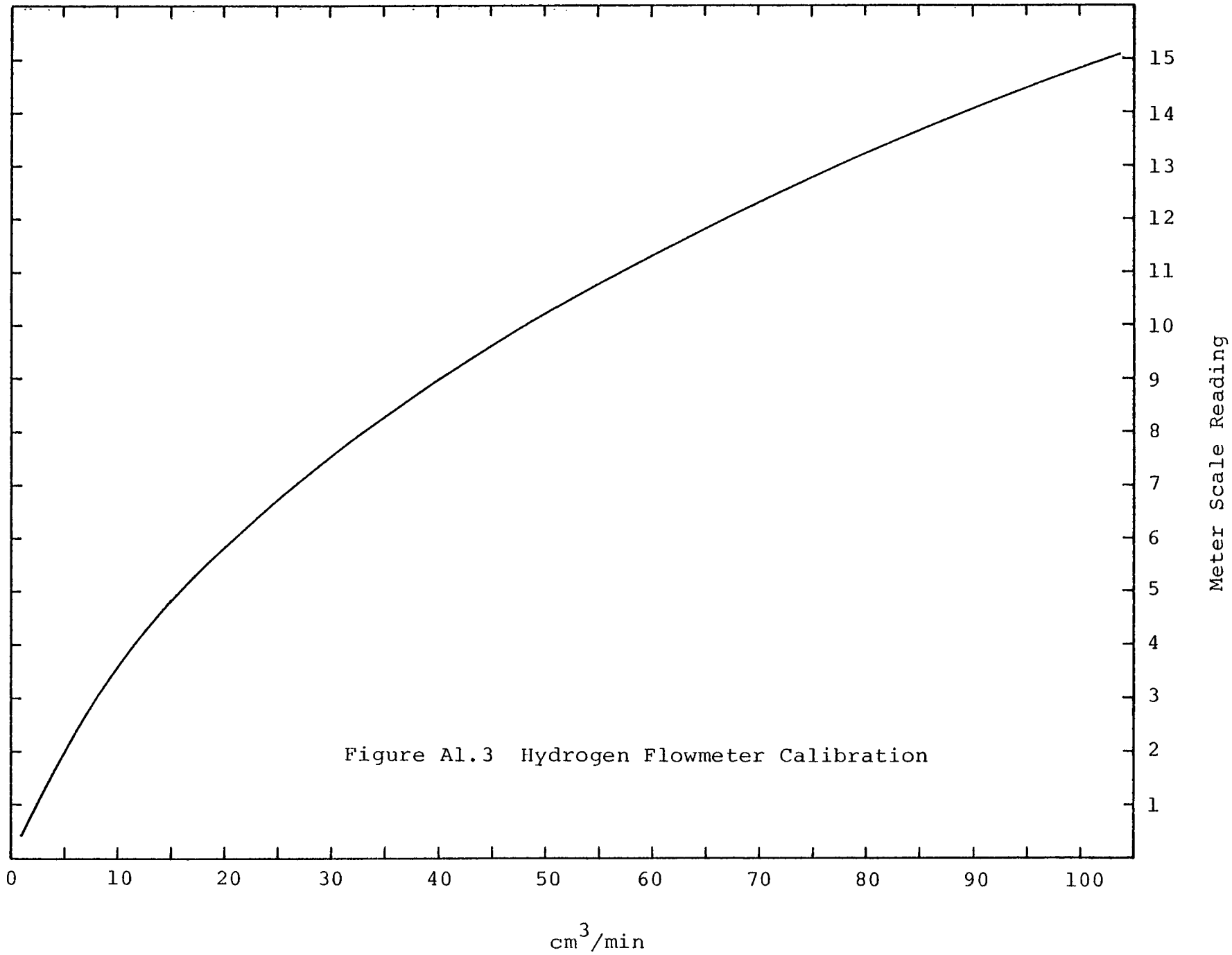


Figure A1.3 Hydrogen Flowmeter Calibration

APPENDIX 2
MULTICHANNEL TIMER SETTINGS

The various periods of oscillation (τ 's) were achieved by the settings on the actuator drum shown below. In each case 15 slots on the big drum correspond to one period.

$\tau = 60s$

To obtain this period, red-colored triangular actuators must be pushed into slots numbered 1, 5, 9, 13, 17, 21, 25, 29, 33, 37, 41, 45, 49, 53 and 57 on the actuator drum.

$\tau = 180s$

To obtain this period, red-colored triangular actuators must be pushed into slots numbered 1, 13, 25, 37, and 49 on the actuator drum.

$\tau = 300s$

To obtain this period, red colored-triangular actuators must be pushed into slots numbered 1, 21 and 41 on the actuator drum.

$\tau = 450s$

To obtain this period, red-colored triangular actuators must be pushed into slots numbered 1 and 31 on the actuator drum.

Only square shaped actuators must be used on the big drum. Different colors may be used to help identify the γ and $(1-\gamma)$ fractions of τ . If triangular actuators are used on the big drum, the solenoid valves will chatter continuously and the gas flow will be irregular.

APPENDIX 3
ESTIMATION OF PARAMETERS

All of the computations shown below represent typical order of magnitude estimates. Since nitrogen is by far the major component of the gas mixture and since the molecular weights of the hydrocarbons are very close to the molecular weight of nitrogen, the property values of the gas mixture will be assumed to be those for nitrogen. Unless mentioned otherwise, property values have been taken from:

- 1) Perry (1963)
- 2) Kothandaraman and Subramanyan (1975)

A3.1 Estimation of Thermal Relaxation Time

The effective thermal conductivity (K_e) was estimated using the correlation proposed by Krupicza (1966) for a packed bed.

$$\frac{K_e}{K_f} = \frac{K_s}{K_f} [0.28 - 0.75 \log e - 0.057 \log (K_s/K_f)]$$

The thermal conductivity of alumina pellets (K_s) similar to those used in this work has been reported by Sehr (1958) to be 8.0×10^{-4} cal/(cm-s-°K) and the thermal conductivity of nitrogen is reported to be 9.19×10^{-5} cal/(cm-s-°K) (Kothandaraman and Subramanyan, 1975).

The void fraction in the basket is approximately $\epsilon = 0.4$ and the effective density and specific heat are estimated as follows:

$$\begin{aligned}\rho_e &= \rho_s(1-\epsilon) + \rho_f\epsilon \\ &= 1.0 \times 0.6 + 0.78 \times 10^{-3} \times 0.4 \\ &= 0.6 \text{ g/cm}^3\end{aligned}$$

$$\begin{aligned}c_p &= c_{ps}(1-\epsilon) + c_{pf}\epsilon \\ &= 0.2 \times 0.6 + 0.25 \times 0.4 \\ &= 0.22 \text{ cal/(g-}^\circ\text{K)}\end{aligned}$$

where ρ and c_p denote the density and specific heat and subscripts s and f refer to the solid and gas phases respectively.

. The thermal relaxation time is given by

$$\begin{aligned}&\frac{L_{\text{basket}}^2 \rho_e c_p}{K_e} \\ &= \frac{(0.23 \text{ cm})^2 \times 0.6 \text{ g/cm}^3 \times 0.22 \text{ cal/(g-}^\circ\text{K)}}{29 \times 10^{-5} \text{ cal/(cm-s-}^\circ\text{K)}} \\ &= 24 \text{ seconds}\end{aligned}$$

A3.2 Estimation of Adiabatic Temperature Rise (β)

A typical value of the effective diffusivity of the reaction mixture in the porous catalyst particle is

$D_e = 10^{-3} \text{ cm}^2/\text{s}$. The bulk concentration of the reactant is
 $C_o = 2.67 \times 10^{-6} \text{ mol}/\text{cm}^3$.

. The dimensionless intrapellet adiabatic temperature rise is given by

$$\begin{aligned}\beta &= \frac{(-\Delta H)D_e C_o}{K_s T_s} \\ &= \frac{42 \times 10^3 \text{ cal/mole} \times 10^{-3} \text{ cm}^2/\text{s} \times 2.67 \times 10^{-6} \text{ mol}/\text{cm}^3}{8 \times 10^{-4} \text{ cal}/(\text{cm}\cdot\text{s}\cdot^\circ\text{K}) \times 439^\circ\text{K}} \\ &= 3.2 \times 10^{-4}\end{aligned}$$

A3.3 Estimation of Weisz's Observable Modulus (ϕ)

For first-order kinetics and spherical particles

$$\begin{aligned}\phi &= \frac{\text{observed rate}}{\frac{D_e}{d_p^2} \times C_o} \\ &= \frac{4.1 \times 10^{-9} \text{ mol}/(\text{cm}^3\cdot\text{s})}{\frac{10^{-3} \text{ cm}^2/\text{s}}{(0.1 \text{ cm})^2} \times 2.67 \times 10^{-6} \text{ mol}/\text{cm}^3} \\ &= 1.5 \times 10^{-2}\end{aligned}$$

APPENDIX 4
CATALYST PROPERTIES*

CATALYST	Nickel Content	Support	Surface Area (m ² /g)	Pore Size Range (μ)	Pore Volume (cm ³ /gm)
I Harshaw Ni0707T 1/8" Tablets	14%	Alumina	140	-	0.38
II Girdler G49A 3/16" x 1/8" Tablets	60%	Keiselguhr	85	0.014 - 0.0029 0.18 - 0.014 175.0 - 0.08	0.10 0.20 -
III Girdler G52 3/16" x 3/16" Tablets	32%	Silica-Alumina	70	0.014 - 0.0029 0.08 - 0.014 18.0 - 0.08 175.0 - 18.0	0.11 1.10 0.08 -

* As reported by manufacturer

CATALYST PROPERTIES cont.

CATALYST	Nickel Content	Support	Surface Area (m ² /g)	Pore Size Range (μ)	Pore Volume (cm ³ /gm)
IV Girdler G87RS 1/8" Extrusions	43%	Refractory	34	0.014 - 0.0029 0.08 - 0.014 1.75 - 0.08 175 - 1.75	0.07 0.11 0.01 -